Rhizopus oryzae FOR FUMARIC ACID PRODUCTION: CONTINUOUS FEED STRATEGIES TO MANIPULATE THE METABOLISM

Reuben Marc Swart

2022-10-28

Rhizopus oryzae FOR FUMARIC ACID PRODUCTION: CONTINUOUS FEED STRATEGIES TO MANIPULATE THE METABOLISM

Reuben Marc Swart

A thesis submitted in partial fulfilment of the requirements for the degree

Doctor of Philosophy

in the

Department of Chemical Engineering
University of Pretoria

2022-10-28

Rhizopus oryzae FOR FUMARIC ACID PRODUCTION: CONTINUOUS FEED STRATEGIES TO MANIPULATE THE METABOLISM

Author:	Reuben Marc Swart
Supervisor:	Professor Willie Nicol
Co-supervisor:	Professor Hendrik Gideon Brink
Department:	Chemical Engineering
Degree:	Doctor of Philosophy in Chemical Engineering

Synopsis

The four-carbon dicarboxylic acid, fumaric acid, of the tricarboxylic acid cycle remains a promising bio-based platform chemical. To date the most promising organism for producing fumaric acid is *Rhizopus oryzae* (ATCC 20344) that naturally excretes fumaric acid under nitrogen limited conditions. In order to investigate the fumaric acid production with *R. oryzae*, a novel immobilised biomass reactor was developed. Fumaric acid excretion in *R. oryzae* is always associated with the co-excretion of ethanol, an unwanted metabolic product from the fermentation. The cause of ethanol production was suspected to be a result of *R. oryzae* being a Crabtree-positive organism. For Crabtree-positive organisms like *Saccharomyces cerevisiae*, ethanol overflow is negated by controlling the glucose input to the fermentation. The same strategy was employed for *R. oryzae* during a continuous production fermentation. It was shown that ethanol could be eliminated entirely during fumaric acid production, achieving a yield of $0.802\,\mathrm{g\,g^{-1}}$ fumaric acid on glucose [1]. The medium pH was identified as a key parameter affecting fumaric acid excretion. It was found that the selectivity for fumaric acid production increased at high glucose consumption rates for a pH of 4, different from the trend for pH 5 and 6, achieving a yield of $0.93\,\mathrm{g\,g^{-1}}$ [2]. This yield is higher than previously reported in the literature.

The use of lignocellulosic hydrolysate, predominantly comprised of glucose and xylose, for the production of fumaric acid would greatly improve the industrial viability of the process. A synthetic lignocellulosic hydrolysate (glucose-xylose mixture) was used in batch and continuous fermentations to investigate the feasibility of this substrate. The batch fermentation of the synthetic hydrolysate at the optimal conditions (urea feed rate $0.625\,\mathrm{mg\,L^{-1}\,h^{-1}}$ and pH 4) produced a fumaric acid yield of $0.439\,\mathrm{g\,g^{-1}}$. A specific substrate feed rate ($0.164\,\mathrm{g\,L^{-1}\,h^{-1}}$) which negated ethanol production and selected for fumaric acid was determined. Using this feed rate in a continuous fermentation a

fumaric acid yield of $0.735\,\mathrm{g\,g^{-1}}$ was achieved; a 67.4 % improvement [3]. Metabolic analysis helped to identify a continuous synthetic lignocellulosic hydrolysate feed rate that selected for fumaric acid production, while achieving co-fermentation of glucose and xylose, avoiding the undesirable carbon catabolite repression.

Because this work demonstrates the viability of fumaric acid production from lignocellulosic hydrolysate, the process developments discovered will pave the way for an industrially viable process.

Acknowledgements

The process to this point has been one of many late nights, feelings of inadequacy and fear of whether it will all work out. I thank the Lord Jesus for providing for me at every difficult turn and for the ability to have studied up until this point, it is such a privilege.

Willie, thank you this would not have been possible without you. Thank you for the continued encouragement along the way, you are the best supervisor I could have asked for. The environment that you build around your students is the key to success.

To the research group Nico, Naas, Maria, Dominic, Kwanele, Lonestar, Joy, Roger, Felix, Eleanor and Charles, thank you so much for the support throughout the last few years. It has been an absolute pleasure working next to you!

To all of my friends, the family, thank you so much for all the good times (i.e. hikes, dinners and runs) that we have had during these years. It has been a blessing to meet you all, thank you for making me a better person along the way.

Berné thank you for the support at the lowest points and your continued friendship, thank you for being so interested in the work. Thank you proofreading the papers and this thesis, I appreciate it greatly.

Dedication

Mom and Dad, your overwhelming love and continued prayers have brought us to this point. Thank you for always having my back, pushing me in the right direction and for being there when I needed you. None of this would have been possible without your support. Thank you immensely.

Contents

List of Figures

List of Tables

Nomenclature

α	Carbon dioxide yield coefficient	$Cmol\ CO_2\ Cmol\ X^{-1}$
β	NADH yield coefficient	$mol\ NADH\ Cmol\ X^{-1}$
γ	ATP yield coefficient	$mol\ ATP\ Cmol\ X^{-1}$
μ_{max}	Maximum specific growth rate	h^{-1}
A	Acid concentration	$mol\ L^{-1}$
C	Carbon mole concentration of specie	$Cmol\ L^{-1}$
e	Effluent	-
eq	Equilibrium	-
F	Faraday's constant	96.5 kJ Volt^{-1}e-mol^{-1}
f	Feed into reactor	-
i	Intracellular	-
j	Designation of a specie	-
K_m	Monod constant	$g\ L^{-1}$
MM_j	Molar mass of species j	$g\ Cmol^{-1}$
N	Moles of species	$Cmol_i$
n	Number for proton transported with fumarate	-
o	Inlet	-
pKa	Dissociation equlibrium constant	-
pmf	Proton motive force	V
Q	Volumetric flow rate	$L\ h^{-1}$
R	Gas constant	8.314×10^{-3} kJ mol^{-1} K^{-1}
r	Rate of production	$Cmol_i\ L^{-1}\ h^{-1}$
r_i	Rate of production of species i	$g\ g^{-1}\ h^{-1}$
r_x	Rate of biomass growth	$g\ g^{-1}\ h^{-1}$

r_{CO2}	Rate of CO_2 production	$mol\ L^{-1}\ h^{-1}$
S_j	Matrix specification	-
T	Temperature	K
t	Time	h
V	Liquid volume of the fermenter	L
V_g	Gas volume of the fermenter	L
v_j	Metabolic flux mode rate of pathway j	$Cmol\ L^{-1}\ h^{-1}$
Y_{sj}	Yield of species j on the substrate (glucose/xylose)	$g\ g^{-1}$, $Cmol\ Cmol^{-1}$
V	Flux model rate matrix	-
X	Mass balance rate matrix	-
ATP	Adenosine triphosphate	-
B	Biomass	-
CCR	Carbon catabolite repression	-
DO	Dissolved oxygen	-
ET	Ethanol	-
FA	Fumaric acid	-
$FADH_2$	Flavin adenine dinucleotide	-
G	Glucose	-
GL	Glycerol	-
GTP	Guanosine triphosphate	-
GY	Glycogen	-
LH	Lignocellulosic hydrolysate	-
MA	Malic acid	-
NADH	Nicotinamide adenine dinucleotide	-
NADPH	Nicotinamide adenine dinucleotide phosphate	-

P/O	Oxidative phosphorylation value	$mol_{ATP}\ mol^{-1}_{NADH}$
PA	Pyruvic acid	-
SA	Succinic acid	-
TCA	Tricarboxylic acid	-
U	Urea	-
W	Water	-
X	Xylose	-

Publications

RM Swart, F Le Roux, A Naude, NW De Jongh, and W Nicol. "Fumarate production with Rhizopus oryzae: Utilising the Crabtree effect to minimise ethanol by-product formation". In: *Biotechnology for Biofuels* 13.1 (2020), pp. 1–10. ISSN: 17546834. DOI: 10.1186/s13068-020-1664-8. URL: https://doi.org/10.1186/s13068-020-1664-8

RM Swart, DK Ronoh, H Brink, and W Nicol. "Continuous Production of Fumaric Acid with Immobilised Rhizopus oryzae: The Role of pH and Urea Addition". In: *Catalysts* 12.1 (Jan. 2022), p. 82. ISSN: 2073-4344. DOI: 10.3390/catal12010082. URL: https://www.mdpi.com/2073-4344/12/1/82

RM Swart, H Brink, and W Nicol. "Rhizopus oryzae for Fumaric Acid Production: Optimising the Use of a Synthetic Lignocellulosic Hydrolysate". In: *Fermentation* 8.6 (June 2022), p. 278. ISSN: 2311-5637. DOI: 10.3390/fermentation8060278. URL: https://www.mdpi.com/2311-5637/8/6/278

NW de Jongh, RM Swart, and W Nicol. "Fed-batch growth of *Rhizopus oryzae*: Eliminating ethanol formation by controlling glucose addition". In: *Biochemical Engineering Journal* 169.November 2020 (2021). ISSN: 1873295X. DOI: 10.1016/j.bej.2021.107961

DK Ronoh, RM Swart, W Nicol, and H Brink. "The Effect of pH, Metal Ions, and Insoluble Solids on the Production of Fumarate and Malate by Rhizopus delemar in the Presence of CaCO3". In: *Catalysts* 12.3 (2022). ISSN: 20734344. DOI: 10.3390/catal12030263

1 Introduction

In the current climate the world's population is growing at a rapid rate and is predicted to reach 8.5 billion people by 2030 [6]. Combined with the growing middle class in developing countries, the pressure on the energy and food industries has never been so high [7, 8]. Considering moreover the impact that each person's lifestyle has on the environment as well as our current trajectory of climate change, a grim picture is painted for our future. In the Sixth Assessment Report from the Intergovernmental Panel on Climate Change it has been clearly found that human influence has warmed the climate. The only course of action to curb further climate change is to limit both CO_2 and other greenhouse gas emissions [9]. The push to develop environmentally sustainable and innovative pathways for producing fuels, food, and materials is front of mind. The world's reliance on fossil fuels needs to be broken.

The question arises, how can fossil fuels be replaced? Fossil fuels are predominately used for the production of energy of which transportation fuels form a large part. Our source of energy will likely be replaced by a combination of wind, solar, nuclear, hydroelectric, and biomass energy [10]. Fossil fuels are also widely used for the production of organic chemicals and plastics. These materials will have to come from renewable biomass-based sources. The proposed biorefinery solves both of these problems because it would use renewable biomass to produce biofuels and bio-based chemicals [11]. In 2004, the US Department of Energy released a report identifying promising bio-based chemicals that could be produced from carbohydrate sources. The chemicals were identified on the basis of a number of factors including versatility, ease of production, attention from literature, commercial applications and whether it is a platform chemical [12].

The dicarboxylic acids of the tricarboxylic acid cycle: succinic acid, fumaric acid, and malic acid were named as Top Value Added Chemicals from Biomass because of their versatility as platform chemicals [12]. These were identified as building block chemicals that can serve to replace chemicals derived from crude oil and natural gas. The imagined process uses metabolic pathways directing the conversion of sugars to the desired metabolite. This process would avoid the use of fossil fuels, prone to produce CO_2, and would use lignocellulosic biomass as the feed stock instead. Production through a fermentative process would reduce or negate the by-production of CO_2, moving towards a carbon-neutral process. Lignocellulosic biomass is plant matter comprised of cellulose, hemicellulose, and lignin, either being a waste stream from industry (sugarcane) or purposefully grown for the biorefinery [13]. The growth of the biomass consumes the CO_2 that would later be present in the final chemical. Hydrolysis of this material yields the monomeric or dimeric sugars: glucose, fructose, sucrose, lactose, galactose, xylose, and

arabinose [14]. The proportions of these sugars depends on the biomass source as well as the hydrolysis process used. However, glucose and xylose are usually the predominant sugars produced [15].

Most studies have been performed on the biological production of succinic acid and since 2012 four commercial startups have employed a fermentative strategy to produce succinic acid [16]. Fumaric acid differs from succinic acid in degree of reduction, where the internal double bond of fumarate, in addition to the two terminal carboxylic acid groups, opens up various downstream possibilities. Fumaric acid hydrogenation to succinic acid is a straightforward catalytic step. A potential bulk market for the C4 dicarboxylic acids lie in the replacement of petrochemically derived maleic anhydride, a 2.77 billion USD market [17]. Fumaric acid also has a global market size of 660.9 million USD and is expected to grow at a rate of 5.5% annually for the period 2021–2026 [18]. It is a versatile chemical that is currently used in the food and beverage industry, resins, polyesters, animal feeds, and in the production of pharmaceuticals [19, 20, 21]. All fumaric acid is currently produced from butane, a by-product of the petrochemical industry [22, 21].

Moving to the biological production of fumaric acid is crucial for a transition away from unsustainable petrochemical practices. Multiple avenues have been explored to identify the ideal organism to produce fumaric acid. The avenues include *Rhizopus* species, which have been found to naturally excrete fumaric acid and then *Saccharomyces cerevisiae* and *Escherichia coli*, which are well researched organisms allowing for genetic engineering to enable fumaric acid production [19]. However, fumaric acid production by *Rhizopus oryzae* has not been matched by any other natural organism or by a genetically modified strain. Frits Went and Hendrik Coenraad Prinsen Geerligs first discovered *R. oryzae* ATCC 20344 in 1895. Although it has since been correctly renamed *Rhizopus delemar*, it is still referred to as *Rhizopus oryzae* in most of the literature [23].

R. oryzae is one of the most prominently studied *Rhizopus* species for fumaric acid production. Genetic modifications on *R. oryzae* have resulted in small differences in the fermentation outcome [24, 25], but most open literature studies employ the wild strain where fumaric acid titres range from $25\,\mathrm{g\,L^{-1}}$ to $103\,\mathrm{g\,L^{-1}}$ and volume-based productivity's range from $0.19\,\mathrm{g\,L^{-1}\,h^{-1}}$ to $1.21\,\mathrm{g\,L^{-1}\,h^{-1}}$ are commonly obtained. Although *R. oryzae* has received much attention an industrially viable process has not yet been realised, indicating that there is still room for discovery [20]. The key points which still require attention to make the process industrially viable are: the rate of fumaric acid productivity, the substrate conversion yield to fumaric acid, the cost of neutralising agent required and the downstream separation of fumaric acid from the medium.

R. oryzae excretes fumaric acid under nitrogen-limited conditions with the co-production

of ethanol typically observed in this 'non-growth' production phase. Ethanol is an unwanted by-product that reduces fumaric yield and should be minimised from a processing perspective. Numerous authors attribute ethanol formation to anaerobic zones within the fungal mycelium [26, 27, 28]. *R. oryzae* is a facultative anaerobe that can survive under anaerobic conditions [29] where the ethanol pathway is used for generating intracellular ATP. Most *R. oryzae* fermentations employ suspended biomass pellets and numerous efforts have been made to reduce the pellet diameter by manipulating pH, inoculum size, nitrogen source, and glucose concentration [28, 30, 31]. The postulate that "reduced pellet diameters" will decrease anaerobic zones within the mycelium matrix and hence reduce ethanol formation has been stated but has never been conclusively proven. Accordingly, an uncertainty exists with regard to the influence of oxygen availability on ethanol formation.

The work presented in this study follows on from what was done by Naude, a previous PhD student within the group, who published multiple articles on the production of fumaric acid with *R. oryzae* [32, 33, 34]. This involved the development of a novel reactor bioreactor (250 mL) wherein the fungus could be immobilised and the growth carefully controlled. Immobilisation of the fungus allowed for a simple transition to the production phase from growth, as the reactor could be drained and rinsed, removing the nitrogen without disturbing the biomass. Further it was discovered that continuous addition of nitrogen during the usual nitrogen void production fermentations enhanced the longevity of fumaric acid production. In the conclusion of his work it was discovered that fumaric acid could be bio-catalysed to malic acid with *R. oryzae*.

In the pursuit of developing an industrially viable fumaric acid process, the work was continued by beginning with the investigation into ethanol production. It is claimed in literature that the cause of ethanol production is insufficient oxygen transfer to the organism and by correctly controlling the fungal morphology the oxygen transfer would be improved. In so doing the ethanol production would be negated [35, 32]. It was hypothesised that anaerobic zones in the mycelium were not the cause of ethanol production and that *R. oryzae* was a Crabtree-positive organism, producing ethanol as a result of a limited respiratory capacity in high glucose concentrations. Fermentations that tested for the presence of anaerobic zones were conducted. Further fermentations investigated the response to a closely controlled glucose feed rate. These fermentations shed light on the physiology of *R. oryzae*. The results and implications of this study are discussed in Chapter 4.

The nitrogen content as well as the pH of the medium, were established to be important parameters affecting fumaric acid production. Light was shed on the mechanism by which *R. oryzae* produced fumaric acid. It was found that the urea cycle, which overlaps

with the fumarate producing pathway, becomes highly active under nitrogen starved conditions [29]. Chapter 5 further investigates the interplay between fumarate production and nitrogen addition.

The pH of the medium is known to affect the metabolism and morphology of the organism. Additionally, it was discovered that the transportation of dicarboxylic acids into the medium contribute significantly to the energy costs of the cell [36]. To increase the yield of fumaric acid produced, the distribution of glucose at different pH values needed to be tested. This investigation and optimisation of the medium conditions for fumaric acid production are discussed in Chapter 5.

The production of fumaric acid from glucose is not industrially viable as it would encroach on global food security [37]. A superior alternative would be to use lignocellulosic biomass which is renewable, sustainable and is often a waste stream from other industrial processes. A common hurdle encountered in the fermentation of lignocellulosic hydrolysate is carbon catabolite repression (CCR), where glucose is used preferentially over other sugars. Chapter 6 investigates whether CCR can be overcome in a glucose and xylose mixture and whether fumaric acid production can be optimised with substrate feed strategies. The objective is to bring biological fumaric acid production closer towards industrial viability.

2 Literature

2.1 Fumaric Acid

Fumaric acid is a naturally occurring molecule, initially extracted from the plant *Fumaria officinalis*, after which its name is derived [22]. It is also known as trans-1,2-ethylenedicarboxylic acid, (E)-2-butenedioic acid, and boletic acid. In Figure 1 fumaric acid can be seen to be a dicarboxylic acid with a double carbon bond in the centre. It forms part of the tricarboxylic acid cycle, present in many organisms, but is rarely excreted in large quantities.

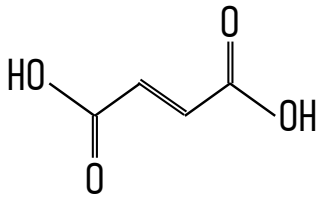

Figure 1: Chemical structure of fumaric acid

Fumaric acid is relatively insoluble with a solubility limit of $5.5\,\mathrm{g\,L^{-1}}$ in water, but the neutralised form sodium fumarate has a solubility of $228\,\mathrm{g\,L^{-1}}$ [38, 36]. Fumaric acid is a moderately strong acid with pKa values of 3.09 and 4.60 (25 °C) [36].

2.2 Fumaric Acid Applications within the Market

Fumaric acid has a global market size of 660.9 million USD and is expected to grow at a rate of 5.5 % annually for the period 2021–2026 [18]. All fumaric acid is currently produced from butane, a by-product of the petrochemical industry. Butane undergoes a catalytic reaction to produce maleic anhydride, which is then hydrolysed to maleic acid — the isomer of fumaric acid. The oxidation of butane to maleic anhydride over the $(VO)_2P_2O_7$ catalyst is an exothermic reaction, producing large amounts of CO and CO_2 [35]. This is a well-researched reaction chain with over 225 related US patents published [21]. The chemical structure of fumaric acid causes it be a versatile platform chemical with many potential industrial applications and was named as one of the top sugar-derived building blocks [12]. This included the other dicarboxylic acids of the TCA cycle, malic acid and succinic acid. Both of these chemicals are a single enzymatic step away from fumaric acid and therefore share many applications. The industries that use

fumaric acid include the food and beverage, pulp and paper, and polyester resin [35]. The food and beverage industry is the largest consumer of fumaric acid using it as an acidulant, flavour enhancer, buffer and as an anti-microbial agent [18]. As a result of the chemical structure of fumaric acid, which allows for polymerisation and esterification, the resin industry (paper resins, alkyd resins, and unsaturated polyester resins) find a number of applications for it.

A potential application for fumaric acid lies in the animal feed industry. It has been established that the addition of fumaric acid to ruminant feed increases the energy absorption by decreasing the methane production. This reduced the methane production by 32 % when fumaric acid was added to the feed [39]. The livestock industry contributes approximately 25 % of the world's methane production. Considering also that methane has a global warming potential 21 times that of CO_2, decreasing the emissions would greatly help reduce the impact of the animal industry [9, 40].

The pharmaceutical industry has recently discovered that fumaric acid esters can be used as a treatment for the incurable diseases psoriasis and multiple sclerosis. It has been found that fumaric acid esters have anti-oxidative, anti-inflammatory and immune-modulating effects. Dimethyl fumarate, the most widely studied ester, has been found to be a safe and effective treatment option for the management of psoriasis and, in recent years, has also been approved for the treatment of psoriasis and multiple sclerosis [41, 42].

Another potential application for fumaric acid is the conversion to its chemically similar derivatives. Malic acid, the favoured acid in the food and beverage industry, can be produced from fumaric acid by a simple hydration reaction, which is even possibly in situ with the organism *R. oryzae* [34, 5]. Maleic anhydride, an intermediate in the petrochemical production of fumaric acid, has a global market size of USD 2.77 billion and is expected to grow annually at a rate of 6.7 % [17]. Fumaric acid could possibly feed this market since a high-yielding dehydration reaction can be employed to convert fumaric acid to maleic anhydride [43].

2.3 Biorefinery

The biorefinery concept is born out of the necessity to move toward renewable biomass based sources for the production of fuels and chemicals. As with the oil refineries, the biorefinery will be composed of a number of processes in order to achieve economic feasibility [44]. The most suitable raw material is lignocellulosic biomass. Note that lignocellulosic biomass is an umbrella term for any plant biomass predominately comprised of cellulose, hemicellulose and lignin. Cellulose and hemicellulose are polysaccharides —

polymers comprised of many sugar molecules. Lignocellulosic biomass has a recalcitrant nature owed to its complex structure and composition [37]. The biomass is impervious to many simple enzymatic conversions; for this reason the lignocellulosic biomass needs to be pretreated before the polysaccharides can be broken apart into smaller fermentable sugars. Pretreatment changes the physical or chemical structure to make the cellulose and hemicellulose more vulnerable to hydrolysis, the next step. The two main procedures used to convert the polysaccharides to fermentable sugars are acid hydrolysis and enzymatic hydrolysis [45, 46]. Acid hydrolysis works by using acidic solutions (HCl or H_2SO_4) and high temperatures to break apart the polymers. This procedure is often not environmentally friendly and produces inhibitory compounds that affect the fermentation process. Enzymatic hydrolysis is therefore the preferred method as it does not come with these draw backs; it uses cellulolytic and hemicellulolytic enzymes which cleave off smaller monomeric sugars. This procedure requires lower temperatures, is not corrosive, and crucially, does not produce inhibitory compounds.

Hydrolysis yields the monomeric or dimeric sugars: glucose, fructose, sucrose, lactose, galactose, xylose and arabinose [14]. The proportions of these sugars depend on the biomass source as well as the hydrolysis process used. Glucose and xylose are usually the predominant sugars produced, with concentrations ranging from 60 % to 70 % glucose, and 30 % to 40 % xylose [15]. The fermentation of hexose (glucose, fructose) through glycolysis — a central enzymatic pathway — is a common process because many organisms possess these enzymes. Pentose (xylose, arabinose), on the other hand, needs to be catabolised through the pentose phosphate pathway that is not as prevalent in organisms [47]. This has led to glucose being the favoured sugar of the fermentation industry for many years. However, in order to use lignocellulosic hydrolysate as a feed stock both hexose and pentose must necessarily be utilised.

Fermentation is often the final step in converting biomass into value added chemicals. Fermentation is a process by which microorganisms catabolise the sugar molecules to produce metabolites. A wide range of metabolites can be produced; each determined by the organism's enzymatic pathways. Screening of potential organisms or bioprospecting are often involved to find an organism capable of producing the desired chemical. The yield, titre and production rate of the desired chemical is used for the evaluation. Naturally occurring organisms often have the capability of producing the desired chemical; in cases where it cannot genetic engineering is used. *Saccharomyces cerevisiae* and *Escherichia coli* are the favoured organisms for genetic engineering because their genomes have been fully sequenced and they are both well-studied [14]. The pathways from other organisms producing the desired metabolite or consuming the prospective substrate will be inserted into the selected organism. Genetic engineering combined with process engineering has the ability to revolutionise the ways in which chemicals are produced, moving

towards more sustainable practices. The biorefinery will likely produce many varied products and therefore the exact procedure outlined here may not be followed for all products; for instance the production of paper or vanillin will not involve fermentation.

2.4 Microbial Production of Fumaric Acid

The *Rhizopus* specie was first identified as a good producer of fumaric acid by Foster, J.W. and Waksman, S.A. in 1939 and was selected out of 41 organisms from 8 genera [48]. It was established that *Rhizopus nigricans* is able to convert 50.4 % of the loaded glucose to fumaric acid. Two important additional discoveries were that the addition of $CaCO_3$ and the absences of nitrogen enhanced the production of fumaric acid. After this, *Rhizopus oryzae* was found to be the superior producer of fumaric acid with even Pfizer, the USA based pharmaceutical company, using *Rhizopus oryzae* to produce fumaric acid in the 1940's [35].

2.4.1 *Rhizopus oryzae*

R. oryzae ATCC 20344 was first discoverd by Frits Went and Hendrik Coenraad Prinsen Geerligs in 1895. This filamentous fungus is commonly used to produce fermented foods in eastern Asia. There has been much confusion in literature when referring to *R. oryzae* due to the fact that many names have been designated to the same specie, including *R. nigiricans*, *R. arrhizus* and *R. delemar*[49]. The Rhizopus specie has now been correctly divided into two distinct organisms; the proposed names are *R. oryzae* for the lactic acid producing specie and *R. delemar* for the fumaric acid producing specie. Literature, however, has been slow to change and the fumaric acid specie is still commonly referred to as *R. oryzae*.

The production of fumaric acid with *R. oryzae* is a relatively well-studied field with multiple articles published on the topic. The results from the most prominent *R. oryzae* fermentation studies are displayed in Table 1. The production rate can be seen to vary between $0.19\,\mathrm{g\,L^{-1}\,h^{-1}}$ and $1.21\,\mathrm{g\,L^{-1}\,h^{-1}}$, and the yields of fumaric acid on the specific substrates varied between $0.21\,\mathrm{g\,g^{-1}}$ and $0.81\,\mathrm{g\,g^{-1}}$. The substrate used in the majority of the studies was glucose; this includes the studies where waste streams were used, because the predominant carbon source in these feedstocks is likely glucose. Although not an exhaustive list of all studies, it can clearly be seen that fewer studies have been conducted with xylose. It has been found that the production rate and yield of fumaric acid is generally lower on xylose compared to glucose.

Table 1: A literature compilation of the most prominent fumaric acid production studies with *R. oryzae*

Substrate	Reactor	Titre ($g\,L^{-1}$)	Productivity ($g\,L^{-1}\,h^{-1}$)	Yield ($g\,g^{-1}$)	Reference
Glucose	Stirred tank	103	-	0.65	[50]
Glucose	Stirred tank	56.2	0.7	0.54	[51]
Glucose	Stirred tank	41.1	0.37	0.48	[52]
Glucose	Stirred tank	32.1	0.32	0.45	[25]
Glucose	Stirred tank	30.2	0.19	0.27	[53]
Glucose	Immobilised	32.03	1.33	0.36	[54]
Glucose	Immobilised	40.13	0.32	0.75	[32]
Glucose	Immobilised	40.13	0.30	0.81	[33]
Glucose	Immobilised	30.3	0.39	0.21	[55]
Glucose-glycerol	Shake flask	22.81	0.34	0.35	[56]
Cornstarch	Shake flask	44.1	0.53	0.44	[24]
Brewery wastewater	Shake flask	31.3	-	-	[57]
Apple juice waste	Shake flask	25.2	0.35	-	[58]
Dairy manure	Stirred tank	31	0.32	0.31	[59]
Brewery wastewater	Immobilised	43.67	1.21	-	[60]
Xylose	Shake flask	28.4	-	0.43	[61]
Xylose	Shake flask	45.3	-	0.60	[62]
Glucose-xylose	Shake flask	34.2	0.24	0.43	[63]
Glucose-xylose	Shake flask	46.7	-	0.58	[64]
Glucose-xylose	Shake flask	27.8	0.33	0.35	[65]

2.4.2 Metabolic engineered organisms

The production of fumaric acid via a metabolic route has not yet become economically viable, nor is it able to compete with synthetically produced fumaric acid [35, 19]. Metabolic engineering has thus been employed to drive the biological production with the goal of improving fumaric acid yield, titre, and production rate. *R. oryzae* is a natural starting point. Inducing mutation of an organism and selecting for the improved strain is a route that has been taken to improve fumaric acid production. Nitrogen ion implantation was carried out on *R. oryzae* and the mutant strains were then screened for fumaric acid production [24, 65]. Production rates were found to have improved, but the yields achieved were substantially lower than that of the pure culture. Ultra-violet radiation

and femtosecond laser irradiation were two other procedures used to induce mutagenesis but were unable to produce strains that improved fumaric acid production [19].

Genetic engineering *R. oryzae* has yielded improvements. Fumaric acid in *R. oryzae* is produced via a reductive portion of the tricarboxylic acid cycle present in the cytosol. This takes pyruvate and CO_2 to oxaloacetate by pyruvate carboxylase, then forms malate with malate dehydrogenase, and finally produces fumaric acid with fumarase [66]. To improve the production of fumaric acid, it was hypothesised that increasing the production of oxaloacetate, the amount of carbon directed through the reductive TCA cycle would increase. Phosphoenolpyruvate carboxylase (PEPC), an enzyme exogenous to *R. oryzae*, and pyruvate carboxylase (PYC), an endogenous enzyme, were overexpressed. It was established that overexpressing the PYC had a negative effect by increasing the amount of malic acid produced. However, in the PEPC experiments it was found that fumaric acid production was improved and the yield increased by 26 % [67]. The strain developed was an uracil auxotroph and must therefore be supplied with a complex nitrogen source. The fumarase enzyme was also overexpressed in *R. oryzae*, resulting not in a higher production of fumaric acid as expected, but rather that fumarate was catalysed to malate, which in turn increased the production of malic acid [68]. Genetic engineering of *R. oryzae* still requires further research, although these initial findings shed light on how the organism functions.

E. coli and *S. cerevisiae* are both well studied organisms, genetically engineered strains of each are used in industry to produce a range of chemicals [16, 19]. In a recent study *E. coli* was modified to produce fumaric acid. Multiple metabolic pathways were tested, and it was established that using the TCA cycle to produce fumaric acid via succinate was the most successful approach [69]. A yield of $0.55\,\mathrm{g\,g^{-1}}$ fumaric acid from glucose was achieved, an improvement from a previous study in 2013 that achieved $0.389\,\mathrm{g\,g^{-1}}$ [70].

The use of *S. cerevisiae* is particularly favoured because of its high acid tolerance which would prove useful in the production of fumaric acid. The large cost of producing fumaric acid with *R. oryzae* is due to the need for a constant neutralising agent addition to maintain the pH [71]. Genetic engineering of *S. cerevisiae* to produce fumaric acid has, however, proved unsuccessful. The reductive TCA cycle was inserted and PYC was overexpressed, the final titre achieved was only $3.18\,\mathrm{g\,L^{-1}}$[72]. In a following study production via the reductive and oxidative TCA cycle was investigated. Medium optimisation was also conducted with the addition of biotin and control of the carbon-nitrogen ratio. The highest titre achievable was $5.64\,\mathrm{g\,L^{-1}}$ [71]. The failures of genetic engineering to outcompete the natural strain *R. oryzae* suggest that the mechanism by which it produces fumaric acid is not yet fully understood.

2.5 *Rhizopus oryzae* Fermentation

R. oryzae is affected by multiple medium conditions, including pH, substrate concentration, metal ion concentration, morphology, nitrogen availability, temperature, O_2 supply, CO_2 gas composition, and the neutralising agent used [53, 33, 26, 73, 30, 74].

2.5.1 Metabolism

The metabolism of glucose begins with glycolysis, a series of enzymatic reactions that convert glucose to two pyruvate molecules. In the process energy-related molecules such as adenosine triphosphate (ATP) and nicotinamide adenine dinucleotide (NADH) are also produced [29]. The metabolism of xylose is largely different to that of glucose: xylose has to be catabolised to xylitol, then D-xylulose and next D-xylulose-5-P, which enters the Pentose phosphate pathway from which D-glucose-6-P is produced — the start of glycolysis [75, 47]. This is a longer pathway compared to the catabolism of glucose that undergoes a single enzymatic step to D-glucose-6-P.

Once pyruvate has been formed, it is directed primarily down one of three pathways: the reductive TCA cycle producing fumaric acid, the TCA cycle, and ethanol production. Although the fumarase enzyme responsible for producing fumaric acid is present in the TCA cycle, it was discovered that there is in fact an isoenzyme of fumarase present in the cytosol used to produce the high quantities of fumaric acid [76]. The exact mechanism by which fumaric acid accumulation occurs is not yet fully understood, as previously mentioned [68]. It has, nevertheless, been discovered that there is a close relation between the urea cycle and fumarate production [29]. The urea cycle proteins were overexpressed in high fumarate producing fermentations, which are always associated with nitrogen-starvation conditions. It is hypothesised that nitrogen starvation expresses the urea cycle in *R. oryzae* which catabolises amino acids to produce de novo proteins, and has the by-production of fumarate through argininosuccinate lyase. This mechanism has not been further proven.

The TCA cycle's function is the production of energy. Pyruvate is converted to acetyl-CoA which then enters the cycle. Pyruvate is fully catabolised to CO_2 with the by-production of energy molecules, NADH, flavin adenine dinucleotide (FADH), and guanosine triphosphate (GTP). NADH and FADH are redox-carrying molecules that are used in oxidative phosphorylation to produce ATP in the presence of O_2. GTP is primarily used in the synthesis of proteins [14].

The production of ethanol is primarily understood as a means to produce ATP. Anaerobi-

cally, *R. oryzae* uses the production of ethanol to generate ATP when it is unable to use oxidative phosphorylation. Pyruvate cannot be directed to the TCA cycle since the redox molecules cannot be oxidised; pyruvate is therefore directed to ethanol. This is, however, an inefficient route as only 2 mol of ATP can be made per glucose mole compared with a possible 38 mol when the TCA cycle and oxidation phosphorylation are used [77].

Figure 2 shows the central carbon metabolism of glucose and xylose for the production of biomass, fumaric acid, ethanol and CO_2. The metabolic pathways were determined by correlating a number of enzymatic studies of *R. oryzae* [29, 47, 66, 75, 78, 79]. The anabolism has been simplified into a single enzymatic step from the respective carbon source [14].

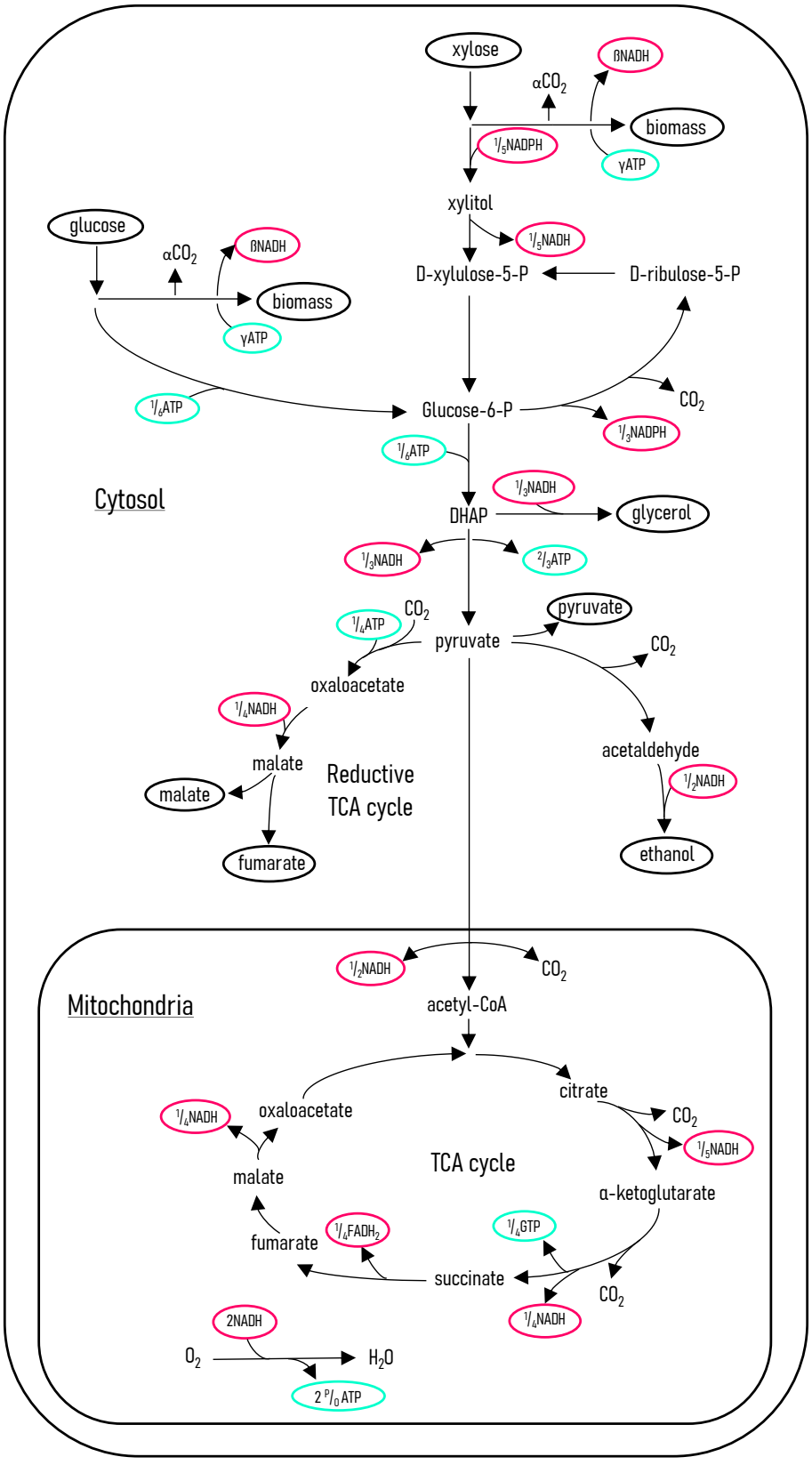

Figure 2: *R. oryzae* metabolic flux model. The metabolic pathways were determined by correlating a number of enzymatic studies of *R. oryzae* [29, 47, 66, 75, 78, 79]. The flux model is written on the basis of carbon moles; resulting in the illustrated fractional amounts of the energy-related compounds. The compounds circled in black are either substrates or metabolites.

2.5.2 Morphology

The filamentous fungal nature of *R. oryzae* is not as convenient for industrial fermentation since it does not form a homogenous fermentation broth. Many studies have focused on the optimisation of the morphology, largely focused on developing pellets [28, 30, 26]. This is when the mycelium forms small spherical clumps as shown in Figure 3.

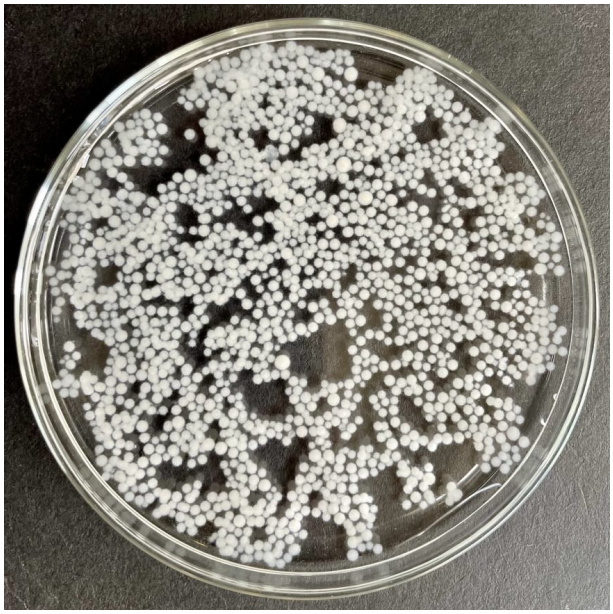

Figure 3: *R. oryzae* pellets formed in a shake flask experiment for a parallel study [5]

The motivation for forming pellets is multi-faceted. Allowing the mycelium to grow uninhibited results in the mycelium forming over any non-smooth surface which could be the reactor impeller, sparger or narrow port; this is not industrially acceptable as it will likely cause reactor failures [26]. The other important motivation is aeration, the mycelium tends to form large clumps that over time inhibit the mass transfer limitation of O_2 to the entire fungal mass, decreasing the efficiency of production. Anaerobic zones forming within mycelium clumps have been claimed to cause the ethanol production found in glucose fermentations [53]. Under fully anaerobic conditions *R. oryzae* does produce large amounts of ethanol instead of fumaric acid [80].

A drawback of using pellets is that repeat or continuous fermentations are difficult when the mycelium is suspended in the medium. The formation of pellets has only been achieved in shake flasks because of its reliance on high shear conditions. In studies where stirred tank reactors have been used, the pellets were prepared in shake flasks and transferred to the production reactor [30, 25] — an operation which is not industrially scalable. Immobilised fungal biomass is better suited to industrial production since the biomass is easily separated from the medium, which allows for continuous or repeat batch

fermentations. It can also be easily scaled by increasing the surface area on which the biomass is grown. By comparing the yields and production rates of fumaric acid achieved for immobilised reactor studies to that of shake flask studies in Table 1 it can be seen that the highest production parameters were achieved from immobilised studies.

2.5.3 The Crabtree Effect

The production of ethanol by *S. cerevisiae* under fully aerobic conditions is referred to as the Crabtree effect; named after Herbert Grace Crabtree who first discovered the phenomena in 1929 [81]. Much research has been conducted as to the mechanism by which it occurs, but it was not until Bradford and Hall [82] developed the explanation currently accepted. The Crabtree effect is caused by a limited respiration capacity. Glucose is converted to pyruvate which is then directed to the TCA cycle. Once the glucose uptake rate surpasses the capacity of the TCA cycle, ethanol production begins [83]. The reason for ethanol production can be seen to be twofold: first it provides a carbon sink for the carbon from glycolysis, and secondly it allows for higher ATP production rates. The Crabtree effect is well illustrated in glucose-limited continuous chemostat fermentations as the dilution rate, which essentially controls the growth rate, can be finely adjusted. The O_2 uptake rate increases with an increased dilution up to a point, after which the O_2 uptake rate remains stable, and ethanol production begins [82]. The stable O_2 rates above the specific dilution indicates a limitation of oxidative phosphorylation — and therefore respiration. Figure 4a illustrates normal glucose respiration in *S. cerevisiae* fermentations — once the glucose uptake rate surpasses a threshold the metabolism in Figure 4b is observed and the respiration capacity is reached. All additional glucose is henceforth metabolised to ethanol.

The production of baker's yeast is a large industry wherein the by-production of ethanol is an unwanted product. A method has been developed whereby the glucose medium concentration is closely controlled below the ethanol breakthrough threshold [84]. The threshold concentration has been found to be $150\,\mathrm{mg\,L^{-1}}$. This enables the yeast to grow without the associated low production rates and yields once ethanol production begins [82].

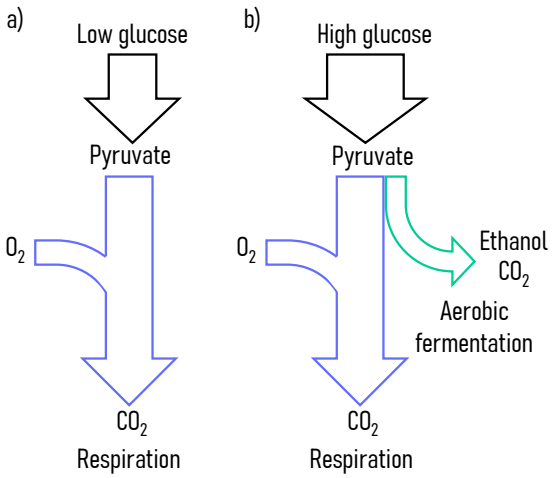

Figure 4: The metabolism of *S. cerevisiae* illustrating the Crabtree effect. (**a**) A low glucose uptake rate can be fully accommodated by respiration. (**b**) Above a glucose uptake threshold rate aerobic ethanol production is observed.

2.5.4 Neutralising Agents

The production of fumaric acid decreases the pH of the medium as a result of the protons released by the dissociation of the produced acid. It has been established that excessively low pH conditions (below pH 4) negatively affect the production of fumaric acid [53]. For this reason a neutralising agent must be titrated to maintain the pH. Many neutralising agents ($CaCO_3$, $Ca(OH)_2$, $NaHCO_3$, NaOH, Na_2CO_3, KOH) have been investigated for their effects on fumaric acid production [50, 38, 35]. $CaCO_3$ has often been named for producing the highest fumaric acid yields, but it must be noted that this largely occurs in studies where NaOH was not tested [50]. Another reason that $CaCO_3$ achieves higher fumaric acid production is due to the released CO_2 which can then be used by pyruvate carboxylase; increased CO_2 liquid concentrations have been shown to improve fumaric acid production [53]. $CaCO_3$ is very convenient for shake flask fermentations — because of its insolubility (2.1 % at 30 °C), all the neutralising agent can be added at once. When acid is produced the $CaCO_3$ dissolves maintaining the pH at 5.5 [35].

The drawbacks of $CaCO_3$ outweigh the advantages. Once fumaric acid forms, an insoluble salt — calcium fumarate — also forms which greatly increases the viscosity of the medium [35]. This leads to increased fermentation costs to move the medium and separate the medium downstream. Moreover, $CaCO_3$ can also not be easily separated from the fungal biomass, and so it can neither be used as animal feed, nor for the production of chitin. The insolubility of $CaCO_3$ is not convenient for industrial production as it has to be handled as a solid and does not form a concentrated solution. The ideal neutralising agent is therefore found to be NaOH; it is a strong base that can be made into concentrated

solutions to limit dilution when it is titrated [14], it produces a soluble fumarate salt ($228\,\mathrm{g\,L^{-1}}$), it allows the biomass to be reused, and it simplifies downstream processing because there are no solids present.

2.5.5 Medium pH

Dicarboxylic acids can be present as dissolved undissociated acid, solid undissociated acid or in a dissociated form, of which there is a first and second conjugated base. The equilibrium ratio between these forms depends on the temperature and pH. Although, the temperature effect is minor compared with pH. There are two equilibrium reactions (the abbreviation Fum will be used for fumarate in this section) that describe the dissociation of fumaric acid:

$$H_2Fum \leftrightarrow HFum^- + H^+ \tag{1}$$

$$HFum^- \leftrightarrow Fum^{2-} + H^+ \tag{2}$$

Using the pKa values of fumaric acid (3.09, 4.60 at 25 °C) the molar concentrations of the dissociated species can be calculated as functions of the pH (the effect of temperature was determined to be minor) with Equations 3 and 4 [36].

$$\frac{[HFum^-]}{[H_2Fum]} = 10^{(pH-pKa_1)} \tag{3}$$

$$\frac{[Fum^{-2}]}{[HFum^-]} = 10^{(pH-pKa_2)} \tag{4}$$

Fumaric acid has a low solubility ($0.047\,\mathrm{mol\,L^{-1}}$); once the undissociated acid forms and the concentration reaches the solubility limit, solid acid will precipitate. Taking this account while conserving the ionic charge and the total acid in the medium, Figure 5 can be drawn to describe the dissociation as a function of pH.

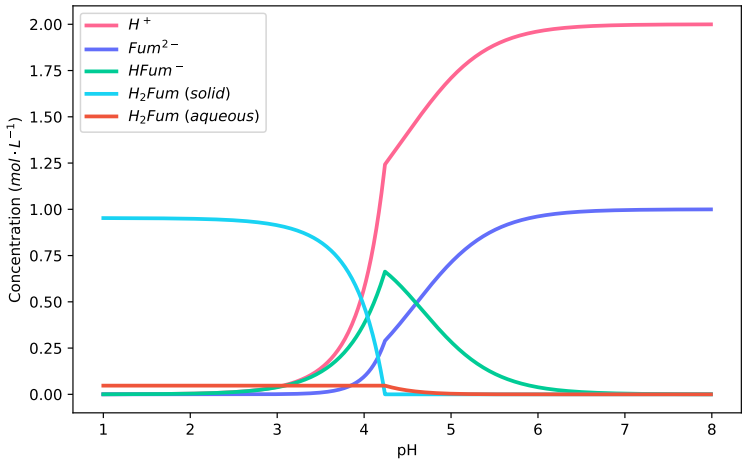

Figure 5: The dissociation of fumaric acid ($1\,\mathrm{mol\,L^{-1}}$) with respect to pH

At pH 6 and above all the acid is fully dissociated. This then transitions as the pH decreases — firstly to form the first conjugated base and undissociated fumaric acid. Decreasing the pH further causes the solubility limit to be reached, and thus precipitating fumaric acid. This provides an interesting downstream processing possibility where solid fumaric acid could be removed. The exact pH at which the solubility limit is reached is a function of the acid concentration; the higher the concentration, the higher the pH at which solid fumaric acid forms. A higher molar concentration causes the equilibrium ratios dictated to encounter the solubility limit at an early stage as the acid becomes less dissociated. The implications of this are best described by the proton (H^+) concentration in Figure 5, this concentration directly corresponds to the concentration of alkali that would be required to maintain the pH at a specific value. 342 % more alkali is required at pH 6 compared to the amount required at pH 4. The cost of acid-base addition has been cited multiple times as a large production cost [19, 53] which can mostly be overcome by operating at a lowed pH.

The pH of the medium also affects the ionic strength and osmotic stress on the cell. A high pH increases the osmotic stress — Figure 6 shows the ionic and osmotic strength as the pH changes. The osmotic pressure increases to a maximum at pH 6. A pH 4 results in an osmotic pressure 3 times less than that at pH 6. The osmotic stress on a cell affects the intracellular water abundance, the cell growth and the anabolism, which has been found to lead to by-product production [36, 85, 86].

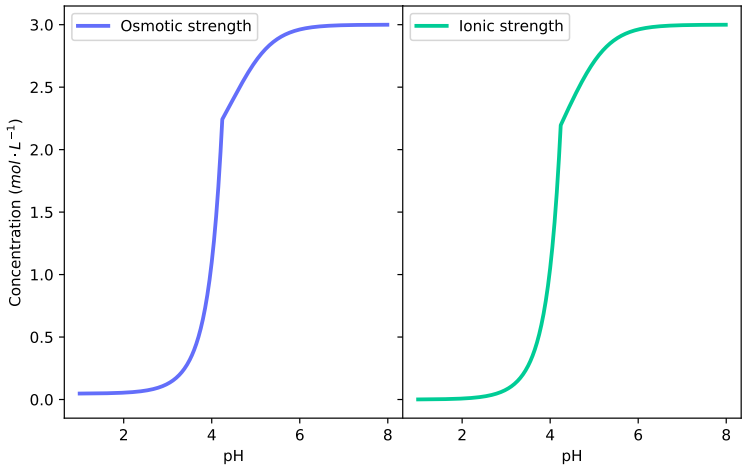

Figure 6: The osmotic and ionic stress related to a fumaric acid solution ($1\,\mathrm{mol\,L^{-1}}$) with respect to pH

2.5.6 Carboxylic Acid Transport

The transportation of carboxylic acids into the medium requires specific transporters; since acids are charged molecules they do not passively diffuse across the cell membrane as other metabolites may. The proton gradient between the intracellular pH, widely assumed to be 7, and the extracellular pH needs to be overcome to excrete fumaric acid into the medium and resulting in an ATP cost [36]. The enzyme ATP-ase is used to export protons into the medium from the cell. For eukaryotes this is a cost of one ATP per proton. Figure 7 shows the mechanisms by which fumarate can be exported into the medium (the mechanism differs based on the porter used). The porter selected is dependent on the acid equilibrium ratio between the intracellular and extracellular fumarate concentration that needs to be maintained and the proton gradient across the cell membrane (proton motive force).

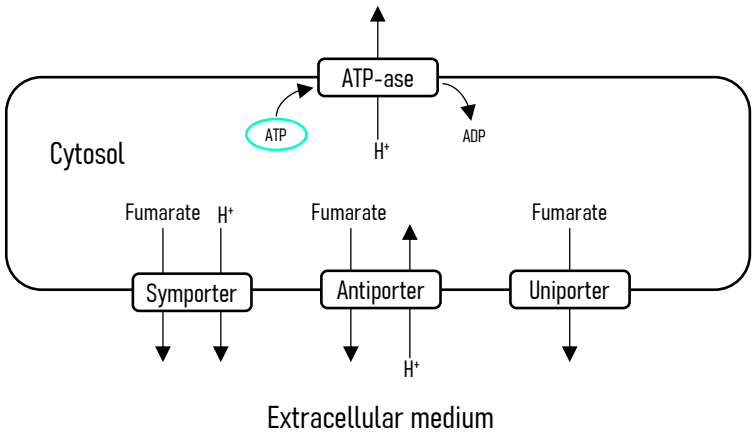

Figure 7: The dissociation of fumaric acid ($1\,\mathrm{mol\,L^{-1}}$) with respect to pH

The ATP cost of each transporter varies as a result of the number of protons, n, that need to be exported for each molecule of acid to balance the charge. Equations 5 and 6 are used to relate the medium pH to the ratio between the intracellular and extracellular acid concentrations for a specific transporter. There are three transporters that are ordinarily present: uniport (n = 0), symport (n = 1), and antiport (n = -1). The proton motive force, pmf, and the intracellular acid concentration, A_i, values were suggested to be 0.15 V and 1×10^{-3} mol L^{-1} respectively [36]. Varying these parameters has not been found to greatly affect the energy costs predicted. Figure 8 shows the achievable equilibrium ratio for each porter as a function of the pH. The transporter used at a specific pH is selected by the proximity of its achievable concentration ratio to the required minimum concentration ratio dictated by the medium. The minimum concentration ratio refers to the ratio between the total amount of acid dissolved in the medium and the intracellular concentration that needs to be overcome by the transporter. As the pH decreases the minimum concentration ratio decreases once fumaric acid begins to precipitate. The cost of exporting monoprotic acids, such as pyruvic acid, into the medium can be calculated similarly [87].

$$log\left(\frac{A_o}{A_i}\right)^{eq} = 2(pH_o - pH_i) + \frac{(n-2)(-pmf)F}{ln(10)RT}, \tag{5}$$

$$\left(\frac{A_o}{A_i}\right)^{eq} = \left(\frac{10^{pKa_1+pKa_2-2pH_o} + 10^{pKa_2-pH_o} + 1}{10^{pKa_1+pKa_2-2pH_i} + 10^{pKa_2-pH_i} + 1}\right)\left(\frac{A_o^{2-}}{A_i^{2-}}\right)^{eq}. \tag{6}$$

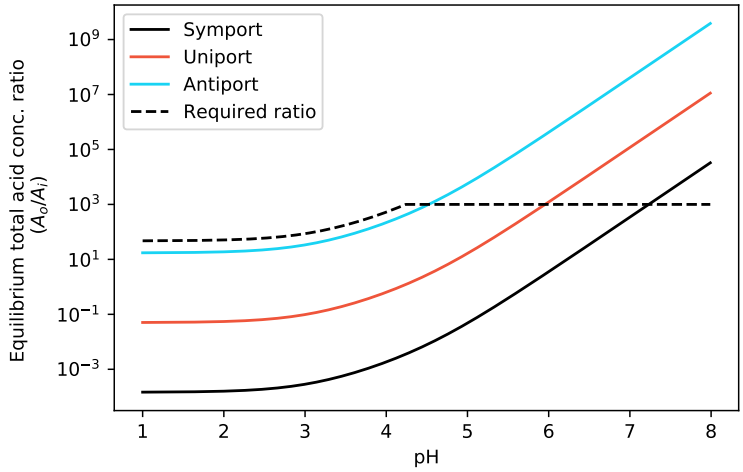

Figure 8: The dissociation of fumaric acid (1 mol L^{-1}) with respect to pH

Taking the energy cost of exporting carboxylic acids into account when producing fumaric acid as well as the added loss of carbon to CO_2 from the production of energy, it is clear

that to optimise the production of fumaric acid the energy cost must be minimised. Using glucose as the substrate, it has been found that the theoretical maximum yield is $1.5\,\mathrm{mol\,mol^{-1}}$ of fumaric acid per glucose [36]. This translates to a mass-based yield of $0.97\,\mathrm{g\,g^{-1}}$.

2.5.7 The Role of Nitrogen

The production of fumaric acid is closely linked to the presence of nitrogen in the medium. In the first screening of organisms for fumaric acid production, the carbohydrate-nitrogen-ratio was found to be a critical condition in the production of fumaric acid [48]. The production of fumaric acid was later isolated to an isoenzyme of fumarase which is present in the cytosol [76]. It has been discovered that cytosolic fumarase is particularly sensitive to the urea concentration in the medium. Using isolated cytosolic fumarase, urea concentrations between $0.1\,\mathrm{g\,L^{-1}}$ and $2.0\,\mathrm{g\,L^{-1}}$ were tested [73]. The activity of fumarase was inhibited by the higher concentrations of urea, which in turn affected the yield and rate of fumaric acid production.

In a whole cell *R. oryzae* study it was found that long-term fumaric acid production was affected by nitrogen starvation [33]. A fermentation void of urea produced an initial high rate of fumaric acid, but it was also associated with a high decay rate of fumaric acid production. Testing various urea feed rates it was established that continuous addition of urea at $0.625\,\mathrm{mg\,L^{-1}\,h^{-1}}$ maintained a low urea concentration and improved the stability of fumaric acid production. A higher feed rate of $1.875\,\mathrm{mg\,L^{-1}\,h^{-1}}$ urea was discovered to enhance the fumaric acid production rate over time. This was attributed to an increased biomass concentration made possible by the increased nitrogen availability.

2.5.8 Lignocellulosic Hydrolysates as Feedstock

Research on the use of lignocellulosic hydrolysate for the production of fumaric acid is limited and only covers batch shake flask fermentations of xylose and glucose feedstocks [64, 88, 59, 63]. The reported fumaric acid yields from these studies range from $0.31\,\mathrm{g\,g^{-1}}$ to $0.58\,\mathrm{g\,g^{-1}}$ — considerably lower than pure glucose fermentations that reach $0.81\,\mathrm{g\,g^{-1}}$ [33]. It has been found that glucose is metabolised preferentially over xylose, commonly referred to carbon catabolite repression (CCR). This is a well known phenomena where the most energy-efficient substrate (often glucose) is used preferentially such that use of other substrates is inhibited [89]. Overcoming CCR is a major hurdle for the use of lignocellulosic hydrolysates as feedstocks. This is especially true when considering continuous

operation where accumulation of substrates cannot be allowed [90]. Genetic manipulation is often used to modify organisms and to improve co-utilisation of substrates.

It has also been found in the glucose-xylose fermentations that increasing the proportion of xylose decreases the amount of ethanol produced [64] — indicating the xylose produced less or no ethanol. The catabolism of xylose was found often to be incomplete whereas glucose was always fully consumed. This does suggest a greater preference and capability of catabolising glucose compared to xylose [88].

2.5.9 Additional Conditions that Affect *R. oryzae*

The mineral composition of the medium was established to have a great effect on the growth of biomass and production of fumaric acid. Four metal ions were tested in various concentrations to determine the optimal medium composition [26]. The composition of $0.6\,\mathrm{g\,L^{-1}}$ KH_2PO_4, $0.507\,\mathrm{g\,L^{-1}}$ $MgSO_4 \cdot 7\,H_2O$, $0.0176\,\mathrm{g\,L^{-1}}$ $ZnSO_4 \cdot 7\,H_2O$, and $0.0005\,\mathrm{g\,L^{-1}}$ $FeSO_4 \cdot 7\,H_2O$ was proven to provide all the crucial elements for both spore germination and fumaric acid production.

The addition of CO_2 to the gas composition sparged has been found to improve fumaric acid production. This is likely as a result of the CO_2 requirement of PYC, indicating that CO_2 produced from the TCA cycle may not fully satisfy the requirement [53]. A $10\,\%$ CO_2 gas composition was found to be optimal; increasing the CO_2 composition further reduced the O_2 availability and the overall fermentation. There is, however, still space for optimisation of the CO_2 composition since the cited study did not investigate compositions between $0\,\%$ and $10\,\%$ CO_2.

3 Methods

The shared experimental techniques and apparatus used in Chapters 4, 5 and 6 will be discussed in this chapter. Investigation-specific techniques will be discussed in the respective chapters.

3.1 Microorganism and Culture Conditions

Rhizopus oryzae (ATCC 20344, CECT 2774), was obtained from the Spanish collection of cultures (Colección Espanola de Cultivos Tipo, Valencia, Spain) and used for all fermentations in this study. The culture was grown on potato dextrose agar and incubated at 30 °C for 5 days. Stock culture vials were created by suspending spores in an aseptic solution of 50 % volume basis, glycerol, and water. These stock cultures were then frozen at −40 °C. Preceding any fermentation a stock culture vial was transferred to agar plates and grown as previously mentioned. The spores from these plates were suspended in sterile distilled water to achieve a spore concentration of $8 \times 10^6\,\mathrm{mL}^{-1}$. A total of 10 mL of the spore solution was injected aseptically, through a silicone septum, into each of the batch growth fermentations as the inoculum.

3.2 Growth Medium

All fermentations used the same medium for the initial biomass growth, after which the production mediums were varied depending on the experiment. The growth medium contained the following mineral salts (all values have units of $\mathrm{g\,L}^{-1}$): 0.6 KH_2PO_4, 0.507 $MgSO_4 \cdot 7\,H_2O$, 0.0176 $ZnSO_4 \cdot 7\,H_2O$, and 0.0005 $FeSO_4 \cdot 7\,H_2O$ [26]. The biomass was grown under batch conditions with $3.1\,\mathrm{g\,L}^{-1}$ glucose and $2.0\,\mathrm{g\,L}^{-1}$ urea [32]. All the solutions were sterilised at 121 °C for 60 min. All chemicals used were obtained from Merck (Modderfontein, South Africa). After the completion of the biomass growth phase with all glucose consumed, the reactor was drained and rinsed aseptically twice with the production medium to remove all nitrogen from the system. The immobilised biomass remained in the reactor.

3.3 Fermenter Design and Operation

3.3.1 Construction and Instrumentation

The reactor consisted of a glass tube and a stainless steel housing with a liquid volume of 1.08 L. A rough polypropylene tube was inserted into the centre of the reactor onto which *R. oryzae* could attach. A scalpel was used to score the outer part of the tube and thereby create the attachment surface. The tube had a length of 386.5 mm, with an internal and outer diameter of 32 mm and 40 mm respectively. Silicone tubing connected to the housing allowed for the recycling of the liquid phase, the gas phases, and the aseptic addition or removal of the liquid solutions. A Watson and Marlow 323U peristaltic pump (Johannesburg, South Africa) was used to recycle the liquid phase. 8 mm Marprene tubing was inserted into the pump and connected to the silicone tubing. The liquid was recycled past an Endress + Hauser CPS171 pH-probe (Gerlingen, Germany), which measured the temperature and pH of the medium, and an Endress + Hauser COS81D oxygen sensor, which measured the dissolved oxygen in the medium. Figure 9 shows a piping and instrumentation diagram of the reactor.

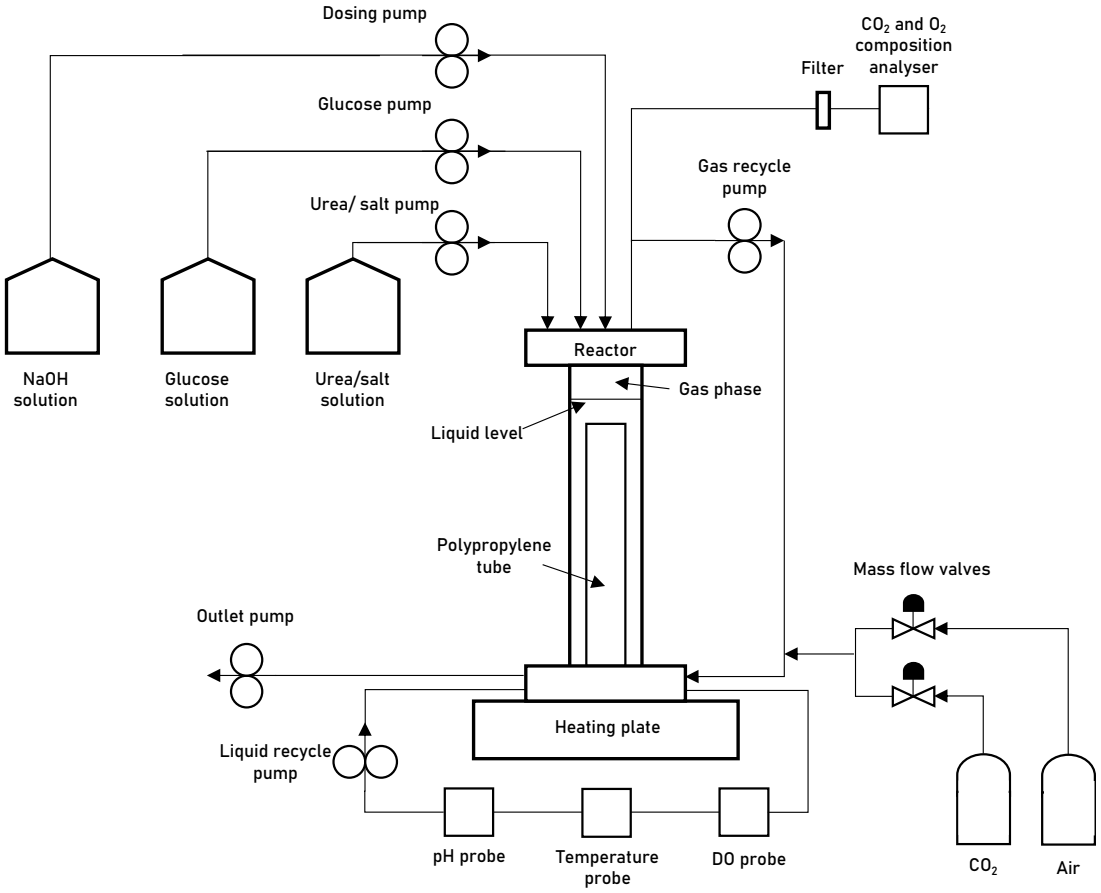

Figure 9: Process flow diagram of the reactor and instrumentation.

The reactor was continuously sparged with CO_2 and instrumental air — both lines were controlled using a SLA5850 mass flow controllers from Brooks (Hatfield, PA, USA). The gas mixture had a composition of 8 % CO_2 and 16 % O_2 with the complement N_2 sparged at a rate of 108 mL min^{-1} for all fermentations. The exhaust gas composition was analysed online with the Tandem Gas Analyser 0588 from Magellan Biotech (Borehamwood, UK). The liquid level of the reactor (1.08 L) was controlled by the gas exhaust line positioned inside at the top of the reactor. The liquid and gas mixture was separated in a knock-out bottle, gas was directed to the analyser and the liquid was then trapped in the knock-out bottle that was periodically drained. A 120U Watson and Marlow peristaltic pump with 4.8 mm marprene tubing was used to recycle the gas phase. 0.2 µm PTFE membrane filters (Midisart 2000, Sartorius, Germany) were fitted in the gas lines to prevent contamination.

Glucose, urea/salt and NaOH feed lines were inserted into the top reactor cap, allowing the solutions to drip into the reactor medium. Each line had a 120U Watson and Marlow pump and the entire line was 0.5 mm maprene tubing. The reactor pH was controlled with the addition of a 10 M NaOH solution. The stainless steal reactor base was positioned on a heating plate which maintained the temperature at 35 °C. The reactor was sterilised at 121 °C for 60 min before all fermentations.

3.3.2 Control System and Data Acquisition

In order to control and monitor the various instruments a centralised control system was built. A National Instruments DAQ (Austin, TX, USA) fitted with an input module, two output modules and a relay module was used to send and receive signals between the instruments and a computer. The computer run a purpose built Labview program from which the operator could control each of the instruments as well as monitor each of the displayed data fields. Figure 10 shows the graphical user interface of the control system. This program also recorded the data at a frequency of 1 s to a text file that could later be retrieved and analysed. Most notably the recorded parameters included: temperature, pH, dissolved oxygen (DO), NaOH dosing rate, glucose and urea feeds rates, gas feed rates, outlet gas composition, and the liquid sampling times.

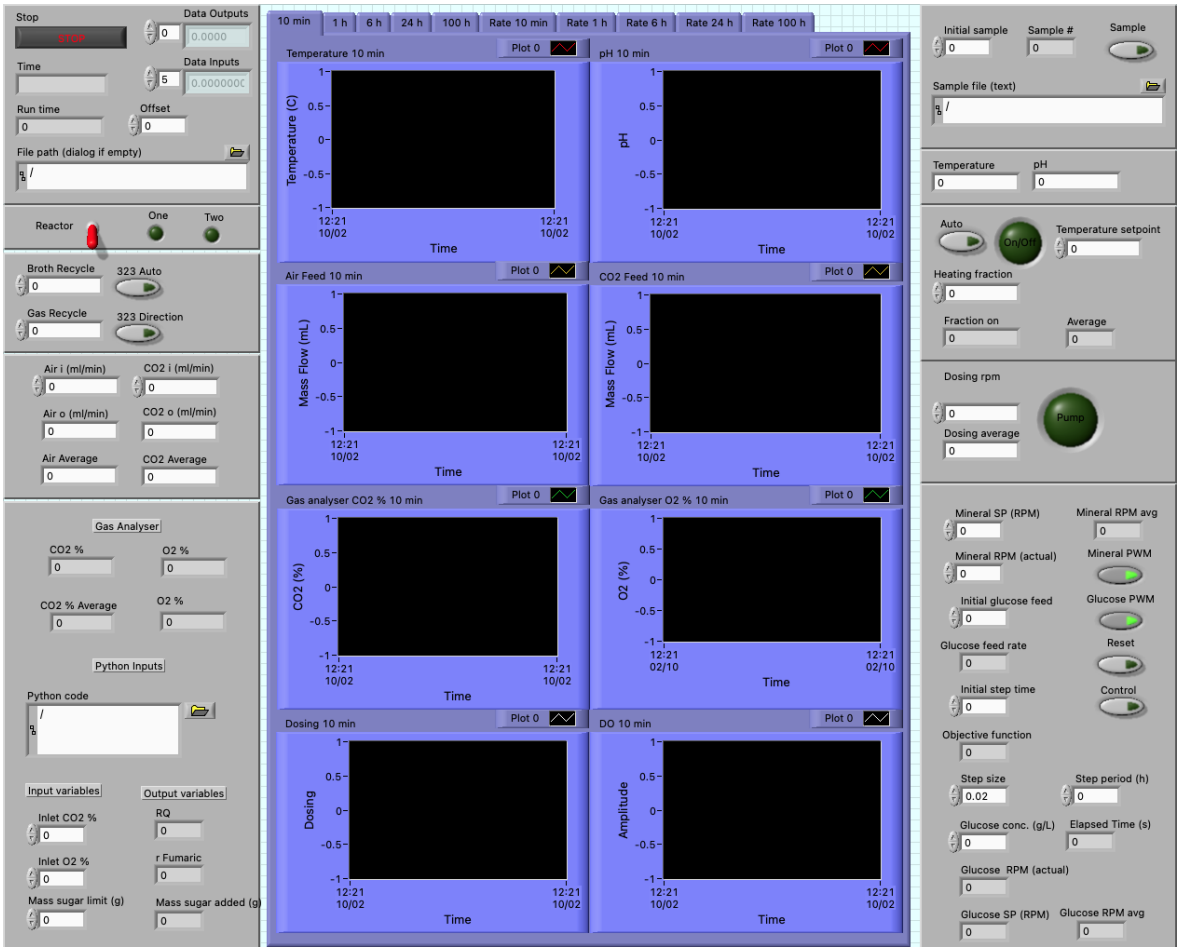

Figure 10: Custom built Labview control system.

Revolutions per minute (RPM) of each of the peristaltic pumps could be controlled via this program. Pumps were calibrated within the operating ranges and the RPM-to-liquid-flow-rate was established. Pumps were operated at multiple RPM values and the amount of liquid pumped over a specific time was recorded. Linear regression was then used to determine the pump equation that was coded into Labview.

3.3.3 pH Control

The pH probe was connected to the Endress + Hauser Liquiline CM442 (Gerlingen, Germany), this was then wired to the National Instruments DAQ and all measurement were recorded. The Liquiline has a functionality were a pH limit can be set and, if surpassed, trigger a relay. This was used to control the medium pH. The pH limit was set and the relay was wired to turn on the NaOH dosing pump. This would titrate the medium until the pH was above the limit, the relay would then open, turning off the pump. This system provided fine control of the pH.

3.3.4 Temperature Control

The temperature of the reactor medium was measured by a thermocouple within the pH probe. This measurement was relied on to the control system. The heating plate, on which the reactor base was positioned, was wired to a relay on the National Instruments DAQ. This allowed the control system to turn the heating plate on and off as needed. In order to achieve stable temperatures and, most importantly, a controlled heating profile on startup that did not overshoot the required temperature, proportional and integral (PI) control was deemed necessary. The reactor was filled with room temperature water (22 °C) and the heating plate was then turned on. The heating response was measured and a first-order model was fit to the data (as can be seen in Figure 11) [91].

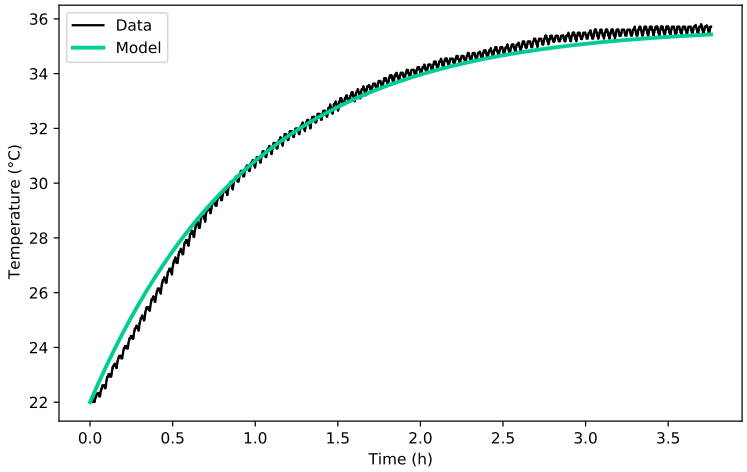

Figure 11: A model fitted to the temperature response of the reactor once the heating plate was switched on.

The model was then used to tune a PI control algorithm that controlled the heating plate based on the temperature received from the thermocouple. Figure 12 shows the control response that was achieved, the liquid is quickly brought to temperature with a slight overshoot and then the temperature is maintained at 35 °C. The control system was robust since changes to the laboratory ambient temperature had a negligible effect on the reactor temperature.

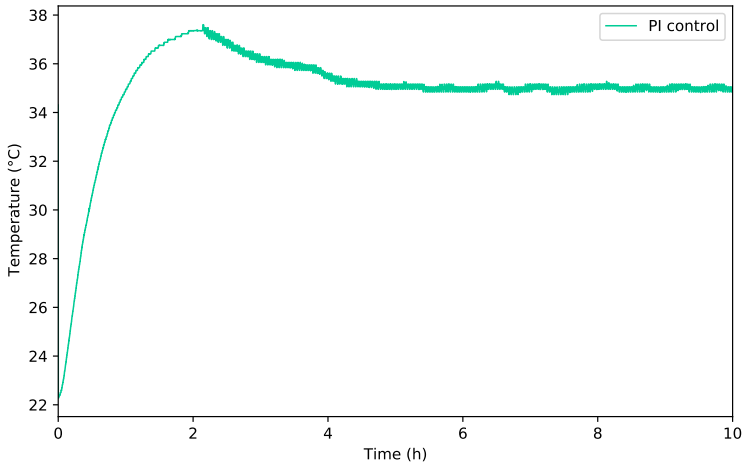

Figure 12: The PI temperature control response.

3.3.5 Feed Rate Control

In this study the feed rate of glucose to the system became an important parameter to control. As mentioned, the feed rates were controlled by the Labview program that was connected to a peristaltic pump. The pump has an RPM range of 0–200 RPM with 0.1 increments. To minimise dilution, concentrated substrate solutions were used which required low pump feed rates. This meant that even the 0.1 increments were too large to control the feed rate finely enough. To overcome this a pulse width modulation algorithm was implemented on Labview, which allowed for any RPM value to be achieved as the algorithm could turn the pump off and on to achieve the desired averaged RPM. Figure 13 shows how the algorithm turned the pump on and off to achieve the selected RPM.

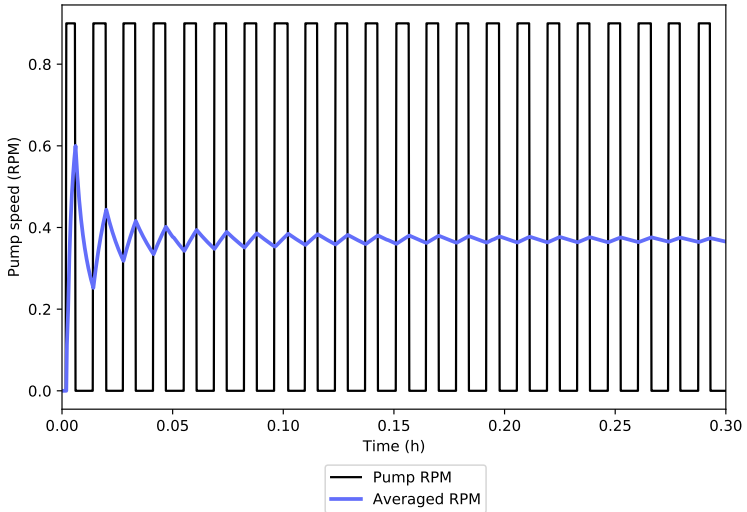

Figure 13: Pulse width modulation algorithm achieving the desired averaged pump RPM

Additionally, the algorithm would initially determine if the RPM required for the substrate feed rate was a discrete pump RPM or not. If not, it would determine the optimal RPM necessary to minimise the error between the desired and the achieved feed rate.

3.4 Analytical Techniques

3.4.1 High-Performance Liquid Chromatography

Samples were taken from the fermentations at varied increments to achieve a satisfactory resolution for the changing concentration profiles. Sampling intervals were determined from previous fermentations [32, 33], and was iteratively corrected if the concentration profiles changed faster than expected. A sampling frequency was considered satisfactory if it produced a smooth concentration profile. The samples were analysed using High-Performance Liquid Chromatography (HPLC). The Agilent 1260 Infinity HPLC (Agilent Technologies, Santa Clara, CA, USA) system was used to analyse for glucose and ethanol. It was equipped with a refractive index detector operated at 55 °C and a 300 × 7.8 mm Aminex HPX-87C column (Bio-Rad Laboratories, Hercules, CA, USA) operated at 60 °C. The mobile phase was a 0.005 M solution of H_2SO_4 with a flow rate of 0.6 mL min^{-1}. For the analysis of glycerol and the organic acids (namely fumaric acid, malic acid, succinic acid, and pyruvic acid), the mobile phase was altered to 0.02 M, with all other specifications remaining constant.

3.4.2 Dry Cell Weight

The dry cell mass was measured at the end of all experimental runs. Biomass measurements were not possible between the growth and production phases. The same biomass growth procedure was used for all experimental runs. Growth runs were terminated in order to determine the dry cell mass after growth and before production. The biomass was removed from the polypropylene tube and centrifuged at 2000 RPM for 10 min; the supernatant was then re-suspended in distilled water and the biomass was centrifuged for a second time. The entire process was repeated a total of three times. The biomass was finally dried at 70 °C for 48 h before being weighed. This procedure was followed for the first study in Chapter 4 and then the following method was used to minimise biomass handling in the later chapters. The biomass was washed with 1 L of distilled water, and then filtered through pre-weighed 110 mm Grade 541 Whatman filter paper. The filter paper and biomass were then dried at 70 °C for 48 h before being weighed to establish the final dry cell weight.

4 Utilising the Crabtree Effect to Minimise Ethanol By-product Formation

The contents of this chapter is based on an article published in *Biotechnology for Biofuels* [1].

4.1 Background

R.oryzae excretes fumaric acid under nitrogen limited conditions with the co-production of ethanol typically observed in this "non-growth" production phase. Ethanol is an unwanted by-product that reduces fumarate yield and should be minimised from a processing perspective. Numerous authors attribute ethanol formation to anaerobic zones within the fungal mycelium [26, 27, 28]. *R. oryzae* is a facultative anaerobe that can survive under anaerobic conditions [29] where the ethanol pathway is used for generating intracellular ATP. Most *R. oryzae* fermentations employ suspended biomass pellets and numerous efforts have been made to reduce the pellet diameter by manipulating pH, innoculum size, nitrogen source and glucose concentration [28, 30, 31]. The postulate that reduced pellet diameters will decrease anaerobic zones within the mycelium matrix and hence reduce ethanol formation has never been conclusively proven. Accordingly, an uncertainty exists with regard to the influence of oxygen availability on ethanol formation.

Organisms like the yeast *Saccharomyces cerevisiae* are known to produce ethanol under full aerobic conditions [82]. The phenomena, referred to as the Crabtree effect [81], is characterised by the formation of ethanol when ample glucose is available in the extracellular environment. Crabtree-positive organisms have the ability to consume glucose at a rate faster than the corresponding maximum respiratory rate whereby excess carbon exits in the form of ethanol. The overflow mechanism is independent of the oxygen supply rate to the cell. Commercial production of baker's yeast (*S. cerevisiae*) targets maximum biomass yield on glucose and attempts to avoid the formation of ethanol in an aerobic fermenter. This is achieved by controlling the glucose feed rate to the fermenter in order to manipulate the maximum cellular uptake rate of glucose. The fed-batch scheme is successful in avoiding ethanol formation as long as the uptake rate of glucose results in a respiratory carbon flux less than the maximum [84]. Glucose uptake rates are dependent on the extracellular glucose concentration and ethanol overflow can be avoided at concentrations below $150\,\mathrm{mg\,L^{-1}}$ [92].

In this chapter it is postulated that *R. oryzae* is a Crabtree-positive organism and that ethanol formation can be avoided by manipulating cellular glucose uptake rates. *R.*

oryzae fermentations typically consist of a growth and fumaric acid production stage [33] where the growth stage shares a similarity with the production of baker's yeast. In Figure 14a it is illustrated how glucose flux is balanced between energy consumption and energy production pathways. For growth conditions where excess nitrogen is supplied two fermentation strategies can be employed — one where the glucose uptake rate is regulated by the organism (batch fermentation) and the other where the glucose uptake rate is controlled by selective glucose addition (continuous fermentation). Figure 14 indicates selective addition of glucose via a control valve on the glucose flux. It is postulated that by controlling the glucose addition, ethanol production should be negated since the respiratory capacity is sufficient to process all catabolic carbon. For production conditions under limited nitrogen supply a similar scenario exists where glucose uptake can be regulated via continuous fermentation. Here the energy consuming pathway cannot be the formation of biomass since nitrogen absence prohibits protein formation. Fumarate excretion from the cell is known to be energy intensive where the amount of ATP required by the acid transporter depends on the extracellular pH [36]. Under nitrogen limitation, fumarate export thus replaces biomass formation as an energy-consuming pathway and a likely scenario exists where ethanol overflow can be suppressed under these conditions.

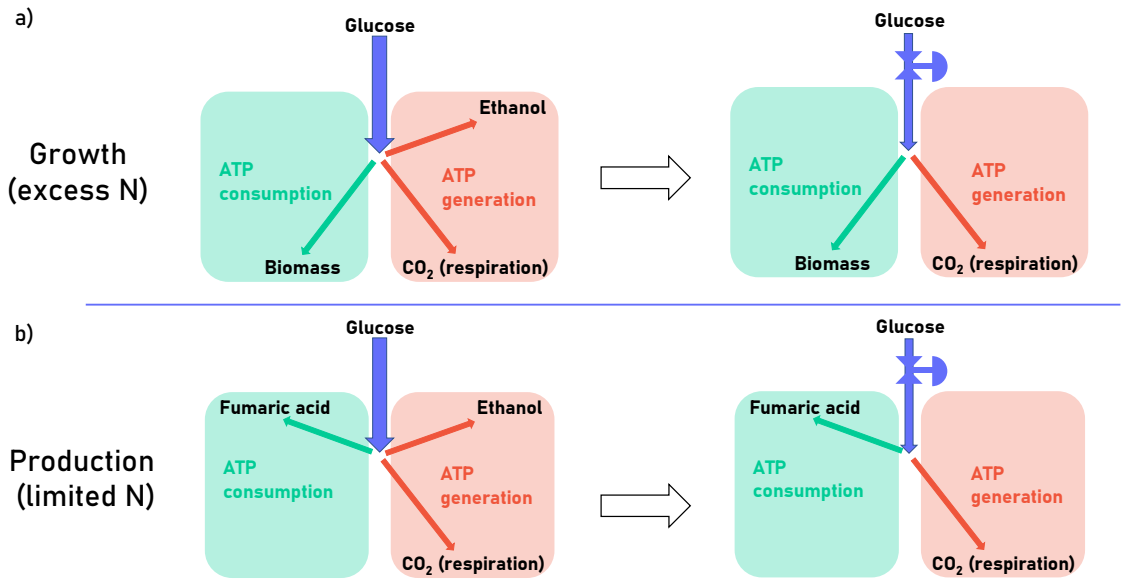

Figure 14: The postulated effect of glucose limitation on growth and fumarate production fermentations. Glucose uptake rate's are controlled via the glucose feed rate and are indicated with a reducing valve on the incoming glucose flux. It is postulated that glucose throttling will reduce ethanol formation in both growth and fumaric acid production fermentations.

In this chapter an immobilised form of *R. oryzae* is used to investigate the organism's Crabtree characteristics. The initial experimental work explores the effect of oxygen availability in the medium on ethanol formation, while subsequent experiments investigate

the effect of glucose limitation on the growth and fumaric acid production (nitrogen limited) response in order to test the postulated response depicted in Figure 14b.

4.2 Methods

4.2.1 Microorganism and Culture Conditions

R. oryzae was used in all fermentations, it was cultivated and inoculated as described in Section 3.1.

4.2.2 Growth Fermentations

Biomass was grown under batch conditions with $3.1\,\mathrm{g\,L^{-1}}$ glucose, $2.0\,\mathrm{g\,L^{-1}}$ urea and the mineral medium outlined in Section 3.2. The nitrogen source (urea) was added in excess, this allowed for the biomass concentration and thickness to be controlled by the initial glucose concentration. The medium was drained once the glucose was fully consumed, leaving the biomass intact on polypropylene tube. The reactor was then rinsed twice with the respective production medium to remove all nitrogen and then filled again with the production medium to begin the production fermentation.

The medium for the fed-batch growth of biomass contained the $2.0\,\mathrm{g\,L^{-1}}$ urea but no glucose at the beginning of the fermentation as this was fed continuously at a rate of $0.07\,\mathrm{g\,L^{-1}\,h^{-1}}$. In order to achieve a low dilution rate a high concentration solution of glucose was made ($342\,\mathrm{g\,L^{-1}}$). The growth fermentation was controlled at pH 5 using a 10 mol NaOH solution that constantly titrated the medium.

4.2.3 Production Fermentations

The batch production fermentations contained $50\,\mathrm{g\,L^{-1}}$ glucose, $0.1\,\mathrm{g\,L^{-1}}$ urea and the mineral solution. The continuous production fermentations began with only the mineral solution, urea was fed at a rate of $0.625\,\mathrm{mg\,L^{-1}\,h^{-1}}$ and glucose fed at a rate between $0.131\,\mathrm{g\,L^{-1}\,h^{-1}}$ to $0.329\,\mathrm{g\,L^{-1}\,h^{-1}}$. In order to achieve low dilution rates high concentration solutions of both glucose and urea were made with $342\,\mathrm{g\,L^{-1}}$ and $16\,\mathrm{g\,L^{-1}}$respectively. The dilution rate for the continuous production fermentations varied between $0.0018\,\mathrm{h^{-1}}$ to $0.0027\,\mathrm{h^{-1}}$, taking into account the glucose and urea additions, as well as the NaOH dosing. The urea solution incorporated the mineral solution to ensure that the mineral composition in the reactor remained constant over the duration of the experimental run.

The production fermentations were controlled at a pH 5. All the solutions were sterilised at 121 °C for 60 min.

4.2.4 Analytical Techniques

The medium samples were analysed to establish the glucose and metabolite concentration using an HPLC as described in Section 3.4.1. The dry cell weight of the biomass was determined using the first method describe in Section 3.4.2.

4.2.5 Model Description

In order to determine the growth rate of biomass during the growth fermentations a model was developed. Equation 7 is the overall chemical reaction of glucose, O_2 and urea being consumed to produced biomass and metabolites. The general formula for biomass was used [14]. The matrix below shows the mass balance used, taking into account all the metabolites produced to correlate the metabolite production rates to a growth in biomass. Solving the matrix for the **X** matrix yielded the production or consumption rates. The first four rows are carbon, hydrogen, oxygen and nitrogen elemental balances. S_1 is the growth rate specification that is fit to the data and then S_2 to S_8 are yield specifications using HPLC determined yields.

$$\begin{gathered} C_6H_{12}O_6 + Y_{so_2}O_2 + Y_{su}CH_4N_2O \rightarrow \\ Y_{sb}CH_{1.8}O_{0.5}N_{0.2} + Y_{sco_2}CO_2 + Y_{sw}H_2O + Y_{sfa}C_4H_4O_4 + Y_{ssa}C_4H_6O_4 \\ +Y_{sma}C_4H_6O_5 + Y_{se}C_2H_6O + Y_{sgl}C_3H_8O_3 + Y_{spa}C_3H_4O_3 \end{gathered} \tag{7}$$

$$\begin{bmatrix} & G & O_2 & U & B & CO_2 & W & FA & SA & Et & GL & MA & PA \\ C & 1 & 0 & 1 & 1 & 1 & 0 & 1 & 1 & 1 & 1 & 1 & 1 \\ H & 2 & 0 & 4 & 1.8 & 0 & 2 & 1 & 1.5 & 3 & {}^{8}/_{3} & 1.5 & {}^{4}/_{3} \\ O & 1 & 2 & 1 & 0.5 & 2 & 1 & 1 & 1 & 0.5 & 1 & {}^{5}/_{4} & 1 \\ N & 0 & 0 & 2 & 0.2 & 0 & 0 & 0 & 0 & 0 & 0 & 0 & 0 \\ S_1 & 0 & 0 & 0 & 1 & 0 & 0 & 0 & 0 & 0 & 0 & 0 & 0 \\ S_2 & Y_{sb} & 0 & 0 & 1 & 0 & 0 & 0 & 0 & 0 & 0 & 0 & 0 \\ S_3 & Y_{sfa} & 0 & 0 & 0 & 0 & 0 & 1 & 0 & 0 & 0 & 0 & 0 \\ S_4 & Y_{sma} & 0 & 0 & 0 & 0 & 0 & 0 & 0 & 0 & 0 & 1 & 0 \\ S_5 & Y_{ssa} & 0 & 0 & 0 & 0 & 0 & 0 & 1 & 0 & 0 & 0 & 0 \\ S_6 & Y_{spa} & 0 & 0 & 0 & 0 & 0 & 0 & 0 & 0 & 0 & 0 & 1 \\ S_7 & Y_{sgl} & 0 & 0 & 0 & 0 & 0 & 0 & 0 & 0 & 1 & 0 & 0 \\ S_8 & Y_{se} & 0 & 0 & 0 & 0 & 0 & 0 & 0 & 1 & 0 & 0 & 0 \end{bmatrix} \mathbf{X} = \begin{bmatrix} 0 \\ 0 \\ 0 \\ 0 \\ \mu \\ 0 \\ 0 \\ 0 \\ 0 \\ 0 \\ 0 \\ 0 \end{bmatrix}$$

The biomass growth rate was described using Equation 8 the Monod equation relating the growth rate to the glucose concentration [14]. The rate of biomass was then used together with the matrix to determine the consumption and production rate of the other species. Equation 9 was then integrated over the fermentation period to produce concentration profiles. In order to fit and establish the growth rate, a non-linear least-squares minimisation and curve-fitting Python package, LMFIT, was used to fit the model to the data. The algorithm minimised the error between the model curve and the HPLC concentration profiles to determine the best fit.

$$\mu = \mu_{max} \frac{C_G}{K_m + C_G} \tag{8}$$

$$\frac{dC_j}{dt} = r_j C_B \tag{9}$$

4.3 Results and Discussion

4.3.1 Growing Biomass in Excess Glucose

All fermentations consisted of a growth and a production phase. Growth was always performed with excess nitrogen in order to establish the biomass that will be used for

fumaric acid production. Production always occurs after growth in a limited nitrogen environment to trigger fumarate excretion. Figure 15 depicts the metabolite concentration profiles obtained under growth conditions for 2 repeat fermentations at pH 5. Complete consumption of all glucose (3.1 g) occurred within 25.6 ± 1.8h. Complete consumption was longer than the reported period if NaOH was used for initial pH correction prior to inoculation. The biomass yield on glucose was found to be $0.196 \pm 0.033 \mathrm{g\,g^{-1}}$.

The fermentation profile in Figure 15 commences with an extended lag phase after which glucose consumption rapidly occurs. Notable amounts of ethanol and fumaric acid formed during the fermentation with the final mass yield of ethanol higher than that of biomass. Malic acid, succinic acid and pyruvic acid where also produced but only in trace concentrations. A model described in Section 4.2.5 was fitted to estimate the growth rate of *R. oryzae*. Constant yield coefficients on glucose were used for ethanol and fumaric acid, there values were 0.211 and 0.058 respectively; this resulted in a reasonable fit as observed in Figure 15. The specific growth rate was estimated to be $0.255\,\mathrm{h^{-1}}$.

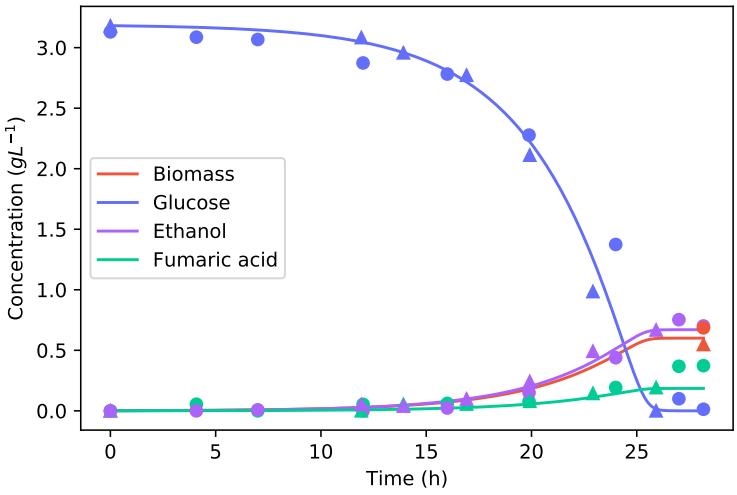

Figure 15: Repeat profiles of metabolite accumulation under growth conditions using 3.1 g/L of glucose and nitrogen excess. The circles and triangles identify the two repeat runs. Notable production of ethanol and fumaric acid was observed, with $0.62 \pm 0.097 \mathrm{g\,L^{-1}}$ of biomass obtained at the end of the run. Fitted model indicate biomass accumulation up to the final measured point. The model employed fixed yield coefficients of ethanol and fumaric acid on glucose (0.211 and 0.058, respectively). The estimated maximum specific growth rate was found to be $0.255\,\mathrm{h^{-1}}$ and the Monod constant was $0.176\,\mathrm{g\,L^{-1}}$.

The extensive ethanol produced, despite fully aerobic conditions, reminds one of *S. cerevisiae* aerobic growth. The results in Figure 15 therefore suggest that *R. oryzae* might be a Crabtree-positive organism where the respiratory capacity reaches a maximum under excess glucose supply. The ethanol formed during the fermentation can accordingly be interpreted as an overflow from glycolysis, where additional ATP is obtained via

ethanol fermentation. Interestingly a small amount of fumarate also forms during the fermentation despite excess nitrogen conditions. From an energetic point of view the ethanol and fumarate excretion will counter each other because 3 ATPs are required to excrete a mole of fumarate at pH 5 [36], while ethanol will produce only 1 mole of ATP per mole of ethanol. Given the final ethanol to fumarate mole ratio of 3.05, it appears that most ATP generated via ethanol production is used for fumarate excretion, indicating that there is little energy gained from the ethanol overflow when compared to the aerobic batch growth of *S. cerevisiae*.

4.3.2 Fumaric Acid Production with DO Variation

The results in Figure 15 suggest that *R. oryzae* might be a Crabtree-positive organism. Other authors [26, 27] suggest an alternative explanation for ethanol formation, where anaerobic zones within fungal pellets are the reason for ethanol production. In order to examine the alternative explanation, an experiment was performed where the DO in the fermenter was increased significantly from 18.4 % to 85 % under production conditions where significant fumarate excretion occurs. The experiment relies on the premise that the higher partial pressure of oxygen will eradicate anaerobic zones. Since the driving force for oxygen mass transfer will be increased by a factor of 4.6. The external liquid oxygen tension (DO) was established to be proportional to the partial pressure, indicating fast gas to liquid mass transfer.

The results of the two runs at different DO values can be seen in Figure 16. Note that growth similar to the results in Figure 15 preceded the reported production phase. The biomass produced during the growth phase has a thickness of 1 mm to 2 mm, similar to ideal pellet diameters as reported in literature [26, 30]. From Figure 16 it is clear that the production characteristics of *R. oryzae* is unaffected by the dissolved oxygen concentration, with ethanol, fumaric acid and glucose profiles exhibiting almost identical behaviour.

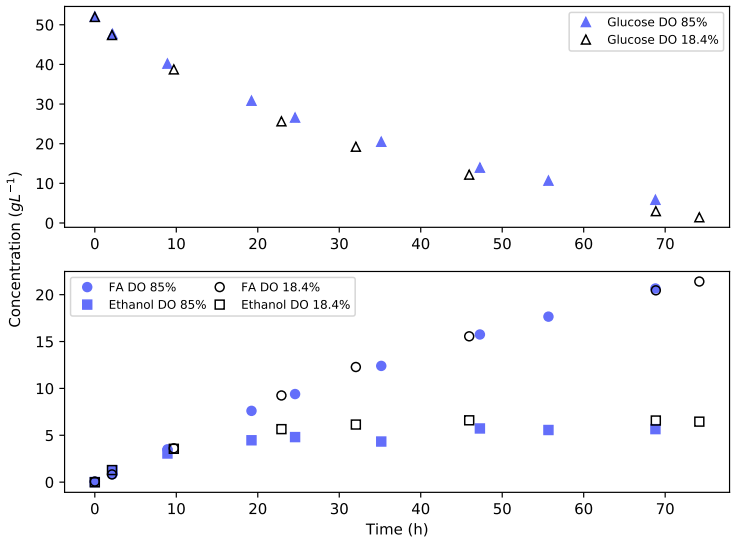

Figure 16: The effect of DO on fumaric acid production where 50 g L^{-1} of glucose was initially used. The DO was varied from 18.4 % to 85 %. A negligible difference was observed between the two runs.

The notion that biomass morphology relates to the extent of ethanol formation in *R. oryzae* is often used [26, 27]. However, the production of ethanol has not been negated as a result of varied morphology in any study. The results from the experiment in Figure 16 provide evidence that perceived anaerobic zones do not exist in the mycelium matrix when the depth of the matrix is 2 mm or less. It is clear that improved oxygenation within the matrix has zero effect on the ethanol response. This observation provides further evidence of the Crabtree-positive characteristics of *R. oryzae*, where ethanol production or overflow is unrelated to oxygen availability.

4.3.3 Manipulating Glucose Uptake Rates Under Growth Conditions

The results from Figure 15 & 16 provide preliminary evidence of the Crabtree-positive nature of *R. oryzae*. In order to comprehensively verify the observation, a link should be made between the glucose uptake rate and the ethanol excretion rate. Aerobic ethanol formation with *S. cerevisiae* is typically negated by reducing the glucose uptake rate [93]. This is achieved by maintaining low concentrations of glucose in the extracellular space. The Monod effect describes a low concentration regime where substrate uptake rates are proportional to substrate concentration. At higher substrate concentrations a zero-order regime is typically observed where substrate concentration has no influence on uptake rate. Accordingly, glucose uptake rates can be manipulated by operating the fermenter at low glucose concentrations. This can be achieved by a continuous fermenter where the glucose addition rate is operated at a similar value to that of the volumetric glucose

consumption rate [84]. In the following sections the continuous strategy will be employed on both growth and production of *R. oryzae* in order to see if the perceived Crabtree characteristics can be utilised to minimise ethanol production.

Figure 17 presents the glucose, ethanol and fumaric acid profiles for the growth run where glucose was added at a constant rate of $0.07\,\mathrm{g\,L^{-1}\,h^{-1}}$. Zero glucose was present in the growth medium prior to spore inoculation. It is clear that ethanol formation is completely avoided by the slow supply of glucose. Trace amounts of fumaric acid were present from the start of the fermentation with negligible additional amounts formed during the fermentation. The glucose concentration also remained close to zero, except right at the beginning where initial growth was unable to consume all the supplied glucose. The situation rectified at 30 hours once biomass accumulation increased in the fermenter. The slight overshoot in the initial glucose concentration ($0.46\,\mathrm{g\,L^{-1}}$) was not accompanied by ethanol overflow, hinting that the glucose uptake rate is always less than the corresponding maximum respiratory rate. The results are in close agreement with glucose controlled *S. cerevisiae* growth, suggesting that the Crabtree traits of *R .oryzae* can be utilised to negate ethanol production.

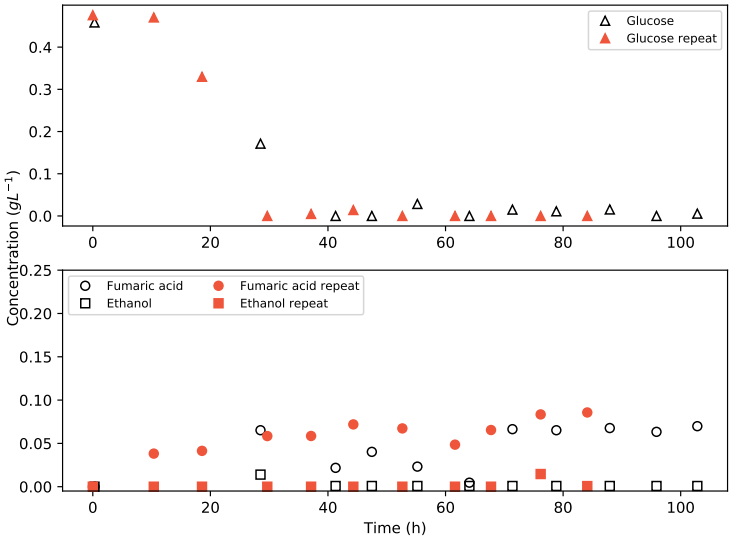

Figure 17: Glucose, ethanol and fumaric acid concentrations during continuous growth of *R. oryzae*. Glucose was added at a constant rate of $0.07\,\mathrm{g\,L^{-1}\,h^{-1}}$. All concentrations approximate zero, except glucose in the initial stages of the experiment. Ethanol overflow clearly avoided.

4.3.4 Manipulating Glucose Supply Under Production Conditions

The results presented thus far provides clear evidence of the Crabtree characteristics of *R. oryzae* under growth conditions. The main objective of the fermentation is to produce

fumaric acid and not biomass. Accordingly, the Crabtree response should be tested under production conditions where the nitrogen supply is limited. For this phase of the fermentation the energy consumption within the cell will be predominantly used for exporting fumarate where 3 moles of ATP are required to export one mole of fumarate [36]. The export cost under production conditions will effectively replace the energy expenditure used for biomass synthesis in the growth phase of the fermentation. The main question is whether the overflow mechanism under production conditions emulate that of the growth conditions and whether the main carbon metabolism reacts in a similar manner. To address this question, the same glucose feed rate employed under glucose limited growth conditions were used ($0.07\,\mathrm{g\,L^{-1}\,h^{-1}}$) from the start of the production phase. Zero fumaric acid (or ethanol) production was observed for 80 hours, indicating that all glucose was respired to obtain energy for the cellular transition from growth metabolism to production metabolism. The transition period for production fermentations with excess glucose ($50\,\mathrm{g\,L^{-1}}$) typically takes 20 hours after which fumaric acid production commences [33]. Accordingly, it was decided to increase the initial glucose addition rate to $0.131\,\mathrm{g\,L^{-1}\,h^{-1}}$ to see whether the transition period could be reduced. In this experiment fumaric acid production commenced after 20 hours and consequently this glucose addition rate was employed as the minimum value in further experiments.

Two extended production fermentations were performed for approximately 200 hours each. Both fermentations employed a growth strategy similar to the results presented in Figure 15. The only difference between the two runs is the glucose addition strategies as can be seen in Figure 18. Both runs initiated with the minimum glucose feed rate of $0.131\,\mathrm{g\,L^{-1}\,h^{-1}}$ up to 66 hours when the feed rate was increased by 50 % ($0.197\,\mathrm{g\,L^{-1}\,h^{-1}}$).

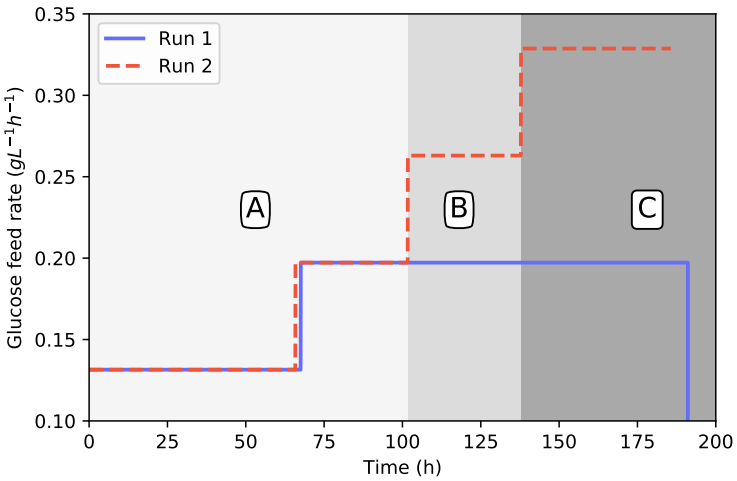

Figure 18: Glucose dosing rates for run 1 and 2. The dosing rate of run 1 was increased by 50 % once. Towards the end of the fermentation, dosing was stopped and the glucose concentration was depleted. The dosing rate of run 2 was increased three times by 50 % of the original rate.

Run 1 remained at this value for the remainder of the fermentation while run 2 had two subsequent increases (see Figure 18). The fumaric acid, ethanol and glucose response of the two runs can be seen in Figures 19, 20 and 21.

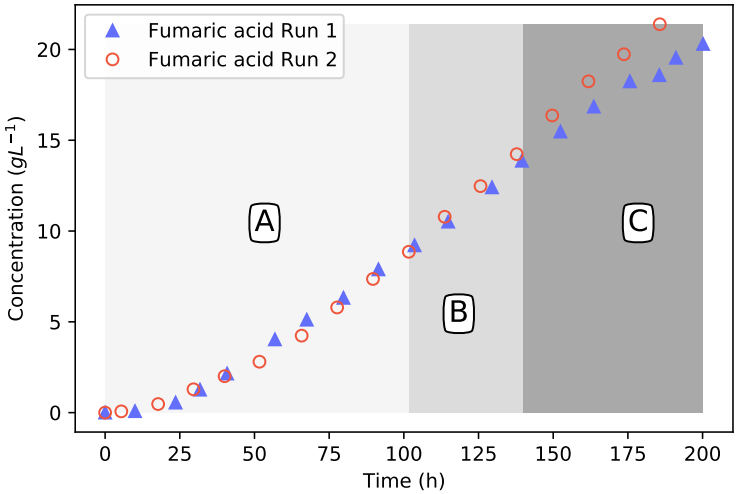

Figure 19: Fumaric acid production profiles for runs 1 and 2. Note the slight increase in fumarate excretion rates in regimes B and C.

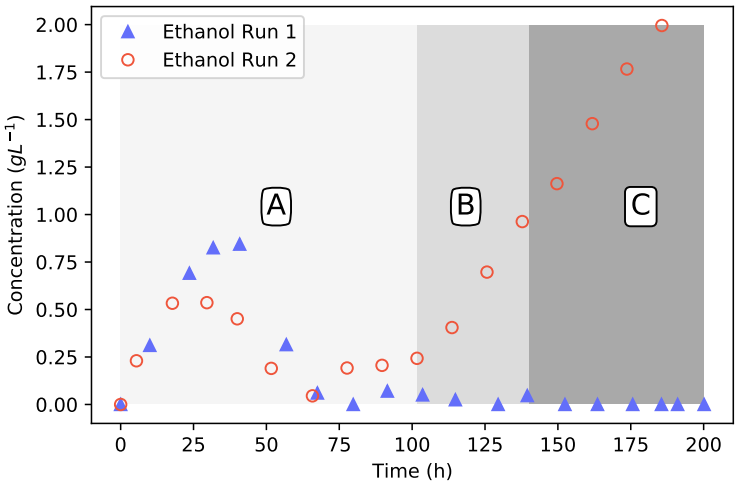

Figure 20: Ethanol profiles for runs 1 and 2. Beyond the first 25 hour transition phase, no ethanol overflow is observed in run 1. Run 2 exhibits clear ethanol overflow in regimes B and C where glucose addition rates were increased.

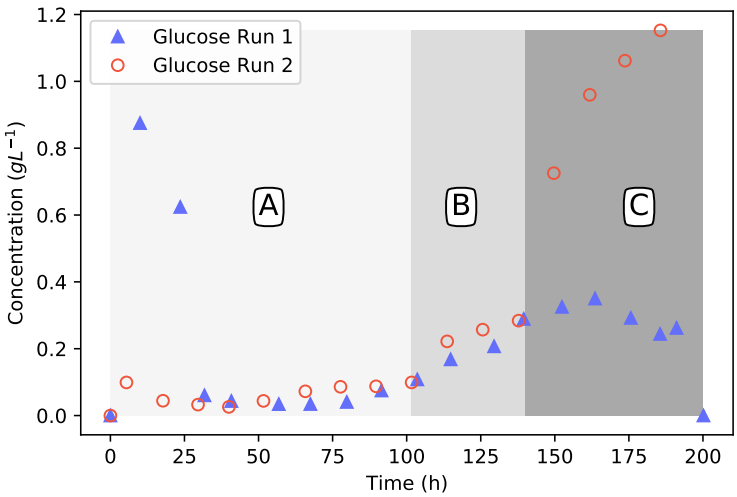

Figure 21: Glucose profiles for runs 1 and 2. Glucose breakthrough is observed for run 2 in regime C, where glucose addition rates exceeds the glucose consumption rate.

The experimental conditions of run 1 and 2 for the first 100 hours were identical and hence presents a repeat run. Figure 19-21 clearly show good repeatability with regards to the metabolic response. The ethanol response of run 1 indicates a regime after 75 hours where zero ethanol is produced. These results are in alignment with the results presented in Figure 17 (continuous growth) and indicates that the metabolic overflow to ethanol can be completely avoided at a glucose addition rate of $0.131\,\mathrm{g\,L^{-1}\,h^{-1}}$. It is clear from these results that ethanol excretion can be avoided by controlling the glucose addition rate. During the first 75 hours of production an ethanol peak was observed, indicating initial production followed by the metabolic consumption of ethanol. This implies that the transition period (first 25 hours) is associated with a slight oversupply of glucose and hence the initial ethanol production. The behaviour switches once fumaric acid production commences and ethanol consumption is observed between 25 and 75 hours. This indicates that once the production mode is established at around 25 hours, the supplied glucose rate on a biomass basis is less than the corresponding maximum respiratory rate and accordingly ethanol breakdown can be accommodated within the mitochondria. This is further illustrated by the first step-up in glucose addition at 75 hours, where zero ethanol formation is observed despite an increase in cellular glycolytic flux. Both results suggest that a feed rate of $0.131\,\mathrm{g\,L^{-1}\,h^{-1}}$ corresponds to a glycolytic flux below the ethanol overflow point.

When looking at the complete duration of run 1 a constant fumaric acid production rate of $0.158\,\mathrm{g\,L^{-1}\,h^{-1}}$ is observed after 75 hours (see Figure 19). Given the glucose supply rate $0.197\,\mathrm{g\,L^{-1}\,h^{-1}}$ it is evident that this rate also corresponds to a glycolytic flux below the ethanol overflow point. When considering the glucose concentration profile in Figure 21 a slight glucose increase is observed towards the end, with a maximum value of $0.28\,\mathrm{g\,L^{-1}}$

obtained at 175 hours. It is evident that this glucose concentration is below the overflow threshold concentration and is in close agreement to the value of $0.15\,\mathrm{g\,L^{-1}}$ reported for *S. cerevisiae* [92]. Run 1 clearly illustrates that the Crabtree effect of *R. oryzae* can be utilised to avoid ethanol by-product formation, a very useful result for further development of the *R. oryzae* fumaric acid process.

Run 2 was performed to establish the ethanol overflow and glucose breakthrough point. The results of the first 100 hours of run 2 were in good agreement with that of run 1, indicating repeatability in the method. The first deviation between run 1 and run 2 occurs at 100 hours when the glucose addition rate was increased to $0.263\,\mathrm{g\,L^{-1}\,h^{-1}}$ in run 2 while the glucose addition rate of run 1 remained at a feed rate of $0.197\,\mathrm{g\,L^{-1}\,h^{-1}}$ for the remainder of the run. Figures 19, 20 and 21 are mapped with 3 separate regimes A,B and C. Regime A represents similar operation between run 1 and run 2, regime B represents the time when run 2 glucose feed rate is 33% higher than in run 1 and regime C represents the time when run 2 glucose feed rate is 67% higher than in run 1.

The major difference between run 1 and 2 in regime B can be seen in the ethanol profiles of Figure 20. It is clear that ethanol overflow starts occurring when the glucose feed rate is increased to $0.263\,\mathrm{g\,L^{-1}\,h^{-1}}$. The glucose uptake rate in regime B exceeds that of the carbon flux that can be accommodated by respiration and fumarate excretion, resulting in the excess carbon overflowing as ethanol. From Figure 21 it can be observed that the glucose profiles of run 1 and run 2 remain similar, hinting that almost all of the glucose fed is consumed when the glucose concentration is below the threshold value of $0.28\,\mathrm{g\,L^{-1}}$. In Figure 19 it can be seen that the fumaric acid profile of run 2 starts exhibiting a steeper upward gradient once regime B commences. The difference, however, is clearly observed in regime C. This observation suggests that the ethanol overflow point (indicated by the glucose addition rate) is slightly higher than $0.197\,\mathrm{g\,L^{-1}\,h^{-1}}$ although less than $0.263\,\mathrm{g\,L^{-1}\,h^{-1}}$ where ethanol overflow clearly occurs. The increase in fumarate excretion in regime B can be calculated using the fumaric acid concentration measurements or the NaOH dosing rates in regime B where the trace amount of succinic and malic acid formed are subtracted from the neutralisation calculation. Given these two calculations the ethanol overflow point was calculated to occur at a glucose feed rate of $0.244\,\mathrm{g\,L^{-1}\,h^{-1}}$.

In regime C the glucose feed rate was increased to $0.329\,\mathrm{g\,L^{-1}\,h^{-1}}$. From Figure 20 it is clear that the ethanol overflow further increases, indicating that additional glucose uptake by *R. oryzae* is diverted to ethanol. Figure 21 shows a major deviation between the glucose profiles of run 1 and 2. It is evident that glucose breakthrough occurs in run 2, implying that the addition rate of glucose exceeds the uptake rate of *R. oryzae*. The maximum glucose uptake rate accordingly lies somewhere between $0.263\,\mathrm{g\,L^{-1}\,h^{-1}}$ to $0.329\,\mathrm{g\,L^{-1}\,h^{-1}}$ and additional experimental work is required to quantify the maximum

uptake rate more accurately.

When defining and quantifying the maximum glucose uptake rate (breakthrough rate) as well as the glucose uptake rate where ethanol excretion commences (overflow rate), it is preferable to use a biomass basis as opposed to the volumetric basis used in the discussion above. Quantification of biomass can only be performed at the end of the production run where $2.49\,\mathrm{g\,L^{-1}}$ was obtained for run 1 and $2.51\,\mathrm{g\,L^{-1}}$ obtained for run 2. These amounts differ significantly from the biomass amounts obtained using the growth procedure in Figure 15 where an average of $0.617\,\mathrm{g\,L^{-1}}$ of biomass was obtained. It should be noted that this growth procedure is the exact same as that run 1 and 2 utilised. The major increase in biomass during the production phase is unexpected given that the total urea fed over the production period was only $0.116\,\mathrm{g\,L^{-1}}$. Based on the general biomass formula $CH_{1.8}O_{0.5}N_{0.2}$ [14], additional protein synthesis as a result of urea will only contribute 4 % of additional biomass and cannot explain the five-fold increase in biomass. It is accordingly suspected that carbohydrate accumulation in the biomass is the major reason for the mass increase. Given this it was decided to quantify the biomass-based overflow and breakthrough rates using the biomass amount obtained after growth, where the protein contents of the cell are much higher than compared to the spent production biomass. Accordingly, the ethanol breakthrough rate is calculated to be $0.395\,\mathrm{g\,g^{-1}\,h^{-1}}$ while the glucose break through rate lies between $0.426\,\mathrm{g\,g^{-1}\,h^{-1}}$ and $0.533\,\mathrm{g\,g^{-1}\,h^{-1}}$.

Towards the end of run 1 a yield of $0.802\,\mathrm{g\,g^{-1}}$ fumaric acid on glucose was obtained, this was over 50 hour. The yield over the entire fermentation was $0.713\,\mathrm{g\,g^{-1}}$ since fumaric acid was not produced during the first hours of the fermentation. The yield for run 2 during the highest glucose feed rate was found to be $0.596\,\mathrm{g\,g^{-1}}$. This translates to a $0.206\,\mathrm{g\,g^{-1}}$ improvement in the yield for run 1 as a result of controlling the glucose addition below the ethanol breakthrough rate. This illustrates the effectiveness of the continuous reactor operation and the extent of carbon losses to ethanol that occur under batch conditions. These yields were calculated by accounting for all fumaric acid produced over the period and the amount of glucose added to the reactor.

4.4 Conclusion

The results presented thus far address the production of ethanol during *R. oryzae* fermentations. The production of fumaric acid has always been associated with the unwanted by-production of ethanol. It has now been conclusively shown that anaerobic zones within the mycelium matrix are not the cause of ethanol production. Two production fermentations were conducted at two DO concentrations, varied by a factor of 4.6. It was shown

that there was no effect by the DO on the production of ethanol, indicating that ethanol production is caused by a different mechanism.

The growth of *S. cerevisiae* for the production of baker's yeast has been optimised by controlling the glucose addition to the fermentation and thus negating ethanol production. It was hypothesised that *R. oryzae* was also a Crabtree positive organism, producing ethanol under fully aerobic conditions as a result of a limited respiratory capacity. Growth fermentations were conducted with a continuous glucose addition of $0.07\,\mathrm{g\,L^{-1}\,h^{-1}}$, it was established that no ethanol was produced. The results indicate that *R. oryzae* is a Crabtree positive organism, because the controlled glucose feed rate that in turn controls the glucose uptake rate negated ethanol production.

It was then hypothesised that this Crabtree characteristic could be leveraged to improve the yield and production rate of fumaric acid. Production fermentations were conducted with continuous glucose feed rates, it was discovered that the by-production of ethanol can be avoided during fumaric acid production. A regime was found were all the energy costs of the organism can be accommodated without the production of ethanol, using respiration as the predominant ATP source. A glucose feed rate of $0.197\,\mathrm{g\,L^{-1}\,h^{-1}}$ produced a sustained fumaric acid production rate of $0.158\,\mathrm{g\,L^{-1}\,h^{-1}}$ void of ethanol and a $0.802\,\mathrm{g\,g^{-1}}$ yield of fumaric acid on glucose consumed. By systematically increasing the glucose feed rate an ethanol breakthrough point was identified. This occurred once the glucose feed rate was increased to $0.263\,\mathrm{g\,L^{-1}\,h^{-1}}$. This demonstrated that the ethanol is produced as an overflow mechanism and conclusively proving that *R. oryzae* is a Crabtree-positive organism. The utilisation of this characteristic will be further developed for fumaric acid production in the following chapter.

5 Controlled Nitrogen Addition and Optimal pH for Continuous Fermentation

The contents of this chapter is based on an article published in *Catalyst* [2].

5.1 Background

It has been shown that in fumaric acid production fermentations ethanol production can be negated via a glucose-limitation strategy. The production of fumaric acid by *R. oryzae* is sensitive to a variety of environmental conditions — the most influential being morphology, pH, nitrogen availability, and metal ion concentrations [31, 53, 29, 26]. The effect of these conditions on glucose-limited fumaric acid production is now required to further investigate *R. oryzae* as an industrial cell factory.

An industrially viable process will require a continuously steady high-yielding rate of production. It was established that a continuous low urea (nitrogen source) feed during the production phase prolonged the fermentation and resulted in steady fumaric acid production [33]. This strategy was tested together with the glucose-limited feed strategy and it was found to be successful in eliminating ethanol production while maintaining a steady production rate [1]. The urea cycle has been discovered to also contribute to the production of fumarate during nitrogen starvation conditions [29]. This may be the key to why fumaric acid production is highly dependent on the nitrogen concentration in the medium. The effect of varying the urea feed rate has been previously tested under excess glucose conditions [33]. Further experimental investigation is warranted to better understand the interplay between the glucose uptake rate and the urea feed rate.

The pH of the medium is known to affect on the metabolism and morphology of *R. oryzae*. Investigations as to the effect of pH on fumaric acid production have been focused on cell morphology and production in batch fermentations [26, 94, 63]. A thermodynamic analysis of dicarboxylic acid production highlights the energy cost of acid transport into the extracellular medium [36]. Dicarboxylic acids do not diffuse across the cell wall like ethanol and therefore require a transporter to overcome the concentration gradient over the cell wall. The cost of transporting fumaric acid out of the cell is a function of both the pH and the extracellular concentration. Transport cost is inversely proportional to the pH and proportional to the extracellular concentration. This is counter to the assumption that the production of FA is adenosine triphosphate (ATP) neutral [79]. This implies that more glucose is used in the production of fumaric acid since ATP needs to be produced

for export costs. The role of pH on fumaric acid production with *R. oryzae* has previously been investigated but only in excess glucose batch fermentations [26, 94].

The previous chapter showed how controlled glucose addition increased the yield of fumaric acid on glucose to $0.802\,\mathrm{g\,g^{-1}}$. Still markedly lower than the theoretical maximum yield of $0.97\,\mathrm{g\,g^{-1}}$ [36]. The current chapter aims to utilise the novel bioreactor and the glucose-controlled feed strategy to further investigate medium conditions that influence the yield and production rate of fumaric acid.

5.2 Methods

5.2.1 Microorganism and Culture Conditions

R. oryzae was used in all fermentations, it was cultivated and inoculated as described in Section 3.1.

5.2.2 Production Fermentations

The same growth procedure explained in Section 3.2 preceded all the production fermentations in this chapter. The production fermentations began once the reactor was fully rinsed of growth medium and filled with the nitrogen-void production medium. The production medium filling the reactor consisted only of the mineral medium described in Section 3.2 — urea and glucose were fed separately. Urea was fed at a rate from $0.255\,\mathrm{mg\,L^{-1}\,h^{-1}}$ to $1.25\,\mathrm{mg\,L^{-1}\,h^{-1}}$, and glucose was fed at a rate from $0.132\,\mathrm{g\,L^{-1}\,h^{-1}}$ to $0.329\,\mathrm{g\,L^{-1}\,h^{-1}}$. In order to achieve low dilution rates, high-concentration solutions of both glucose and urea were made with $342\,\mathrm{g\,L^{-1}}$ and $16\,\mathrm{g\,L^{-1}}$, respectively. The dilution rate for the continuous production fermentations varied from $0.0018\,\mathrm{h^{-1}}$ to $0.0027\,\mathrm{h^{-1}}$, taking into account the glucose and urea additions, as well as the NaOH dosing. The urea solution incorporated the mineral solution to ensure that the mineral composition in the reactor remained constant over the duration of the experimental run. All the solutions were sterilised at 121 °C for 60 min. All chemicals used were obtained from Merck (Modderfontein, South Africa).

During the production phase of the experiment, the fermenter was operated as a continuous stirred tank fermenter (CSTR). The reactor liquid recycle rate was multiples greater than the dilution rate to ensure the reactor was well mixed. The feed of liquid into the fermenter was composed of a mineral solution, glucose solution and a NaOH dosing solution. The flow rate of the mineral solution was kept constant for the entire run, whereas

the glucose solution varied depending on the desired glucose feed rate. The flow rate of the NaOH solution varied dependent on the production rate of acids in the fermenter. This resulted in a varied dilution rate as the fermenter was also maintained at a constant volume. The rate at which liquid was fed into the fermenter had to be equal to the flow rate of the liquid removed from the fermenter at any given time. For all the experimental runs, the temperature was constant at 35 °C. Further reactor operation was described in Chapter 3.

5.2.3 Analytical Techniques

All the fermentation medium concentrations were analysed with a HPLC. The method is fully described in Section 3.4.1. Fermentations were sampled at 12 h intervals. The dry cell mass was determined at the end of all experimental runs by using the second method described in Section 3.4.2. The carbon, hydrogen, nitrogen, and sulphur content of the biomass was determined by an Elemental Analyser — the Thermo Scientific Flash 2000 Organic Elemental Analyzer (Waltham, MA, USA). The method is describe next: the gas pressures were 250 kPa for He and 300 kPa for O_2, the flow rates were 140 mL min^{-1} for He measurement, 100 mL min^{-1} for He reference and 250 mL min^{-1} for O_2. The reactor operated at a temperature of 950 °C, the oven at 65 °C. The analytical duration was 620 s, the oxygen injection delay was 5 s, and the sample delay 12 s.

5.2.4 Production Rate Calculations

Because the reactor was operated with a constant feed of liquid, it had a dilution rate. The concentration profiles therefore could not be directly used to determine the production rates. To separate the production rates from the concentration profiles, Equation 10 was used [14]. This equation calculates the molar change of a species in the fermenter by accounting for the entry, exit, and production or consumption of a species. The desired variable is r_j; the equation was accordingly reworked into Equation 11. $\frac{dN_j}{dt}$ was calculated using the concentration profiles obtained from the HPLC analysis. Equation 12 illustrates the manner in which $\frac{dN_j}{dt}$ was calculated. It was assumed that the differential molar change term and the difference molar change terms were approximate for the calculations. The concentrations between sample values were interpolated to calculate the difference. Equation 10 was solved using Euler integration with a time increment of 1 s — the same increment at which all other online measurements were sampled. The effluent volumetric flow rate, Q_e, comprised of the volumetric feed rate and the volume sampled from the fermenter at specific times.

$$\frac{dN_j}{dt} = Q_f C_j^f - Q_e C_j + r_j V, \tag{10}$$

$$r_j = \frac{\left(\frac{dN_j}{dt} - Q_f C_j^f + Q_e C_j\right)}{V}, \tag{11}$$

$$\frac{dN_j}{dt} \approx \frac{\Delta N_j}{\Delta t} = \frac{\Delta C_j}{\Delta t} V, \tag{12}$$

HPLC analysis allowed all products, as well as the concentration of glucose in the medium to be accounted for. This allowed for a mass balance to be used to calculate the rates of CO_2 and O_2. The matrix used to solve the mass balance can be seen below. The mass balance took as input the rates of glucose consumption and the production of fumaric acid, malic acid, succinic acid, pyruvic acid, glycerol, and ethanol — rates corresponding to the specification rows S_2 to S_8 respectively. It was established that there was an accumulation of biomass weight over the production run. The biomass accumulation was attributed to the growth of nitrogen-containing biomass enabled by the constant feed of urea, and the additional biomass was attributed to carbohydrate storage [95]. The amount of nitrogen-containing biomass growth was determined by assuming that the biomass formula remains constant after the growth phase into production and that all the nitrogen present in the urea feed was converted to biomass. Glycogen was chosen as the carbohydrate storage molecule. The rate of glycogen was then calculated as the remaining unaccounted mass, by using specification S_1 and the rate of urea consumption, specified in S_9.

$$\begin{bmatrix}
 & G & O_2 & U & B & GY & CO_2 & W & FA & SA & Et & GL & MA & PA \\
C & 1 & 0 & 1 & 1 & 1 & 1 & 0 & 1 & 1 & 1 & 1 & 1 & 1 \\
H & 2 & 0 & 4 & 1.8 & {}^5/_3 & 0 & 2 & 1 & 1.5 & 3 & {}^8/_3 & {}^3/_2 & {}^4/_3 \\
O & 1 & 2 & 1 & 0.5 & {}^5/_6 & 2 & 1 & 1 & 1 & 0.5 & 1 & 5/4 & 1 \\
N & 0 & 0 & 2 & 0.189 & 0 & 0 & 0 & 0 & 0 & 0 & 0 & 0 & 0 \\
S_1 & Y_{sb}MM_G & 0 & 0 & MM_B & MM_{GY} & 0 & 0 & 0 & 0 & 0 & 0 & 0 & 0 \\
S_2 & 1 & 0 & 0 & 0 & 0 & 0 & 0 & 0 & 0 & 0 & 0 & 0 & 0 \\
S_3 & 0 & 0 & 0 & 0 & 0 & 0 & 0 & 1 & 0 & 0 & 0 & 0 & 0 \\
S_4 & 0 & 0 & 0 & 0 & 0 & 0 & 0 & 0 & 0 & 0 & 0 & 1 & 0 \\
S_5 & 0 & 0 & 0 & 0 & 0 & 0 & 0 & 0 & 1 & 0 & 0 & 0 & 0 \\
S_6 & 0 & 0 & 0 & 0 & 0 & 0 & 0 & 0 & 0 & 0 & 0 & 0 & 1 \\
S_7 & 0 & 0 & 0 & 0 & 0 & 0 & 0 & 0 & 0 & 0 & 1 & 0 & 0 \\
S_8 & 0 & 0 & 0 & 0 & 0 & 0 & 0 & 0 & 0 & 1 & 0 & 0 & 0 \\
S_9 & 0 & 0 & 1 & 0 & 0 & 0 & 0 & 0 & 0 & 0 & 0 & 0 & 0
\end{bmatrix}
\mathbf{X} =
\begin{bmatrix}
0 \\ 0 \\ 0 \\ 0 \\ 0 \\ -r_g \\ r_{fa} \\ r_{ma} \\ r_{sa} \\ r_{pa} \\ r_{gl} \\ r_{et} \\ -r_u
\end{bmatrix}$$

5.2.5 Metabolic Flux Model and Energy Calculations

In order to better understand the effect of the environmental changes on the physiology, a metabolic flux model was set up, (visible in Figure 22). The method followed is described by Villadsen [14]. The metabolic pathways included in the flux model described how glucose is distributed to biomass and all the other metabolites [29, 79, 66]. A lumped approach was used to account for the anabolism, which included accounting for $FADH_2$ and GTP as NADH and ATP, respectively [14]. The model allows for the calculation of energy production and consumption. The matrix that can be seen below, was set up by using mass balances over each reaction as well as energy balances. Each metabolic flux is designated with a number in Figure 22 this corresponds to the column variable in the matrix (v_i) and the letters are used to show the nodal mass balances. The consumption and production rates of the glucose, biomass and the metabolites were used as specifications in the matrix — these are shown in rows S_1 to S_{10}. There were two additional specifications, S_{10} and S_{11} representing O_2 and CO_2, that were not needed to solve the matrix. Rather, they were used to confirm that the metabolic flux model agrees with the mass balance. Solving the flux of all the individual metabolic rates allowed for the calculation of ATP production and consumption rates. The efficiency of oxidative phosphorylation indicated by the P/O number has been assumed to be constant for all the conditions at a value of 1.5 moles of ATP per atom of oxygen consumed. This value, suggested by [14], is unlikely to remain constant, but the assumption will be accounted for in the discussion of the results. Another assumption that needed to be made was the amount of energy used for the production of new biomass enabled by the urea feed. The value chosen is $2.5\,\mathrm{mol_{ATP}/Cmol_X}$, since the system is known to be fully aerobic [1]. The amount of CO_2 released, α, and the amount of NADH produced, β, per mole of biomass were calculated to be 0.116 $\mathrm{mol_{CO_2}\ Cmol_X^{-1}}$ and 0.116 $\mathrm{mol_{NADH}\ Cmol_X^{-1}}$, respectively. These values were calculated using a mass balance over the glucose-to-biomass equation, as well as the biomass formula established from the elemental analysis.

Next, the additional ATP cost of exporting fumaric acid and the other dicarboxylic acids into the medium needed to be determined. Literature outlines the equations and procedure to calculate the ATP cost of exporting dicarboxylic acids into the medium [36]. The ATP cost depends primarily on the medium pH and the concentration of the specific acid. Equations 5 and 6 (the equations have been reprinted below for convenience) are used to relate the medium pH to the ratio between the intracellular and extracellular acid concentrations for a specific transporter. Ordinarily, three transporters are present — namely a uniport ($n = 0$), symport ($n = 1$) and antiport ($n = -1$). The proton motive force, pmf, and the intracellular concentration, A_i, were suggested to be 0.15 V and $1 \times 10^{-3}\,\mathrm{mol\,L^{-1}}$ respectively [36]. It was established that the energy costs predicted

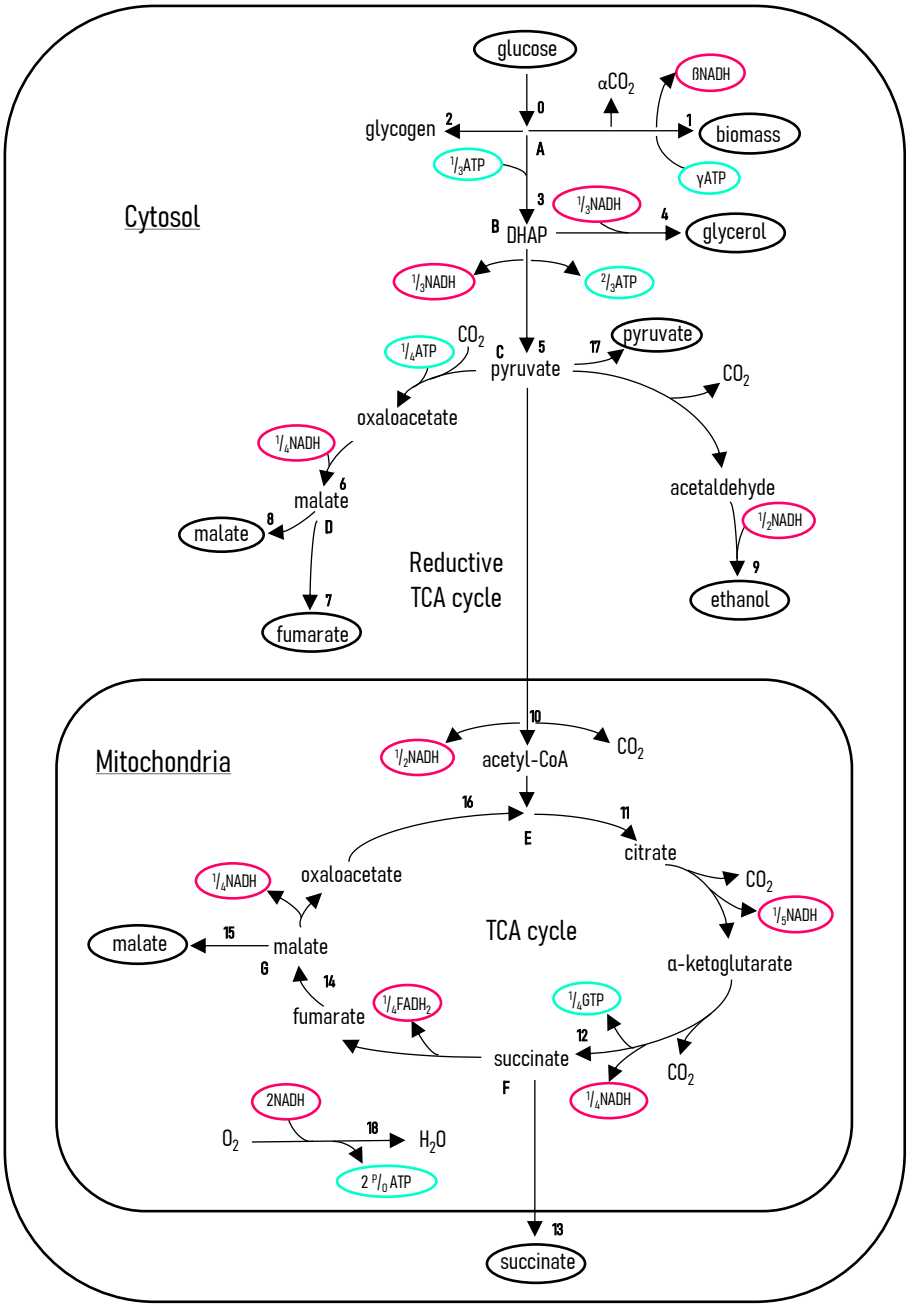

Figure 22: *R. oryzae* metabolic flux model for the consumption of glucose. The flux model is written on the basis of carbon moles; this results in the fractional amounts of the energy-related compounds. The compounds that interact with the medium are circled in black.

were not sensitive to the variation of these parameters. The transporter used at a set of conditions is selected by the proximity of its achievable concentration ratio to the required minimum concentration ratio dictated by the medium. The ATP cost of each transporter varies as a result of the number of protons needing to be exported for each molecule of acid to balance the charge. The cost of exporting pyruvate into the medium was calculated similarly [87].

$$log\left(\frac{A_o}{A_i}\right)^{eq} = 2(pH_o - pH_i) + \frac{(n-2)(-pmf)F}{ln(10)RT},$$

$$\left(\frac{A_o}{A_i}\right)^{eq} = \left(\frac{10^{pKa_1+pKa_2-2pH_o} + 10^{pKa_2-pH_o} + 1}{10^{pKa_1+pKa_2-2pH_i} + 10^{pKa_2-pH_i} + 1}\right)\left(\frac{A_o^{2-}}{A_i^{2-}}\right)^{eq}.$$

$$\begin{bmatrix}
 & v_0 & v_1 & v_2 & v_3 & v_4 & v_5 & v_6 & v_7 & v_8 & v_9 & v_{10} & v_{11} & v_{12} & v_{13} & v_{14} & v_{15} & v_{16} & v_{17} & v_{18} \\
A & -1 & 1.116 & 1 & 1 & 0 & 0 & 0 & 0 & 0 & 0 & 0 & 0 & 0 & 0 & 0 & 0 & 0 & 0 & 0 \\
B & 0 & 0 & 0 & -1 & 1 & 1 & 0 & 0 & 0 & 0 & 0 & 0 & 0 & 0 & 0 & 0 & 0 & 0 & 0 \\
C & 0 & 0 & 0 & 0 & 0 & -1 & {}^3/_4 & 0 & 0 & 1.5 & 1.5 & 0 & 0 & 0 & 0 & 0 & 0 & 1 & 0 \\
D & 0 & 0 & 0 & 0 & 0 & 0 & -1 & 1 & 1 & 0 & 0 & 0 & 0 & 0 & 0 & 0 & 0 & 0 & 0 \\
E & 0 & 0 & 0 & 0 & 0 & 0 & 0 & 0 & 0 & 0 & 1 & -1 & 0 & 0 & 0 & 0 & 1 & 0 & 0 \\
F & 0 & 0 & 0 & 0 & 0 & 0 & 0 & 0 & 0 & 0 & 0 & 0 & -1 & 1 & 1 & 0 & 0 & 0 & 0 \\
G & 0 & 0 & 0 & 0 & 0 & 0 & 0 & 0 & 0 & 0 & 0 & 0 & 0 & 0 & -1 & 1 & 1 & 0 & 0 \\
H & 0 & 0 & 0 & 0 & 0 & 0 & 0 & 0 & 0 & 0 & -1 & 0 & 0 & 0 & 0 & 0 & 0.5 & 0 & 0 \\
I & 0 & 0 & 0 & 0 & 0 & 0 & 0 & 0 & 0 & 0 & 0 & -1 & 1.5 & 0 & 0 & 0 & 0 & 0 & 0 \\
NADH & 0 & 0.116 & 0 & 0 & $-{}^1/_3$ & ${}^1/_3$ & $-{}^1/_4$ & 0 & 0 & -0.5 & 0.5 & 0 & 0.5 & 0 & ${}^1/_4$ & 0 & ${}^1/_4$ & 0 & -2 \\
ATP & 0 & -2.5 & 0 & $-{}^1/_3$ & 0 & ${}^2/_3$ & $-{}^1/_4$ & 0 & 0 & 0 & 0 & 0 & ${}^1/_4$ & 0 & 0 & 0 & 0 & 0 & 3 \\
S_1 & 1 & 0 & 0 & 0 & 0 & 0 & 0 & 0 & 0 & 0 & 0 & 0 & 0 & 0 & 0 & 0 & 0 & 0 & 0 \\
S_2 & 0 & 1 & 0 & 0 & 0 & 0 & 0 & 0 & 0 & 0 & 0 & 0 & 0 & 0 & 0 & 0 & 0 & 0 & 0 \\
S_3 & 0 & 0 & 1 & 0 & 0 & 0 & 0 & 0 & 0 & 0 & 0 & 0 & 0 & 0 & 0 & 0 & 0 & 0 & 0 \\
S_4 & 0 & 0 & 0 & 0 & 0 & 0 & 0 & 0 & 0 & 0 & 0 & 0 & 0 & 0 & 0 & 0 & 0 & 1 & 0 \\
S_5 & 0 & 0 & 0 & 0 & 1 & 0 & 0 & 0 & 0 & 0 & 0 & 0 & 0 & 0 & 0 & 0 & 0 & 0 & 0 \\
S_6 & 0 & 0 & 0 & 0 & 0 & 0 & 0 & 0 & 1 & 0 & 0 & 0 & 0 & 0 & 0 & 1 & 0 & 0 & 0 \\
S_7 & 0 & 0 & 0 & 0 & 0 & 0 & 0 & 1 & 0 & 0 & 0 & 0 & 0 & 0 & 0 & 0 & 0 & 0 & 0 \\
S_8 & 0 & 0 & 0 & 0 & 0 & 0 & 0 & 0 & 0 & 0 & 0 & 0 & 0 & 1 & 0 & 0 & 0 & 0 & 0 \\
S_9 & 0 & 0 & 0 & 0 & 0 & 0 & 0 & 0 & 0 & 1 & 0 & 0 & 0 & 0 & 0 & 0 & 0 & 0 & 0 \\
S_{10} & 0 & 0 & 0 & 0 & 0 & 0 & 0 & 0 & 0 & 0 & 0 & 0 & 0 & 0 & 0 & 0 & 0 & 0 & 1 \\
S_{11} & 0 & 0.116 & 0 & 0 & 0 & 0 & $-{}^1/_4$ & 0 & 0 & 0.5 & 0.5 & 0 & 0.5 & 0 & 0 & 0 & 0 & 0 & 0
\end{bmatrix}
\mathbf{v} =
\begin{bmatrix}
0 \\ 0 \\ 0 \\ 0 \\ 0 \\ 0 \\ 0 \\ 0 \\ 0 \\ 0 \\ 0 \\ -r_s \\ r_x \\ r_{gy} \\ r_{py} \\ r_{gl} \\ r_{ma} \\ r_{fa} \\ r_{sa} \\ r_{et} \\ r_{O_2} \\ r_{CO_2}
\end{bmatrix}$$

5.3 Results and Discussion

5.3.1 Experimental Window Determination and Repeatability

The fermentations conducted in this chapter were primarily focused on the effects of urea and pH on the yield and rate of fumaric acid production. An experimental run, consisting of around 200 h, remained at constant pH and urea addition rate while the glucose

feed rate was altered. Different glucose rates during a run represent processing windows. Each window was considered as a separate processing condition where distinct rates and yields could be calculated. The window spans typically lasted 36 h, and the last 24 h were considered for the calculation of the specific state. Figure 23 indicates the glucose feed rate and NaOH dosing rate for four separate windows; it is evident from the figure that rapid dynamic changes occurred around the step while more stable dosing rates occurred towards the end of the window. In order to calculate the true production rate of metabolites, a mole balance was performed over the last 24 h of operation where differences in HPLC determined concentration values (shown in Figure 23a), and the continuous dilution rate was used (see Section 5.2.4). The procedure enabled four to five separate processing conditions within a single run. The calculated fumaric acid production rates (black squares) can be seen in Figure 23b for each window. The consolidated data from each window will subsequently be used for the analysis of the fermentations.

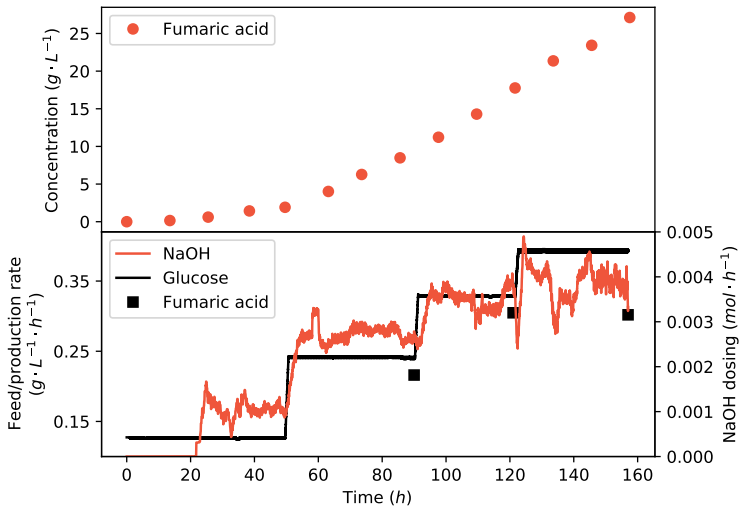

Figure 23: An illustration of how stable acid production was determined and how concentration profiles were used to determine volumetric rates of production. (**a**) The HPLC fumaric acid concentration profile taken from the reactor. This is data from a single fermentation. (**b**) A comparison between the glucose feed rate and the rate of NaOH dosed to maintain the pH. The fumaric acid production rates calculated from the HPLC concentrations and the dilution rate are also shown (black squares).

It is imperative to analyse the repeatability of the operation at the same conditions. Windows can be repeated within an experimental run (at least 75 h apart) or in completely separate runs. In Table 2, four repeat windows are compared at different glucose-addition rates. Some are from the same run while others are from separate runs, as indicated in the table. In the table, it can be seen that the average difference between the fumaric acid production rates is 3.5%, with the average difference between the glucose consumption rates being 2.7%. These repeatable results indicate that the activity of the biomass remained stable over the fermentation for different pH values and urea feed rates. This

accordingly enables comparison between different windows regardless of the time of the fermentation.

Table 2: Repeatability and stability of fumaric acid production evaluated through glucose consumption and distribution.

	Separate Run Repeats				**Repeats within a Run**			
Glucose feed rate ($g\,L^{-1}\,h^{-1}$)	0.132 *		0.197 *		0.227 *		0.263 †	
Glucose consumed ($g\,L^{-1}\,h^{-1}$)	0.133	0.142	0.197	0.195	0.222	0.226	0.240	0.236
Fumaric yield ($g\,g^{-1}$)	0.733	0.774	0.727	0.695	0.900	0.894	0.943	0.912
By-product yield ($g\,g^{-1}$)	0.076	0.073	0.074	0.040	0.093	0.116	0.139	0.108

* Experimental conditions: pH 5 and urea feed rate of $0.625\,mg\,L^{-1}\,h^{-1}$; † Experimental conditions: pH 4 and urea feed rate of $0.255\,mg\,L^{-1}\,h^{-1}$.

5.3.2 The Role of pH and Urea Feed Rate on the Production of Fumaric Acid

Figure 24a–c are parity plots between the glucose fed and the glucose consumed for various conditions. At low glucose feed rates, it can be seen that all the glucose feed is consumed. The $y = x$ line (black line) indicates the point of full glucose consumption. Points below the line indicate glucose accumulation and suggest suboptimal glycolytic flux. For the urea feed rate of $0.625\,mg\,L^{-1}\,h^{-1}$ and pH 4, it can be seen that there was full consumption of glucose at all the glucose feed rates. For pH 5, at the highest glucose feed rate of $0.329\,g\,L^{-1}\,h^{-1}$, a slight drop in glucose consumption can be seen. However, looking at the glucose consumption for pH 6, from a glucose feed of $0.197\,g\,L^{-1}\,h^{-1}$, glucose accumulation is observed. It is clear that at a lower pH, more glucose can be consumed. This indicates that the pH inhibits some crucial pathway in the consumption of glucose, either in the uptake of glucose or in the metabolism of it. The rate at which glucose is consumed is to be maximised, provided the fumaric acid yield is maintained, as this will increase fumaric acid productivity, which is of key importance. It was also found that the urea feed rate affected the glycolytic flux. The lowest urea feed rate of $0.255\,mg\,L^{-1}\,h^{-1}$ has a negative effect on the glycolytic flux. It can be seen that for both pHs 4 and 5, the glycolytic limit is reached first for the lowest urea feed rate. Through the repeatability experiments, it was determined that, at least within the time frame of the experiments conducted (approximately 200 h), no decay of the glucose consumption rate was seen for the urea feeds of 0.255 or $0.625\,mg\,L^{-1}\,h^{-1}$. This shows that the decreased

glycolytic flux seen for the lowest urea feed is a result of the condition and not the length of the experiment.

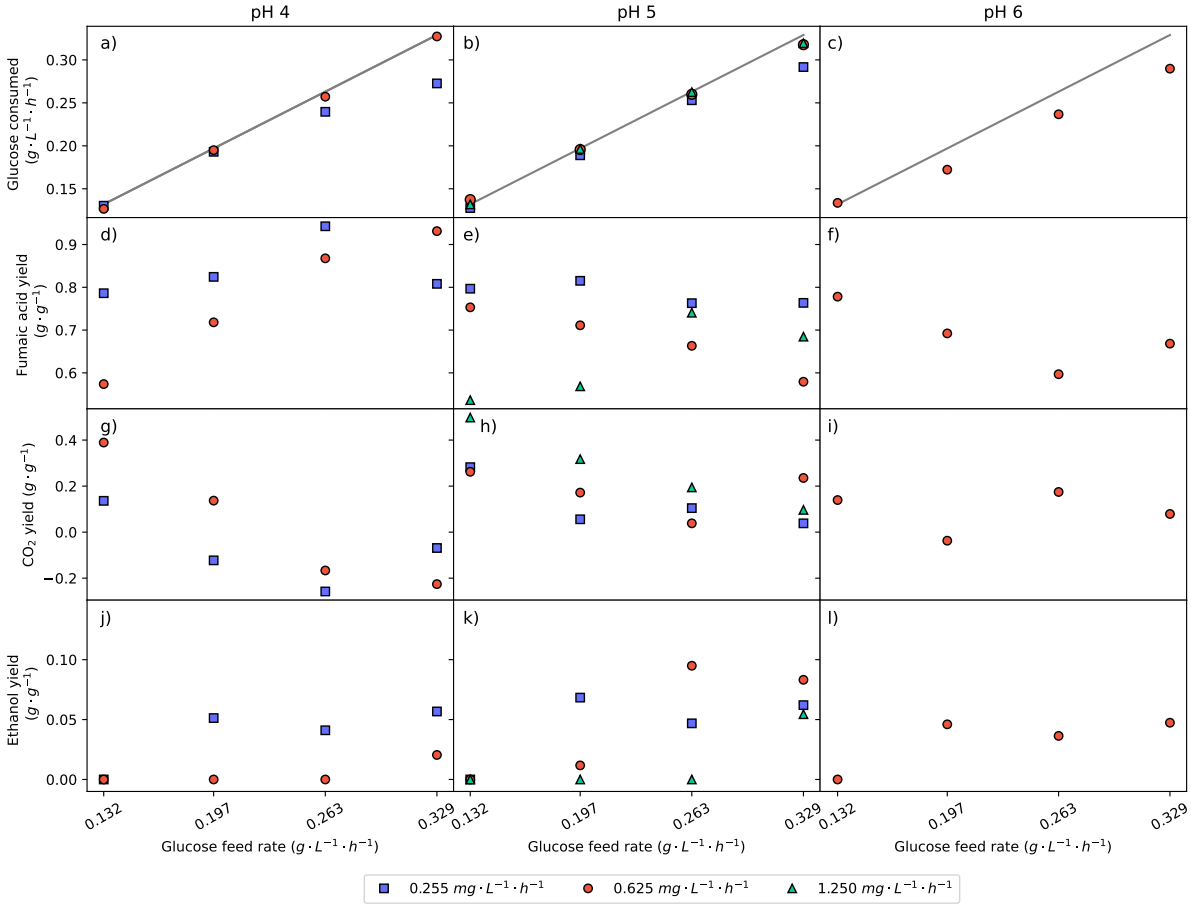

Figure 24: The effect of pH and the urea addition rate on glucose consumption and distribution. (**a**–**c**) A parity plot between the glucose feed and glucose consumed. (**d**–**f**) The yield of fumaric acid from glucose. (**g**–**i**) The yield of CO_2 from glucose. (**j**–**l**) The yield of ethanol from glucose. As indicated in Table 2, repeat experiments were conducted, and the average values of the two experiments are presented. For the conditions that were not repeated, single fermentation values were used.

Clear improvement of fumaric acid production has been found by altering the pH. Comparing the yields of fumaric acid achieved for the different pHs tested (Figure 24d–f), it can be seen that there is a difference in the trends as the glucose feed rate is increased. For pHs 5 and 6, the yield decreased as the glucose feed rate is increased, but the yield for pH 4 increased. The yield of $0.94\,\mathrm{g\,g^{-1}}$ fumaric acid on glucose achieved for pH 4 at a urea feed of $0.255\,\mathrm{mg\,L^{-1}\,h^{-1}}$ is the highest reported in the known literature [19]. This is closely approaching the theoretical maximum of $0.97\,\mathrm{g\,g^{-1}}$ [36]. The yield achieved at the higher urea feed rate of $0.625\,\mathrm{mg\,L^{-1}\,h^{-1}}$ is $0.93\,\mathrm{g\,g^{-1}}$, this has the massive benefit of a higher glycolytic flux, consuming all of the glucose feed. Thereby achieving productivity of $0.305\,\mathrm{g\,L^{-1}\,h^{-1}}$ fumaric acid. Total consumption of glucose will allow for the extended

production of fumaric acid since there will be no problematic accumulation, and downstream processing is simplified. Comparing the yields of CO_2 shown in Figure 24g,h,l), it is seen that the highest fumaric acid yields correspond to the lowest CO_2 yields. At these points, the CO_2 yields are negative, indicating that CO_2 is being consumed by pyruvate carboxylase (EC 6.4.1.1) in the pathway of fumaric acid production. This is a result of the high yield of fumaric acid production but also suggests that less carbon is being directed to the TCA cycle.

A higher urea feed rate is shown to increase the glycolytic flux; however, the effect on the distribution of glucose must also be taken into account. It can be seen for both pHs 4 and 5 that the highest yield of fumaric acid is achieved consistently for the lowest urea feed. This confirms the view that urea addition inhibits the production rate of fumaric acid but shows that there is a greater influence on the yield of fumaric acid. It can clearly be seen that as the feed rate of urea is increased, the yield of fumaric acid decreases. Nitrogen availability influences the glucose uptake rate and how the glucose consumed is metabolised. Looking at the fumaric acid yields achieved for the urea feed of $1.25\,\mathrm{mg\,L^{-1}\,h^{-1}}$, it can be seen for the first two glucose feed rates that the above trend is observed; however, it is not followed for the higher glucose feed rates. There is a clear trade-off when it comes to the effect of urea feed rate on fumaric acid production. On the one side, the glycolytic flux is inhibited by low urea addition, while on the other side, the fumaric acid yield is clearly higher at low urea feeds. Since fumaric acid production will be a key optimisation parameter, a balance between these two effects will result in optimum production.

The point at which glucose accumulation begins is consistently preceded by ethanol production. Ethanol is the major by-product and all other by-products follow a similar trend to ethanol. Figure 24j–l shows the ethanol yields for the various conditions. If one compares the glucose feed rate where glucose accumulation begins, it can be seen that at that feed rate or the preceding feed rate, ethanol production began. This ties into the function of glycolysis; once the carbon sinks of fumaric acid production and the TCA cycle are at capacity, ethanol overflow begins. Increasing the glucose feed rate further leads to glucose accumulation, as no more glucose can be accommodated through glycolysis. Comparing the ethanol yields for the three pHs at the urea feed of $0.625\,\mathrm{mg\,L^{-1}\,h^{-1}}$, it can be seen that the pH clearly shifts the point at which ethanol breakthrough occurs. The ethanol breakthrough point is also influenced by the urea feed rate. At pH 5 it can be seen that as the urea feed rate was increased, the glucose feed rate at which ethanol breakthrough occurred increased. This clearly shows that an increased nitrogen feed rate increases the glycolytic flux that can be accommodated before ethanol breakthrough occurs. It is also evident that the yield of fumaric acid is unaffected by ethanol breakthrough.

The yields of CO_2 (Figure 24g–i) show why the yield of fumaric acid is unaffected by ethanol breakthrough. The increase in fumaric acid yield always corresponds to a decrease in the yield of CO_2. The yield of CO_2 gives insight into ATP production since CO_2 is largely produced through the TCA cycle. Using the metabolic flux model described in Section 5.2.5, the fraction of carbon consumed that is directed to the TCA cycle was calculated (Figure 25a,b). As the yield of fumaric acid increases, the fraction of carbon that is directed to the TCA cycle decreases and this counteracts ethanol breakthrough, maintaining the yield of fumaric acid.

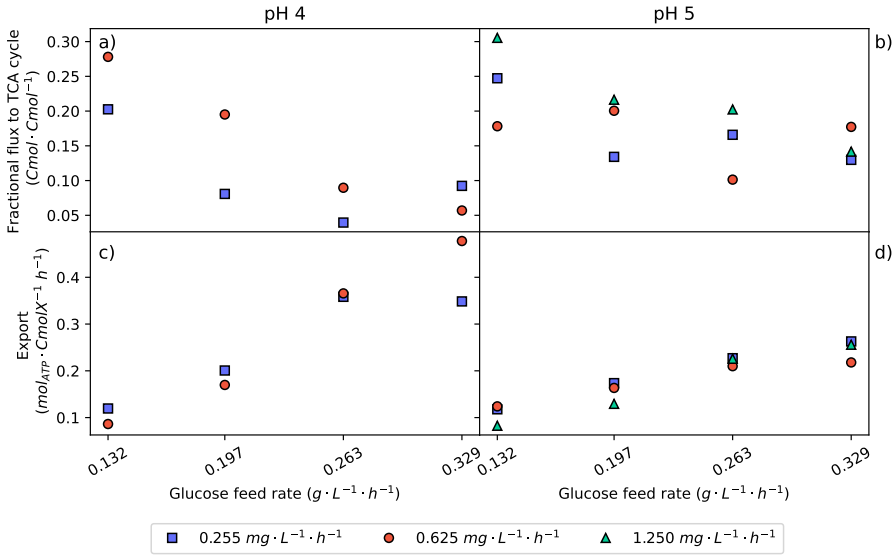

Figure 25: The effect of the urea addition rate on the energy parameters at pHs 4 and 5. (**a**,**b**) The fractional amount of glucose that is directed to the TCA cycle. (**c**,**d**) The ATP required to export the acids produced into the medium. As indicated in Table 2, repeat experiments were conducted, and the average values of the two experiments are presented. For the conditions that were not repeated, single fermentation values were used.

It was found that there was a mass increase of biomass in the reactor during the production of fumaric acid. Figure 26 shows the yields of biomass on glucose consumed for the various conditions. It can be seen that as the urea feed rate is increased, the yield of biomass increases between the low and medium urea feed rates. This trend is not followed for the highest urea feed rate since a higher biomass yield is expected. Looking at the nitrogen to carbon ratios shown in Table 3, it can be seen that the nitrogen contents of the biomass produced during the production runs are less than that produced during the growth phase. The biomass initially grown is in a nitrogen excess medium. The nitrogen-starved environment had a clear influence on the biomass produced and is not equivalent to the biomass initially grown. The nitrogen contents in the final collected biomass were compared to the amount of nitrogen fed during the fumaric acid production phase, and it was found that all the nitrogen was accounted for. This suggests that all urea was ab-

sorbed during production and that higher urea feed rates resulted in biomass with more accumulated nitrogen. The total biomass increase over the fumaric acid production span was between 1.95 and 5.72 times the initial amount of biomass (obtained from the growth phase). This figure does not correspond to the total nitrogen increase in biomass over the production period that was between 41% and 119% (nitrogen accumulated over production divided by nitrogen present in biomass after growth) for the low and medium urea runs, and 247% for the high urea runs. The major difference between nitrogen and total biomass increase can be attributed to the accumulation of carbohydrates, as indicated in the flux model presented in Section 5.2.5. The nitrogen increase does, however, suggest that more proteins were synthesised during production, and it can be anticipated that this will increase the overall activity of the biomass. Activity increases were, however, not observed when considering the stability of the repeatability data. This clearly suggests that fractions of the biomass became inactive during production as biomass steadily grew due to urea addition. The relative stability of the biomass activity further hints that low urea addition resulted in less biomass death than high urea addition. Enhanced usage of the urea cycle at low urea feed rates provides a plausible reason for the slower rate of biomass decay at these conditions.

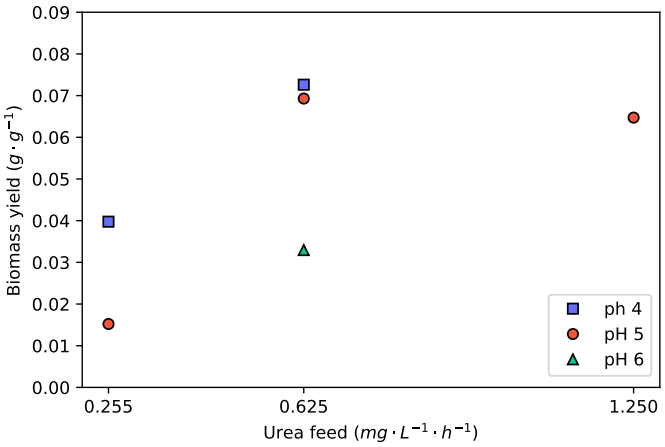

Figure 26: The effect of pH and urea addition on the yield of biomass on glucose. As indicated in Table 2, repeat experiments were conducted, and the average values of the two experiments are presented. For the conditions that were not repeated, single fermentation values were used.

Table 3: Experimental parameters analysing the yield and elemental composition of *R. oryzae* biomass.

Phase	**pH**	**Urea Feed** ($mg\,L^{-1}\,h^{-1}$)	Y_{gb} ($g\,g^{-1}$)	**H:C**	**N:C**
Growth	5	Excess	0.180	1.410	0.189
Production	5	0.255	0.013	0.807	0.128
Production	5	0.625	0.080	0.644	0.120
Production	5	1.250	0.066	1.041	0.148
Production	4	0.625	0.071	1.030	0.123

It has been seen at low pH (pH 4) and especially at low nitrogen (urea feed of $0.255\,mg\,L^{-1}\,h^{-1}$) that there is a very low rate of respiration or carbon flux to the TCA cycle. This indicates that there is a lower rate of ATP production under these conditions. Since it is known that the export of fumaric acid comes at an additional ATP cost [36], it is expected that the export cost is lower under these conditions. Figure 25c,d shows that the export costs are, in fact, the highest under these conditions. This severe contradiction cannot be explained by using enhanced cycling of the urea cycle. The urea cycle is expected to be enhanced under low nitrogen feed conditions, where more ATP expenditure takes place in producing fumarate [96, 29]. The extremely low flux to respiration under these conditions is counterintuitive when considering the enhanced costs of fumaric acid export, as well as the enhanced maintenance cost of the urea cycle. A plausible explanation is that the efficiency of generating ATP in oxidative phosphorylation is severely enhanced under the low pH and nitrogen conditions. This postulate was tested in the flux model, where the oxidative phosphorylation values (P/O) higher than three were obtained to close the energy balance. Since the theoretical maximum for P/O values is three, the observed contradiction could not be elucidated. Accordingly, it is highly likely that the calculated export costs do not represent the functioning of the organism.

Dicarboxylic acids can be present as solid undissociated acid, aqueous undissociated acid and then dissolved in a dissociated form, of which there is a first and second conjugated base. The equilibrium ratio between these forms is dependent on the molar concentration of the acid, temperature and pH. At pH 6 most of the acid will be present, as the second dissociated form requires the most alkali to be added if the pH is to be maintained. At low pH values, the acid becomes undissociated, and depending on the specific acid, solid acid can form. Solids will begin to form for fumaric acid at a pH below 4.11 and a temperature of 25 °C [36]. Assuming an industrial production concentration of $1\,mol\,L^{-1}$ fumaric acid, operation at a ph of 6 would require 2.97 times the amount of NaOH

than would be required at a pH of 4. This is an attractive operating condition since it results in the double benefit of less alkali needed to maintain the pH and less acid used in downstream re-acidification of the medium; thus, decreasing the overall cost of fumaric acid production. Together with the results presented for pH 4 it can be seen that this is the ideal condition for fumaric acid production.

The pH also has an effect on the ionic and osmotic stress on the cell. The osmotic and ionic strength increase from approximately $0\,\mathrm{mol\,L^{-1}}$ at a pH of 2 in an S-curve shape to the maximum of $3\,\mathrm{mol\,L^{-1}}$ at a pH of 6. Operation at pH 4 results in an osmotic pressure that is a third of that at pH 6 [36]. These two factors are important since such stresses have been found to result in the production of unwanted by-products [36, 85, 86]. Through analysis of the pH 6 experiments, it was determined that pH 6 provided unfavourable fumaric acid yields, glucose accumulation and experienced high levels of ethanol production, as shown in Figure 24c,f,i, respectively. In Figure 26, it can also be seen that the production of biomass was disrupted by the high pH. This confirms the literature that suggested high osmotic and ionic stress caused by a high pH favoured by-product production. pH 6 is clearly an unfavourable condition for fumaric acid production.

5.4 Conclusion

The mechanism by which *Rhizopus oryzae* produces fumaric acid has long been debated. By closely varying the medium pH, the urea feed rate and the glucose feed rate, a better understanding of the fumaric acid production has been uncovered. Clear correlations between the point of ethanol breakthrough and the amount of urea supplied have been established. At a higher urea feed rate, ethanol production begins at a higher glucose feed rate. A drastic difference was found in the metabolism of *R. oryzae* between pH 4 and higher pH values. The lower pH experienced a proportional increase in the yield of fumaric acid to the glucose feed rate. This was attributed to an improved metabolic function. An optimum point for fumaric acid production has been identified. It lies at pH 4 with a urea feed rate of $0.625\,\mathrm{mg\,L^{-1}\,h^{-1}}$ and a glucose feed rate of $0.329\,\mathrm{g\,L^{-1}\,h^{-1}}$. The yield of fumaric acid at this point is $0.93\,\mathrm{g\,g^{-1}}$ with productivity of $0.305\,\mathrm{g\,L^{-1}\,h^{-1}}$. This point has total glucose consumption and, accordingly, no glucose is wasted or present in the exit stream.

6 Optimising the use of a Synthetic Lignocellulosic Hydrolysate through Feed Strategies

The contents of this chapter is based on an article published in *Fermentation* [3].

6.1 Background

Optimum conditions for the production of fumaric acid have been identified. These conditions include the morphology, medium composition, growth procedure, pH, glucose feed rate, and urea feed rate. Industrially, however, it is unlikely that a pure glucose feed will be used for the production of fumaric acid as this would have to be sourced from cereal crops, thus encroaching on the food and animal feed industries. The favourable option would be to use a waste stream as feedstock. The lignocellulosic plant biomass is perfectly suited to the biorefining process for the production of bio-based chemicals. Lignocellulosic material is comprised of cellulose, hemicellulose, and lignin, and it is often a waste stream for many processes, making it an ideal feedstock because it is inexpensive and renewable [89]. It has been found that 25 % of municipal waste solids are comprised of lignocellulosic material [97]. The hydrolysis of lignocellulosic biomass breaks down the polysaccharides into the monosaccharide units, of which glucose and xylose are the two predominant sugars [13, 15].

Glucose has been a favourite of the fermentation industry since it is easily utilised by numerous microbes and is a widely available feedstock [15]. Glucose is consumed through the glycolytic pathway, which is common in many organisms, unlike the pentose phosphate pathway that is required for the fermentation of xylose [89]. This has led to the less frequent utilisation of xylose as a feedstock because the required pathways would have to be transferred to the identified organism [98]. However, in recent years, a drive towards more renewable feedstocks has grown. *R. oryzae* does have the ability to consume both xylose and glucose to produce fumaric acid [88]. This ability is highly beneficial as lignocellulosic hydrolysate can be used for the production of fumaric acid. The available literature is limited and only covers batch shake flask fermentations of xylose and glucose feedstocks [55, 88, 59, 63]. The reported fumaric acid yields from these studies range from $0.31\,\mathrm{g\,g^{-1}}$ to $0.58\,\mathrm{g\,g^{-1}}$, considerably lower than pure glucose fermentations that reach $0.93\,\mathrm{g\,g^{-1}}$ as shown in Section 5.3.2.

The utilisation of xylose in the continuous production of fumaric acid as well as the co-fermentation of glucose and xylose need to be further understood. The novel reactor and fermentation strategy can precisely control all critical medium conditions, allowing

for the close monitoring of substrate consumption and metabolite production in order to uncover the physiology of *R. oryzae*.

This chapter aims to compare, analyse, and optimise the production rates and yields of fumaric acid achieved from the fermentation of pure glucose, pure xylose, and a synthetic lignocellulosic hydrolysate (LH). This will give greater insight into the utilisation of xylose as a substrate, the use of lignocellulosic hydrolysate (including only the predominant sugars) as a potential feedstock for fumaric acid production, and the effects that xylose has on the metabolism of *R. oryzae*.

6.2 Methods

6.2.1 Microorganism and Culture Conditions

R. oryzae was used in all fermentations, it was cultivated and inoculated as described in Section 3.1.

6.2.2 Production Fermentations

The batch production medium consisted of $20\,\mathrm{g\,L^{-1}}$ glucose, xylose, or a glucose–xylose mixture as well as the mineral medium salts at the specified concentrations. The continuous production fermentations began with only the mineral solution. Urea was fed at a rate of $0.625\,\mathrm{mg\,L^{-1}\,h^{-1}}$ for all production fermentations. The 50% mass-based glucose–xylose mixture (synthetic LH) was fed at a rate from $0.132\,\mathrm{g\,L^{-1}\,h^{-1}}$ to $0.329\,\mathrm{g\,L^{-1}\,h^{-1}}$ for the continuous fermentations. To achieve low dilution rates, high-concentration solutions of both the synthetic LH and urea were made with $325.85\,\mathrm{g\,L^{-1}}$ and $16\,\mathrm{g\,L^{-1}}$, respectively. The dilution rate for the continuous production fermentations varied from $0.0018\,\mathrm{h^{-1}}$ to $0.0027\,\mathrm{h^{-1}}$ and took into account the substrate and urea additions as well as the NaOH dosing. The urea solution incorporated the mineral solution to ensure that the mineral composition in the reactor remained constant over the duration of the experimental run. All the solutions were sterilised at 121 °C for 60 min.

6.2.3 Analytical Techniques

Samples were taken from the fermentations at varied increments to achieve a satisfactory resolution for the changing concentration profiles. The samples were analysed using High-Performance Liquid Chromatography (HPLC). The system used to analyse for glucose,

xylose, and ethanol was the Agilent 1260 Infinity HPLC (Agilent Technologies, Santa Clara, CA, USA) equipped with a refractive index detector operated at 55 °C and a 300 × 7.8 mm Aminex HPX-87C column (Bio-Rad Laboratories, Hercules, CA, USA) operated at 60 °C. The mobile phase was a 0.005 M solution of H_2SO_4 with a flow rate of 0.6 mL min^{-1}. For the analysis of glycerol and the organic acids (namely fumaric acid, malic acid, succinic acid, and pyruvic acid), the mobile phase was altered to 0.02 M, with all other specifications remaining constant. Peaks of xylose and malic acid overlapped and could not be separated sufficiently with this system. In order to solve this, the concentration of malic acid was determined separately with the Waters HPLC (Waters, Milford, MA, USA) equipped with a UV-Vis detector and a 300 × 7.8 mm Aminex HPX-87H column operated at 35 °C. The mobile phase was a 0.02 M solution of H_2SO_4 with a flow rate of 1.0 mL min^{-1}. Using the determined concentration of malic acid, the area was subtracted from the combined peak of xylose and malic acid to determine the corrected concentration of xylose. The dry cell mass was determined at the end of all experimental runs, using the second method described in Section 3.4.2.

6.2.4 Production Rate and Yield Consolidation

The production rates of all substrates consumed and metabolites produced were determined using the method outlined in Section 5.2.4. In order to confirm that all the metabolites had been accounted for, a mass balance was conducted for the systems. The total amount of substrate initially added or fed over the course of the fermentation was measured (this included glucose, xylose, and urea, depending on the specific fermentation conditions). The total molar amount of carbon added to the reactor was determined. The total amount of metabolites produced was established by integrating the corrected production rates. The metabolites accounted for include fumaric acid, ethanol, malic acid, succinic acid, pyruvic acid, and glycerol. The total mass of the biomass produced during the production fermentation was identified and converted into carbon moles. The molar mass for *R. oryzae* determined in the previous chapter was used.

Finally, the amount of carbon that exited the reactor as CO_2 had to be accounted for. Using the online gas CO_2 composition and the flow rate of the gas sparged into the reactor, together with Equation (13), the rate of CO_2 production was calculated. The total molar amount of CO_2 produced was calculated by integrating the production rate with the fermentation time. The closure of the mass balance was determined by comparing the molar amount of carbon in the reactor with the sum of all the carbon accounted for at the end of the fermentation. The mass balance was conducted for all the fermentations, and it was confirmed that all carbon had been accounted for. This is a valid claim because all HPLC peaks were accounted for. A 10% tolerance was used to indicate a sufficient mass

balance closure. The error was likely due to the assumption that the inlet and outlet gas flow rates were equal. Due to the pressure drop across the gas analyser, the outlet gas flow rate could not be measured.

$$r_{CO_2} = \frac{1}{V}\left(Q_{gas}(C^o_{CO_2} - C_{CO2}) - V_g\frac{dC_{CO2}}{dt}\right) \tag{13}$$

6.2.5 Metabolic Flux Model

To gain a better understanding of how the xylose-glucose mixture was metabolised, xylose catabolism pathways were included into the metabolic flux model (described earlier in Section 5.2.5). Figure 27 shows the metabolic pathways of *R. oryzae* catabolising glucose and xylose to the various metabolites. The metabolic pathways were established by correlating a number of enzymatic studies of *R. oryzae* [75, 29, 78, 79, 66]. A matrix was developed from the model that solved for the individual fluxes, the matrix can be found in Appendix A. Mass balances were drawn around the nodes, indicated by the letters on Figure 27 and corresponding to the rows of the matrix. Additionally, NADH and NADPH balances were also used to solve the matrix. The metabolic rates of production and consumption were used as specifications in the matrix. It can be seen that ethanol production and consumption is possible with the flux model, the model was altered depending on the role of ethanol for that point in the fermentation. The matrix was overspecified since there were more equations than unknowns, meaning that the ATP balance was not required to solve the matrix. The specifications of O_2 and CO_2 were also not required and their solution served as a check on the validity of the metabolic flux model. The metabolic rates of O_2, CO_2 and glycogen were determined using a mass balance for specific instances of the fermentation as was done in Section 5.2.4. The matrix below uses carbon, hydrogen, oxygen and nitrogen elemental balances along with the product rate specifications from the HPLC concentration profiles to determine the unknown rates.

$$
\begin{bmatrix}
 & G & X & \mathrm{O}_2 & U & B & GY & \mathrm{CO}_2 & W & FA & SA & Et & GL & MA & PA \\
C & 1 & 1 & 0 & 1 & 1 & 1 & 1 & 0 & 1 & 1 & 1 & 1 & 1 & 1 \\
H & 2 & 2 & 0 & 4 & 1.8 & {}^{5}/_{3} & 0 & 2 & 1 & 1.5 & 3 & {}^{8}/_{3} & {}^{3}/_{2} & {}^{4}/_{3} \\
O & 1 & 1 & 2 & 1 & 0.5 & {}^{5}/_{6} & 2 & 1 & 1 & 1 & 0.5 & 1 & 5/4 & 1 \\
N & 0 & 0 & 0 & 2 & 0.189 & 0 & 0 & 0 & 0 & 0 & 0 & 0 & 0 & 0 \\
S_1 & Y_{sb}MM_G & Y_{sb}MM_X & 0 & 0 & MM_B & MM_{GY} & 0 & 0 & 0 & 0 & 0 & 0 & 0 & 0 \\
S_2 & 1 & 0 & 0 & 0 & 0 & 0 & 0 & 0 & 0 & 0 & 0 & 0 & 0 & 0 \\
S_3 & 0 & 0 & 0 & 0 & 0 & 0 & 0 & 0 & 1 & 0 & 0 & 0 & 0 & 0 \\
S_4 & 0 & 0 & 0 & 0 & 0 & 0 & 0 & 0 & 0 & 0 & 0 & 0 & 1 & 0 \\
S_5 & 0 & 0 & 0 & 0 & 0 & 0 & 0 & 0 & 0 & 1 & 0 & 0 & 0 & 0 \\
S_6 & 0 & 0 & 0 & 0 & 0 & 0 & 0 & 0 & 0 & 0 & 0 & 0 & 0 & 1 \\
S_7 & 0 & 0 & 0 & 0 & 0 & 0 & 0 & 0 & 0 & 0 & 0 & 1 & 0 & 0 \\
S_8 & 0 & 0 & 0 & 0 & 0 & 0 & 0 & 0 & 0 & 0 & 1 & 0 & 0 & 0 \\
S_9 & 0 & 0 & 0 & 1 & 0 & 0 & 0 & 0 & 0 & 0 & 0 & 0 & 0 & 0 \\
S_{10} & 0 & 1 & 0 & 0 & 0 & 0 & 0 & 0 & 0 & 0 & 0 & 0 & 0 & 0
\end{bmatrix}
\mathbf{X} =
\begin{bmatrix}
0 \\ 0 \\ 0 \\ 0 \\ 0 \\ -r_g \\ r_{fa} \\ r_{ma} \\ r_{sa} \\ r_{pa} \\ r_{gl} \\ r_{et} \\ -r_u \\ -r_x
\end{bmatrix}
$$

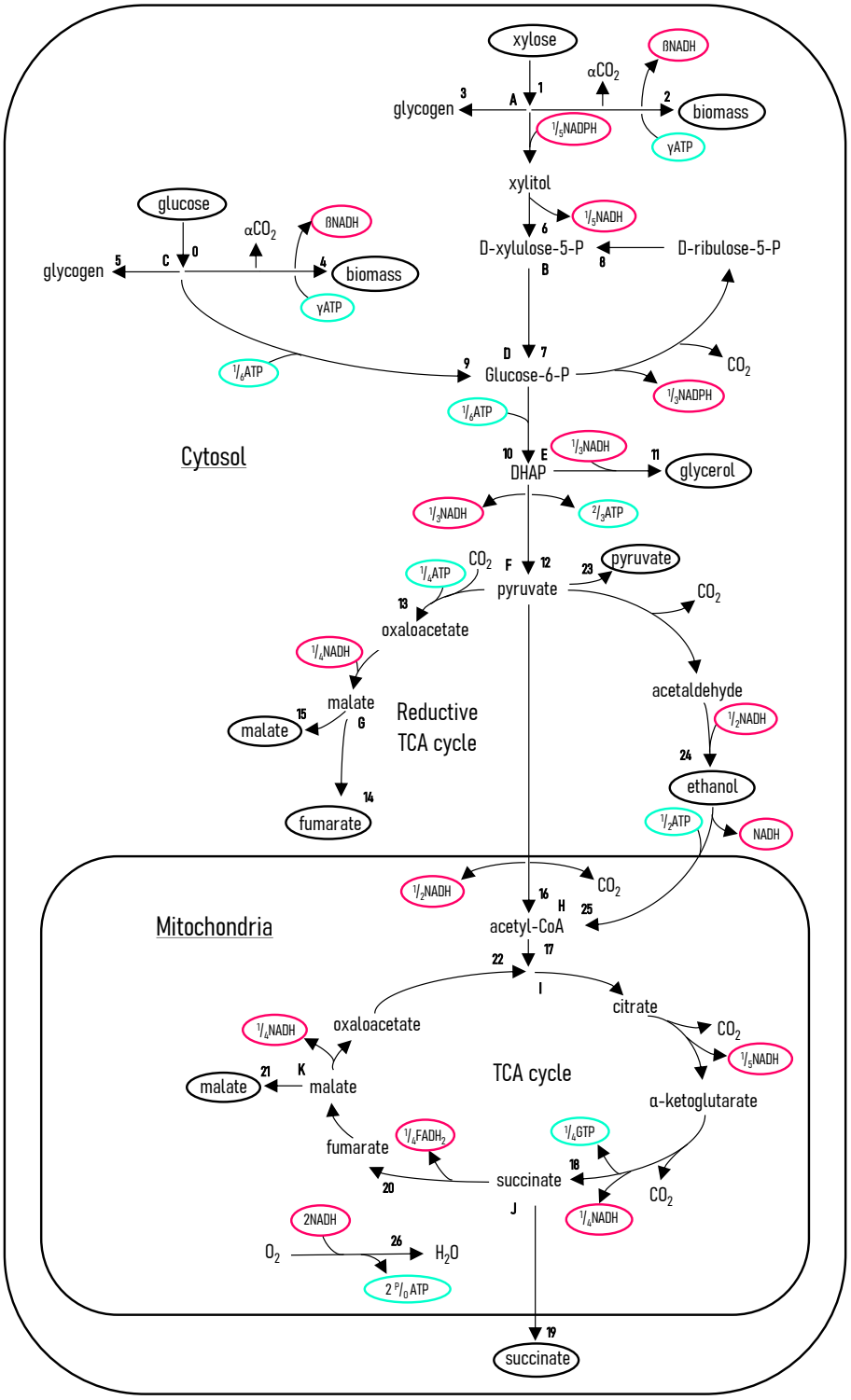

Figure 27: *R. oryzae* metabolic flux model. The metabolic pathways were determined by correlating a number of enzymatic studies of *R. oryzae* [75, 29, 78, 79, 66]. The flux model is written on the basis of carbon moles; this results in the illustrated fractional amounts of the energy-related compounds. The compounds that are either substrates or metabolites are circled in black.

6.3 Results and Discussion

All the fermentations began with the same batch growth of biomass with excess nitrogen. The glucose concentration was used to achieve the correct thickness and covering of biomass on the polypropylene tube [32]. Once all the glucose was consumed, as indicated by online CO_2 production rates, the medium was drained, and the reactor was then rinsed and filled with the respective production medium in order to remove nitrogen from the reactor and induce the production of fumaric acid. The production fermentations were operated at pH 4, with a constant addition of urea at $0.625\,\mathrm{mg\,L^{-1}\,h^{-1}}$. These variables were found to greatly affect the production of fumaric acid, with the values being the optimum operating conditions as found in Chapter 5.

To investigate the feasibility of fumaric acid production with a lignocellulosic hydrolysate, it was first necessary to understand the metabolism of xylose and a glucose–xylose mixture. We conducted batch fermentations of glucose, xylose, and then a 50% glucose–xylose mixture that simulated lignocellulosic hydrolysate. The total sugar concentration for these fermentations was $20\,\mathrm{g\,L^{-1}}$. Figure 28 shows the batch fermentation of glucose. It can be seen that the major products were fumaric acid and ethanol. The minor products of malic acid, succinic acid, and pyruvic acid reached maximum concentrations of $0.83\,\mathrm{g\,L^{-1}}$, $0.37\,\mathrm{g\,L^{-1}}$, and $0.137\,\mathrm{g\,L^{-1}}$, respectively.

The production rate of fumaric acid and ethanol proved to be equivalent during the first 10 h of the fermentation, producing large amounts of ethanol—which is unfavourable. This production of ethanol was induced by the high glucose concentration. *R. oryzae* has been found to be a Crabtree-positive organism, producing ethanol under fully aerobic conditions — as illustrated in Chapter 4. Ethanol is an unwanted by-product because it decreases the yield of fumaric acid and complicates the downstream separation and processing. Although ethanol can be assimilated and metabolised, no fumaric acid is produced from it. Fumaric acid is produced by *R. oryzae* through a reductive tricarboxylic acid (TCA) cycle that is present in the cytosol [29]. Ethanol is likely consumed by its conversion to acetate—and afterwards to acetyl-CoA—from where it can be consumed by the TCA-cycle for the production of energy. Therefore, it offers no benefit to the production of fumaric acid.

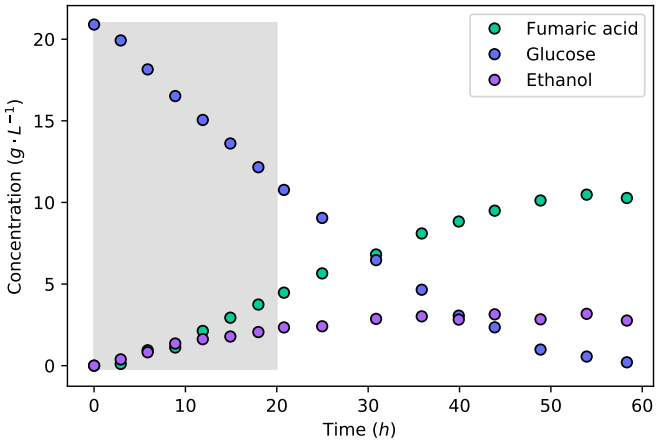

Figure 28: The concentration profiles for a batch fermentation of a $20\,\mathrm{g\,L^{-1}}$ glucose solution. The shaded area indicates the 20 h interval used for metabolic flux calculations further on.

Using the equations and integration method outlined in Section 5.2.4, the effect of the dilution rate was accounted for to accurately determine the consumption and production rates of the organism. For the batch fermentation of glucose, the final accumulative yield of fumaric acid from glucose was $0.553\,\mathrm{g\,g^{-1}}$. The yield of ethanol was found to be $0.191\,\mathrm{g\,g^{-1}}$, which is a large yield for an unwanted by-product. It has been found that the production of ethanol could be avoided by carefully throttling the glucose feed rate on the reactor, which in turn increases the yield of fumaric acid from glucose up to $0.93\,\mathrm{g\,g^{-1}}$ (Chapter 5). The high yield of ethanol and low yield of fumaric acid in this batch fermentation clearly highlights the advantage of throttling the glucose feed rate in order to avoid the production of ethanol. The overall rate of fumaric acid production was $0.186\,\mathrm{g\,L^{-1}\,h^{-1}}$, and the maximum rate was found to be $0.291\,\mathrm{g\,L^{-1}\,h^{-1}}$. This maximum rate of fumaric acid production with the co-production of ethanol ($0.087\,\mathrm{g\,L^{-1}\,h^{-1}}$) is slightly less than the maximum fumaric acid production rate ($0.304\,\mathrm{g\,L^{-1}\,h^{-1}}$) found in a glucose-limited fermentation where no ethanol was produced [2]. The concentration of biomass and all other parameters were identical between these fermentations. The fumaric acid production can be considered to be equivalent for the two conditions. Because the batch fermentation has an unrestricted glucose intake, the rate of glycolysis increases to a point where the TCA-cycle reaches a limit. The residual carbon that cannot be accommodated through the TCA-cycle or fumaric acid production is directed to the production of ethanol. This illustrates the Crabtree effect.

Comparing the fermentation of glucose to that of xylose, as shown in Figure 29, it can firstly be seen that the duration of fermentation was considerably longer for xylose. Glucose fermentation ended after 58 h, whereas the fermentation of xylose took 166 h for the

same mass of substrate. The average fumaric acid production rate was $0.073\,\mathrm{g\,L^{-1}\,h^{-1}}$, and the maximum rate achieved was $0.145\,\mathrm{g\,L^{-1}\,h^{-1}}$. Comparing the average production rates, the production rate of fumaric acid from xylose is 60.8% lower than that from glucose.

The metabolism of xylose is largely different to that of glucose. Xylose has to be catabolised to xylitol, then D-xylulose, and followed by D-xylulose-5-P, which enters the Pentose phosphate pathway from which D-glucose-6-P is produced; this is the start of glycolysis [75]. This is a longer pathway compared to the catabolism of glucose, which undergoes a single enzymatic step to produce D-glucose-6-P. These additional enzymatic steps required for the catabolism of xylose are likely the cause of the slow xylose utilisation and fumaric acid production. In a study on xylose utilisation by a recombinant *Saccharomyces cerevisiae*, it was found that the enzymatic route of xylose to glycolysis was the rate-limiting step which resulted in inefficient metabolism affecting the energy balance of the cell [99].

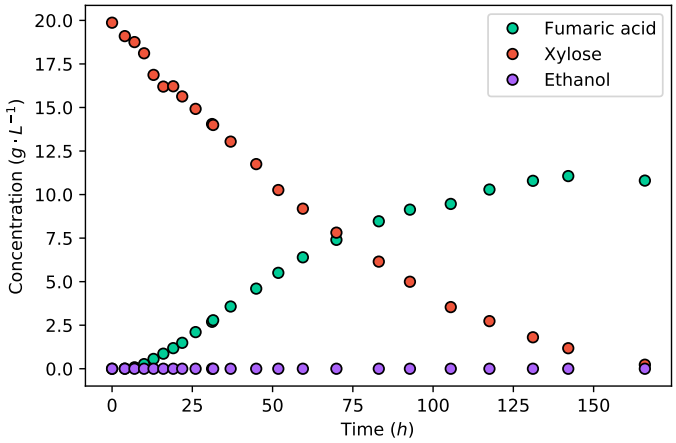

Figure 29: The concentration profiles of a batch fermentation of a $20\,\mathrm{g\,L^{-1}}$ xylose solution.

However, it can be seen in Figure 29 that there is no ethanol produced from xylose. This is a result of the lower glycolytic flux, which does not saturate the metabolism. All carbon can be accommodated by the reductive TCA cycle, producing fumarate, and the TCA cycle; therefore, no ethanol is produced as an overflow. The final accumulative yield of fumaric acid on xylose is $0.682\,\mathrm{g\,g^{-1}}$, which is considerably higher than that found for glucose (Figure 28). The increased yield was caused by the lack of ethanol production. This yield is also the highest yield of fumaric acid from xylose that has been reported in the literature—an improvement resulting from the operating conditions used. All the fermentations in the literature used $CaCO_3$ for pH control, which did not provide the optimal pH, and the carbon–nitrogen ratio was insufficiently controlled. These results

indicate that xylose can be a promising substrate for the production of fumaric acid. However, the co-fermentation of xylose and glucose is of key importance.

Figure 30 shows the concentration profiles of the fermentation of the synthetic lignocellulosic hydrolysate. Glucose is metabolised preferentially over xylose—in the first 21 h, glucose was consumed at a rate of $0.398\,\mathrm{g\,L^{-1}\,h^{-1}}$, while there was no consumption of xylose. This illustrates carbon catabolite repression (CCR), a well-known phenomenon that prioritises the most energy efficient substrate in a mixture and leads to a diauxic or two-phase utilisation of the substrate [89]. Once the glucose concentration was depleted, xylose consumption began and increased to a rate of $0.116\,\mathrm{g\,L^{-1}\,h^{-1}}$. In the pure substrate fermentations, the average rates of glucose and xylose consumption were $0.337\,\mathrm{g\,L^{-1}\,h^{-1}}$ and $0.107\,\mathrm{g\,L^{-1}\,h^{-1}}$, respectively. Thus, it can be seen that the catabolism of glucose was uninhibited by the presence of xylose; only after the complete consumption of glucose did xylose catabolism reach its full capability. The effect of the two-stage substrate utilisation could be plainly seen in the concentration profile of fumaric acid. While glucose was being consumed, the production rate was at $0.247\,\mathrm{g\,L^{-1}\,h^{-1}}$, which then dropped to $0.063\,\mathrm{g\,L^{-1}\,h^{-1}}$ once only xylose was remaining. It can, however, be seen that the ethanol produced during the catabolism of the glucose is now being consumed during the consumption of xylose.

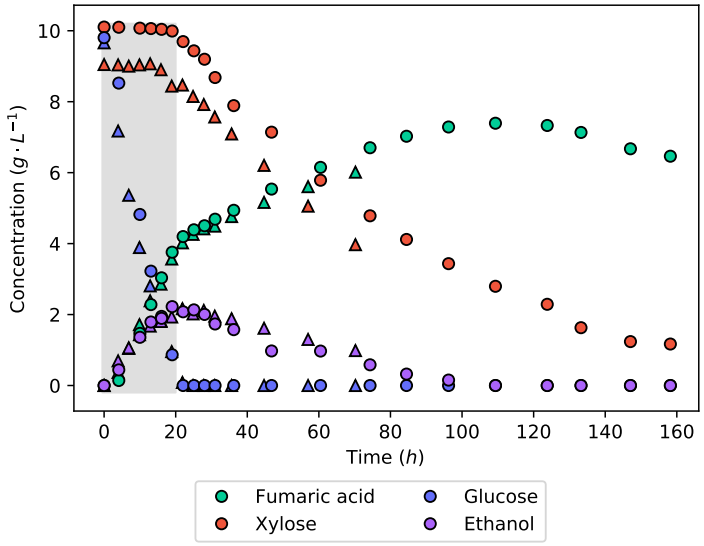

Figure 30: The concentration profiles of a $20\,\mathrm{g\,L^{-1}}$ 50% glucose and xylose batch fermentation. Two sets of concentration profiles can be seen: one shown with circles and the repeat shown with triangles. Good repeatability is demonstrated as the profiles follow near identical trends. The shaded area indicates a 20 h interval used for metabolic flux calculations further on.

The fumaric acid yield from the synthetic LH batch fermentation is $0.439\,\mathrm{g\,g^{-1}}$, which is considerably lower than the yields obtained from either of the pure substrate fermenta-

tions. This value is well within the range found in the literature [55, 88, 59, 63]. The reason for this lower yield is likely a result of the co-fermentation of glucose and xylose. Different metabolic pathways are used to metabolise glucose and xylose; for this reason, the co-fermentation would require the production of more enzymes than necessary if only a single substrate was consumed. It can also be seen that ethanol is produced while glucose is being consumed, certainly contributing to the decreased fumaric acid yield. To make the production of fumaric acid from lignocellulosic hydrolysate viable, the yield will have to be improved. It has been found that minimising the medium glucose concentration negates the production of ethanol and drastically improves the yield of fumaric acid [1].

An effective method of controlling the glucose concentration is by beginning the production fermentation with a medium void of glucose. All glucose is then fed at a specific rate that is equal to the consumption rate. This allows for the rate of glycolysis to be controlled, and we thus have the ability to negate the production of ethanol. Figure 31a–c shows the concentration profiles and substrate feed rate of the fermentation, where a 50% glucose–xylose mixture was continuously fed into the reactor. The fermentation began at a substrate feed rate ($0.132\,\mathrm{g\,L^{-1}\,h^{-1}}$) where an equivalent glucose feed rate did not produce any ethanol [1]. It can be seen that for 48 h, there was no production of ethanol; meanwhile, fumaric acid was still being produced. The substrate feed rate was then stepped up to $0.197\,\mathrm{g\,L^{-1}\,h^{-1}}$, immediately triggering the production of ethanol.

This indicates that the ethanol breakthrough rate is between $0.132\,\mathrm{g\,L^{-1}\,h^{-1}}$ and $0.197\,\mathrm{g\,L^{-1}\,h^{-1}}$. In pure glucose fermentations under the same conditions, it has been found that the ethanol breakthrough rate is between $0.263\,\mathrm{g\,L^{-1}\,h^{-1}}$ and $0.329\,\mathrm{g\,L^{-1}\,h^{-1}}$ [2]. The lessening of the ethanol breakthrough point is an unexpected effect, especially since it can be seen from the pure xylose fermentation (Figure 29) that no ethanol was produced. Ethanol is produced as a result of metabolite overflow (Crabtree effect), or for the production of energy. Adenosine triphosphate (ATP) levels have been found to decrease in the fermentation of xylose as compared to that of glucose [99]. Therefore, the production of ethanol is likely a response to the lower ATP levels, causing glucose to be directed to ethanol in order to produce nicotinamide adenine dinucleotide (NADH) at a faster rate. Although the production of NADH from ethanol is less efficient, it is faster than the TCA cycle [14].

It can also be seen in Figure 31c that there is an accumulation of xylose from the lowest feed rate. There was, however, the complete consumption of glucose at all the feed rates tested. This results from CCR, where glucose is consumed preferentially over xylose. Using a 24 h running average at the end of the feed rate, it was found that xylose was consumed at a rate of $0.052\,\mathrm{g\,L^{-1}\,h^{-1}}$, translating to 72.8% of the xylose fed being con-

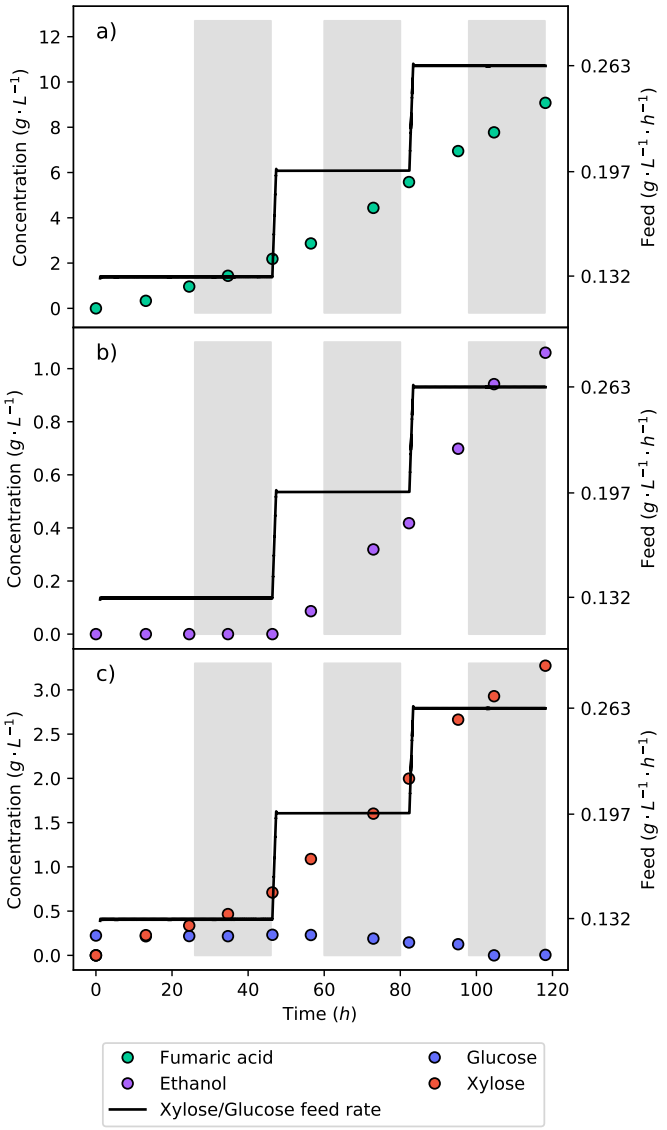

Figure 31: The continuous fermentation of a 50% glucose–xylose mixture. (**a**) The concentration profile of fumaric acid. (**b**) The concentration profile of ethanol. (**c**) The concentration profiles of glucose and xylose. The plot shows the feed strategy of the synthetic lignocellulosic hydrolysate in the reactor and the response of the metabolism to the change in substrate feed rate.

sumed. As the substrate feed rate was increased, the consumption rate of xylose also increased. Because the proportion of glucose to xylose in the feed remained constant, it can be seen that a higher glucose consumption rate enabled a higher xylose consumption rate. This was likely concurrent with the production of ethanol from the glucose, which provided more NADH. The production of ethanol is not a result of xylose accumulation since no ethanol was produced from the batch xylose fermentation.

The calculated yield of fumaric acid produced from the substrate—consumed after the first 48 h and at a feed rate of $0.132\,\mathrm{g\,L^{-1}\,h^{-1}}$ where no ethanol was produced—was found to be only $0.425\,\mathrm{g\,g^{-1}}$. The low yield is a result of a large portion of the substrate being directed to the TCA cycle for cell maintenance. The feed rates of $0.197\,\mathrm{g\,L^{-1}\,h^{-1}}$ and $0.263\,\mathrm{g\,L^{-1}\,h^{-1}}$ achieved yields of $0.693\,\mathrm{g\,g^{-1}}$ and $0.483\,\mathrm{g\,g^{-1}}$, respectively. This shows an initial increased yield with an increase in the feed rate. However, there is the production of ethanol. It has been found that the fumaric acid yield increases with an increased feed rate up to the point of ethanol breakthrough [2], after which the yield decreases. A feed rate of $0.164\,\mathrm{g\,L^{-1}\,h^{-1}}$ was selected as a half-way point between $0.132\,\mathrm{g\,L^{-1}\,h^{-1}}$ and the upper point of ethanol breakthrough ($0.197\,\mathrm{g\,L^{-1}\,h^{-1}}$). The feed rate was tested for 48 h and is shown in Figure 32 by the triangular markers. Figure 32b shows that for the entire fermentation, no ethanol was produced; this indicates that the ethanol breakthrough point lies between $0.164\,\mathrm{g\,L^{-1}\,h^{-1}}$ and $0.197\,\mathrm{g\,L^{-1}\,h^{-1}}$. By negating ethanol production, the fumaric acid yield obtained at the end of the fermentation increased to $0.72\,\mathrm{g\,g^{-1}}$.

Utilising the information gathered from the continuous fermentations where the feed rate was stepped, a strategy was hypothesised to increase the fumaric acid yield on a lignocellulosic hydrolysate feed. The production of ethanol can be avoided by controlling the feed rate on the reactor; all the glucose will be consumed, and the xylose will be allowed to accumulate. Once all the substrate has been fed, the substrate feed will be stopped, and the accumulated xylose will then be allowed to be metabolised. The same mass of substrate feed in the batch fermentations ($20\,\mathrm{g\,L^{-1}}$) will be fed over the course of the fermentation. Figure 32 shows this fermentation.

For the first 24 h, the feed rate was at $0.132\,\mathrm{g\,L^{-1}\,h^{-1}}$, allowing for the organism to adapt and for an inter-run comparison to be conducted. The feed rate was then increased to $0.164\,\mathrm{g\,L^{-1}\,h^{-1}}$ for the remainder of the run until all the substrate had been fed. In Figure 32, it can be seen that the feed strategy was successful: no ethanol was produced, and once the feed rate stopped, the accumulated xylose was consumed. The fermentation was terminated once the production of fumaric acid ceased. The overall fumaric acid yield on the synthetic lignocellulosic hydrolysate feed was $0.735\,\mathrm{g\,g^{-1}}$. Considering that the batch fermentation shown in Figure 30 has the same mass of substrate feed but a fumaric acid yield of $0.439\,\mathrm{g\,g^{-1}}$, the benefit of controlling the metabolism is clear. Manipulating

the substrate feed rate achieved a 67.4% improvement of the fumaric acid yield. The increased yield is a result of the negated ethanol production and the optimal metabolic flux that selects for the production of fumaric acid.

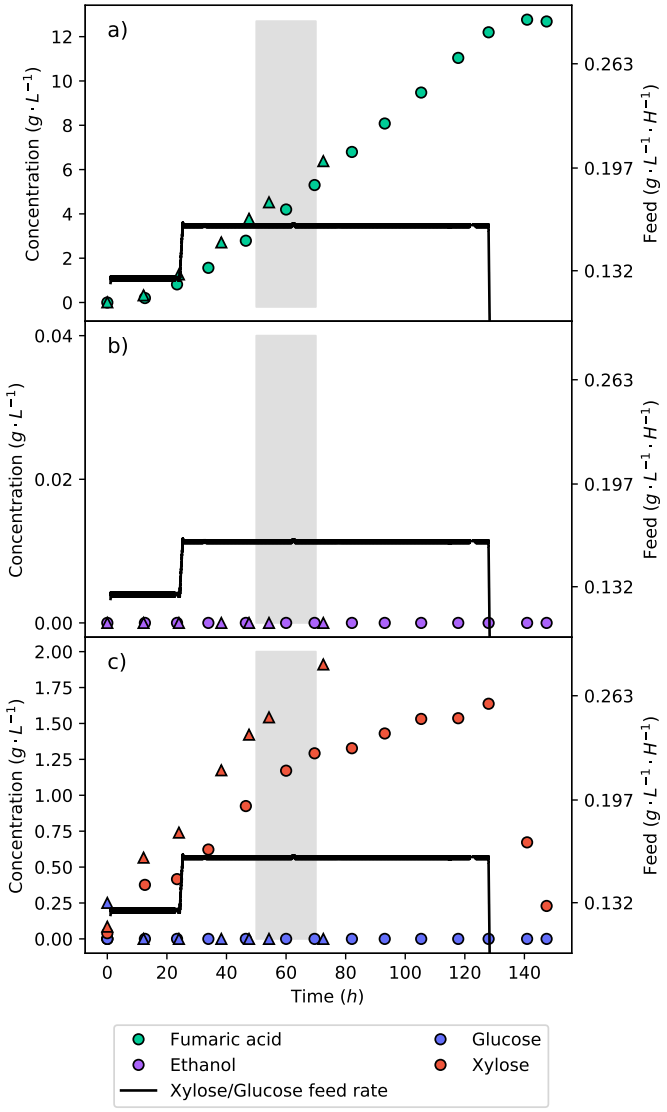

Figure 32: The continuous fermentation of a 50% glucose–xylose mixture fed at a rate of $0.164\,\mathrm{g\,L^{-1}\,h^{-1}}$. Two sets of concentration profiles can be seen: one shown with triangles (a preliminary fermentation) and the other shown with circles, which received $20\,\mathrm{g\,L^{-1}}$ of substrate over the fermentation. Good repeatability is demonstrated since the profiles follow nearly identical trends. The shaded area indicates a 20 h interval used for metabolic flux calculations further on. (**a**) The concentration profile of fumaric acid. (**b**) The concentration profile of ethanol. (**c**) The concentration profiles of glucose and xylose.

It was then considered whether a higher feed rate would produce a higher yield, as was later found by increasing the feed rate from $0.132\,\mathrm{g\,L^{-1}\,h^{-1}}$ to $0.164\,\mathrm{g\,L^{-1}\,h^{-1}}$. This increased the selectivity of carbon directed to fumaric acid. It was found that this relationship holds up to a glucose feed rate of $0.329\,\mathrm{g\,L^{-1}\,h^{-1}}$, which vastly improves the

fumaric acid yield [2]. At this glucose feed rate, a fumaric acid yield of $0.93\,\mathrm{g\,g^{-1}}$ was achieved.

A fermentation of synthetic LH with this feed rate was then conducted, as shown in Figure 33. The feed rate was stepped up to $0.329\,\mathrm{g\,L^{-1}\,h^{-1}}$ after the first 24 h. The same mass of substrate ($20\,\mathrm{g\,L^{-1}}$) was to be fed; since the feed rate was far higher, this implied that the substrate would be delivered over a shorter period of time. Figure 33c shows that there was a considerable accumulation of xylose as a result of the high feed rate, which also had a clear effect on the production of ethanol (Figure 33b). In contrast, the glucose concentration remained low, indicating that the feed rate was matched by the rate of consumption. It can be seen that the production of fumaric acid slowed down and then ceased 24 h later, after the feed rate halted (Figure 33a). This can also be seen in the lower feed rate fermentation in Figure 32, suggesting that the organism adapted to the co-fermentation of glucose and xylose in order to produce fumaric acid. Once glucose was no longer present, the production of fumaric acid stopped. The yield could be further improved if one were able to avoid xylose accumulation. However, this would require the ratio of glucose and xylose to be tailored to the respective uptake rates, and this may not be possible with a hydrolysate. Table 4 summarises the crucial results from the fermentations with equivalent amounts of substrate. It can plainly be seen that the fermentation with the lower LH feed rate that avoided ethanol production outperformed the other strategies.

Table 4: Determining the effect of substrate and fermentation strategy on the yields, rates, and fermentation time. The following subscripts were used: S–substrate, F–fumaric acid, E–ethanol, G–glucose, and X–xylose.

Run	Y_{SF} †	Y_{SE} †	$r_{F,max}$ *	$r_{F,avg}$ *	$r_{G,avg}$ *	$r_{X,avg}$ *	Run Time (h)	Mass Balance Error (%)
Glucose batch	0.553	0.191	0.291	0.186	0.337	-	58.47	4.80
Xylose batch	0.682	0	0.145	0.073	-	0.107	166.05	5.60
LH batch	0.439	0.133	0.253	0.047	0.451	0.048	159.04	3.62
LH High feed rate	0.583	0.07	0.178	0.061	0.129	0.048	177.66	9.85
LH Low feed rate	0.735	0	0.146	0.096	0.076	0.066	148.40	9.25

† Accumulative yield over the run ($\mathrm{g\,g^{-1}}$). * Maximum rate calculated over a 12 h interval or the average rate over the entire run ($\mathrm{g\,L^{-1}\,h^{-1}}$).

Considering the repeatability of the fermentations presented, as visible in Figure 30, a duplicate of the fermentation was conducted. When comparing these two data sets, it can be seen that they are identical with all species following the same concentration profiles. Although the duplicate fermentation did not run to completion, it can still be

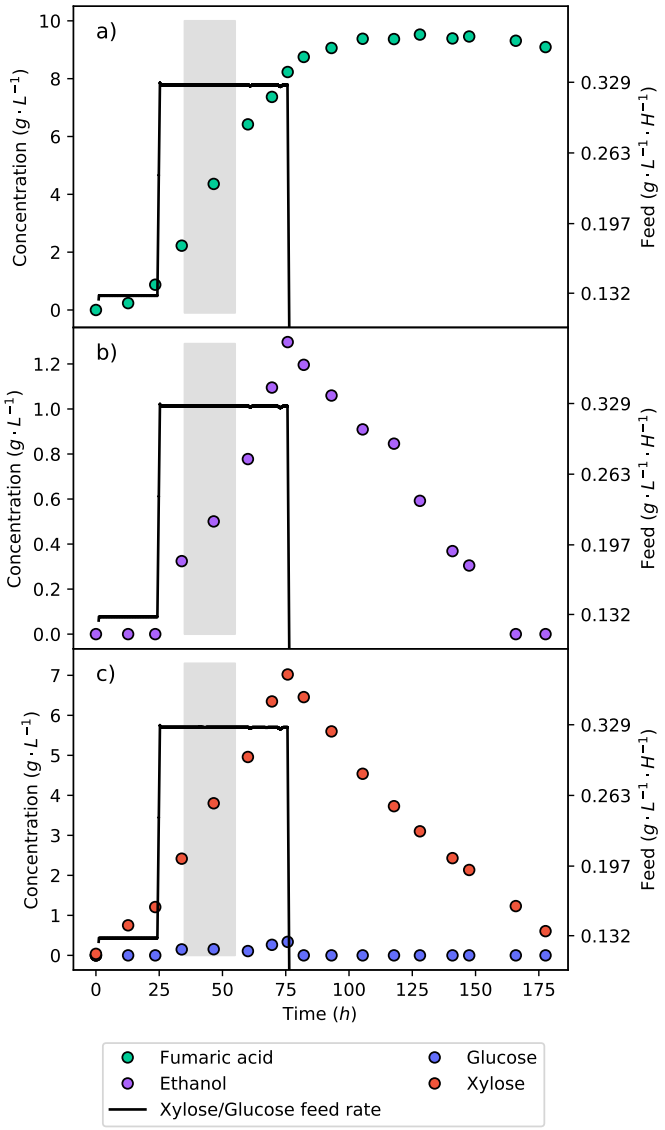

Figure 33: The continuous fermentation of a 50% glucose–xylose mixture at a feed rate of $0.329\,\mathrm{g\,L^{-1}\,h^{-1}}$. The shaded area indicates a 20 h interval used for metabolic flux calculations further on. (**a**) The concentration profile of fumaric acid. (**b**) The concentration profile of ethanol. (**c**) The concentration profiles of glucose and xylose.

said that the result is repeatable. The repeatability of the continuous fermentations has been proven in previous studies [1, 2]; however, it will be discussed here for consistency.

All continuous fermentations were operated with the same conditions and substrate feed rate ($0.132\,\mathrm{g\,L^{-1}\,h^{-1}}$) for the first 24 h. Comparing the fumaric acid concentrations at the end of the 24 h, the mean was found to be $0.980\,\mathrm{g\,L^{-1}}$, with a standard deviation of 0.200; this resulted in a coefficient of variance of 0.204, which proves repeatability. For the 24 h duration of each of these runs, ethanol was expectedly not produced because the feed rate of $0.132\,\mathrm{g\,L^{-1}\,h^{-1}}$ was below the ethanol breakthrough point. This illustrates that the organism was operating in the same metabolic state for all four fermentations.

Using the procedure outlined in Section 6.2.4, a mass balance was conducted over each of the fermentations in order to be certain that all the metabolites were accounted for. The mass balance compared the carbon added to the system to the sum of all the metabolites produced. It was found that the mass balance error for all the fermentations was less than 10%, indicating that the majority of the metabolites were accounted for. Table 4 reports the errors for the specific runs. The errors found are possibly a result of the outlet CO_2 flow rate that had to be assumed and could not be directly measured.

To gain further insight into the metabolism of *R. oryzae*, a metabolic flux model was developed for the metabolism of glucose and xylose. The metabolic flux model was verified by comparing the predicted CO_2 rates to that obtained from a mass balance. It was found that the metabolic flux model predicted the CO_2 production rates accurately, using the other known metabolite rates as input. Figure 27 shows the metabolic pathways determined for *R. oryzae*, metabolising glucose and xylose for the predominant production of fumaric acid, ethanol, and CO_2. The flux model was then solved for specific intervals, shown on the previous figures as shaded areas.

The flux model was solved with carbon balances as well as with NADH and NADPH balances. Further information on the development of the metabolic flux model and specific constants determined for *R. oryzae* are described in Section 6.2.5. Figure 34 shows the metabolic rates determined from the flux model for the batch fermentation of glucose (Figure 28), synthetic LH (Figure 30), and the optimal glucose continuous feed fermentation (Figure 24). The result of a high glucose concentration is clearly demonstrated.

In Figure 34a, it can be seen that the glucose uptake rates of both the pure glucose batch fermentation and the synthetic LH fermentation are equivalent. As a result of CRC, only glucose is consumed in the synthetic LH fermentation, indicating that xylose has no effect on the metabolism. It was found that the optimal glucose feed rate was below this maximum glucose uptake rate. Figure 34b shows the glycolytic flux of carbon to pyruvate; this is the metabolic pathway after which the flux is split between the TCA cycle, fumaric

acid production, and ethanol production. It can be seen that the glycolytic flux for both of the batch fermentations is higher than that of the continuous fermentation. Now, by comparing the ethanol production rates, it can be seen that the optimal glucose feed rate produced considerably less ethanol. This suggests that the production of ethanol is a result of a glycolytic threshold being surpassed. Once the glycolytic threshold has been passed, the proportion of carbon directed to ethanol increases, while fumaric acid production decreases. Operating below this glycolytic threshold improves both the yield and the rate of fumaric acid production.

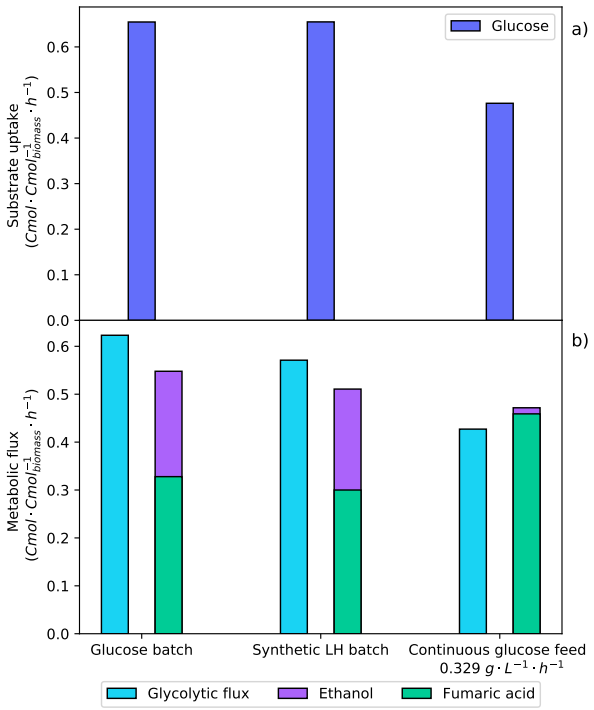

Figure 34: Metabolic flux rates determined for the batch glucose fermentation (Figure 28), the synthetic LH batch fermentation (Figure 30), and the optimal continuous glucose-fed fermentation [2]. The averaged metabolite rates from the shaded regions of these specific fermentations were used to solve the metabolic flux analysis. (**a**) The metabolic uptake rates of glucose and xylose (no xylose was consumed during these intervals). (**b**) The metabolic flux of carbon through the glycolytic pathway and the production rates of fumaric acid and ethanol.

The metabolic flux model was solved for each of the feed rates tested for the continuous synthetic LH fermentations. Figure 35 shows the metabolic fluxes determined. The co-fermentation of glucose and xylose can be seen for each of the feed rates in Figure 35a. A comparison of the glucose and xylose uptake rates shows a visible proportionality between the rates. An R^2 value of 0.983 was found for the first four substrate feed rates between $0.132\,\mathrm{g\,L^{-1}\,h^{-1}}$ and $0.263\,\mathrm{g\,L^{-1}\,h^{-1}}$. This is contrary to what was seen in the synthetic LH batch fermentation, where CRC resulted in the preferential consumption of glucose over xylose. The correlation of the glucose and xylose rates—considering that

there was xylose accumulation at each feed rate—suggests that there is a dependency of xylose on glucose. An increased glucose feed rate enables a higher xylose uptake rate. Considering the feed rate of $0.329\,\mathrm{g\,L^{-1}\,h^{-1}}$, it can be seen that the proportionality between the glucose and the xylose rates no longer holds. The glucose consumption rate has increased proportionally with the increased feed rate; however, the rate of xylose uptake decreased. Considering the glycolytic flux in Figure 35b for the substrate feed rates of $0.263\,\mathrm{g\,L^{-1}\,h^{-1}}$ and $0.329\,\mathrm{g\,L^{-1}\,h^{-1}}$, it can be seen that they are equivalent rates. This suggests an upper limit for the glycolytic flux during the co-fermentation of glucose and xylose. Once the upper limit is reached, glucose is used preferentially over xylose, which results in a decreased xylose consumption rate.

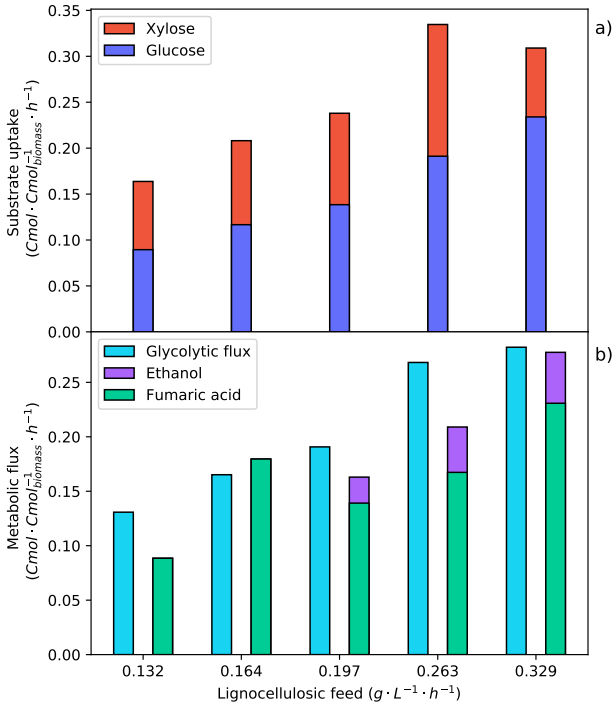

Figure 35: Metabolic flux rates determined for the specific synthetic LH feed rates that were indicated by the shaded intervals in Figures 31–33. The averaged metabolite rates from the shaded regions of the specific feed rates were used to solve the metabolic flux analysis. (**a**) The metabolic uptake rate of glucose and xylose. (**b**) The metabolic flux of carbon through the glycolytic pathway and the production rates of fumaric acid and ethanol.

In Figure 35b, a feed rate of $0.164\,\mathrm{g\,L^{-1}\,h^{-1}}$ is shown to be the optimum, directing the highest fraction of carbon consumed to fumaric acid. The feed rate below ($0.132\,\mathrm{g\,L^{-1}\,h^{-1}}$) has a high fraction that is directed to the TCA cycle, which results in a low fumaric acid yield. This low yield is overcome when the feed rate is increased, and the fraction of carbon directed to the TCA cycle accordingly decreases. The higher feed rate ($0.197\,\mathrm{g\,L^{-1}\,h^{-1}}$) surpasses an upper threshold of the glycolytic flux and induces the production of ethanol, decreasing both the yield and the rate of fumaric acid produc-

tion. Comparing the glycolytic flux at which the ethanol breakthrough occurs for the pure glucose fermentation (Figure 34b) and that of the synthetic LH fermentations (Figure 35b), it can be seen that ethanol production starts at a lower glycolytic flux during the co-fermentation of glucose and xylose. This suggests some effect that xylose has on the glycolytic flux and supports the evidence indicating that xylose causes an inefficient metabolic state, which in turn affects the energy balance [99]. This energy imbalance would explain why the ethanol breakthrough occurs at a lower substrate uptake rate.

6.4 Conclusion

The production of fumaric acid from glucose is a well-studied topic, whereas the more industrially viable option of using lignocellulosic hydrolysate has had little attention. Utilising an immobilised bioreactor and optimal medium conditions, the use of xylose and a synthetic lignocellulosic hydrolysate for the production of fumaric acid was studied. The highest known yield of fumaric acid on xylose was achieved ($0.682\,\mathrm{g\,g^{-1}}$) in a batch fermentation, which was attributed to the closely controlled and optimal medium conditions. In a batch fermentation of the synthetic lignocellulosic hydrolysate, it was found that the high concentration of glucose induced an overflow mechanism, causing ethanol production which greatly affected the yield ($0.439\,\mathrm{g\,g^{-1}}$). By making use of continuous fermentation with a low feed rate ($0.164\,\mathrm{g\,L^{-1}\,h^{-1}}$) for the glucose-xylose mixture, the metabolism was controlled at an optimum point in order to select for the production of fumaric acid and simultaneously negate ethanol production. This greatly improved the fumaric acid yield on the substrate to $0.735\,\mathrm{g\,g^{-1}}$. These findings are a step towards the viable production of fumaric acid through a renewable and environmentally sustainable process. Future work should focus on investigating the use of authentic lignocellulosic hydrolysate.

7 Conclusion

Fumaric acid performs crucial roles in multiple industries, owing to its versatile chemical structure. The shift toward renewable industrial production methods will have to be adopted in all sectors to curb the current climate change — production of fumaric acid forms a crucial part of the shift. The current production of fumaric acid is reliant on the petrochemical industry which produces copious amounts of CO_2. The biorefinery has been suggested as an alternative to the crude oil refinery, substituting the crude oil feed stock for renewable biomass. The goal is to move towards renewable methods while still producing the required chemicals.

R. oryzae fits neatly into the biorefinery as it is the most promising organism to convert biomass derived sugars to fumaric acid. Since its first discovery in 1895 much research has been conducted with *R. oryzae* on the production of fumaric acid. It has focused on shake flask batch fermentations. These fermentations were conducted with a pellet morphology of *R. oryzae* which rely on shake flask conditions to form and is thus inconvenient for industrial production. An immobilised morphology provides lower cost operation as well as simpler separation of the biomass and production medium.

The by-production of ethanol during fumaric acid production was also a major stumbling block for the industrial use of *R. oryzae*. Many authors attributed this to anaerobic zones that formed in the fugal mycelium. Nevertheless, ethanol production was never removed from the *R. oryzae* fermentations.

This thesis aimed to address many of the issues with *R. oryzae* fermentations that are limiting its use as a microbial cell factory for the production of fumaric acid. The first part of the research simulated the presence of anaerobic zones in the mycelium. Conducting fermentations at different DO concentrations produced equivalent ethanol concentrations, proving that oxygen availability was not the cause of ethanol production. It was hypothesised that *R. oryzae* was a Crabtree positive organism, producing ethanol because of a carbon overflow that cannot be accommodated by a limited respiratory capacity. Fermentations were subsequently conducted that systematically increased the glucose feed rate to the system and thereby controlled the glycolytic flux of the organism. It was discovered that ethanol production could be completely negated with a glucose feed rate of $0.197\,\mathrm{g\,L^{-1}\,h^{-1}}$, producing fumaric acid at a rate of $0.158\,\mathrm{g\,L^{-1}\,h^{-1}}$ — a yield of $0.802\,\mathrm{g\,g^{-1}}$.

The pH of the medium was established to be an important parameter in *R. oryzae* fermentations. The organism is particularly sensitive to changes in the pH and therefore during fumaric production the medium has to be continually titrated to maintain the

pH. The neutralised medium has to be re-acidified to remove the fumaric acid in downstream processing — one of the largest costs of fumaric acid production with *R. oryzae*. Fermentations were performed at three different pH's for a range of glucose feed rates. It was discovered that pH 4 greatly improved the glucose uptake and yield of fumaric acid, achieving a yield of $0.93\,\mathrm{g\,g^{-1}}$ fumaric acid on glucose. Operating at pH 4 has the added benefit of decreased neutralising costs since fumaric acid is considerably less dissociated at lower pHs and can even be present as solid acid depending on the operating conditions.

Fumaric acid production has always been closely associated with the nitrogen content of the medium. Cytosolic fumarase, the enzyme responsible for fumaric acid production, has been established as incredibly sensitive to the nitrogen content of the medium. The urea cycle has also been found to be overexpressed during the production of fumaric acid, linking fumaric acid production to nitrogen-starved medium conditions. Additionally, it was discovered that a continuous low feed of urea to production fermentations was crucial to the longevity and stability of fumaric acid production. In this study the feed rate of urea during production fermentations was varied. It was found that a $0.625\,\mathrm{mg\,L^{-1}\,h^{-1}}$ urea feed rate balanced the point of ethanol production and the maximum glucose uptake to achieve the optimum fumaric acid production.

Research into the production of fumaric acid has largely used glucose as the substrate. Industrially this would encroach on the food sector and should be avoided. An alternative and more renewable feed stock is lignocellulosic hydrolysate. Commonly a waste stream, lignocellulosic biomass can be hydrolysed to form a mixture of fermentable sugars. In order to test the viability of this feedstock for fumaric acid production a synthetic glucose-xylose mixture was fermented. It was found that a batch fermentation of the mixture provided a particularly poor yield of fumaric acid ($0.439\,\mathrm{g\,g^{-1}}$). The poor yield was attributed to ethanol production.

Using the substrate feed strategy developed earlier, a glucose-xylose mixture was fed at various feed rates to elucidate the effect on fumaric acid production. The point at which ethanol breakthrough occurs was discovered to be at a lower substrate feed rate than that of a pure glucose feed. This effect was attributed to the catabolism of xylose which caused an energy imbalance in the cell resulting in ethanol production. However, an optimum feed rate was identified that negated ethanol production ($0.164\,\mathrm{g\,L^{-1}\,h^{-1}}$); this feed rate also avoided carbon catabolite repression allowing for co-fermentation of glucose and xylose. The final yield achieved was $0.735\,\mathrm{g\,g^{-1}}$ fumaric acid on the synthetic lignocellulosic hydrolysate — a substantial improvement.

The results presented in this thesis have all been published, Chapter 4 was published in *Biotechnology for Biofuels* [1], Chapter 5 was published in *Catalysts* [2] and Chapter 6

was published in *Fermentation* [3].

This work clearly shows the viable industrial potential for fumaric acid production with *R. oryzae*. Important factors in the production of fumaric acid with *R. oryzae* that still need attention include the fermentation of a real lignocellulosic hydrolysate, optimisation of xylose metabolism and the effect of high titre fermentations. Further research would have to be done on the economic feasibility before such a project could be realised. Larger scale fermentations would also have to be done to investigate how *R. oryzae* would be immobilised in an industrial vessel, as well as how the production parameters optimised in this study translate to different fermenters.

References

[1] RM Swart, F Le Roux, A Naude, NW De Jongh, and W Nicol. "Fumarate production with Rhizopus oryzae: Utilising the Crabtree effect to minimise ethanol by-product formation". In: *Biotechnology for Biofuels* 13.1 (2020), pp. 1–10. ISSN: 17546834. DOI: 10.1186/s13068-020-1664-8. URL: https://doi.org/10.1186/s13068-020-1664-8.

[2] RM Swart, DK Ronoh, H Brink, and W Nicol. "Continuous Production of Fumaric Acid with Immobilised Rhizopus oryzae: The Role of pH and Urea Addition". In: *Catalysts* 12.1 (Jan. 2022), p. 82. ISSN: 2073-4344. DOI: 10.3390/catal12010082. URL: https://www.mdpi.com/2073-4344/12/1/82.

[3] RM Swart, H Brink, and W Nicol. "Rhizopus oryzae for Fumaric Acid Production: Optimising the Use of a Synthetic Lignocellulosic Hydrolysate". In: *Fermentation* 8.6 (June 2022), p. 278. ISSN: 2311-5637. DOI: 10.3390/fermentation8060278. URL: https://www.mdpi.com/2311-5637/8/6/278.

[4] NW de Jongh, RM Swart, and W Nicol. "Fed-batch growth of *Rhizopus oryzae*: Eliminating ethanol formation by controlling glucose addition". In: *Biochemical Engineering Journal* 169.November 2020 (2021). ISSN: 1873295X. DOI: 10.1016/j.bej.2021.107961.

[5] DK Ronoh, RM Swart, W Nicol, and H Brink. "The Effect of pH, Metal Ions, and Insoluble Solids on the Production of Fumarate and Malate by Rhizopus delemar in the Presence of CaCO3". In: *Catalysts* 12.3 (2022). ISSN: 20734344. DOI: 10.3390/catal12030263.

[6] United Nations, Department of Economic and Social Affairs. *Population Division (2019), World population prospects 2019: Highlights*. 141. 2019. ISBN: 9789211483161.

[7] ED Beinhocker, D Farrell, and AS Zainulbhai. "Tracking the growth of India's middle class". In: *McKinsey Quarterly* 3 (2007), pp. 50–61. ISSN: 00475394.

[8] SJ Rose. "The Growing Size and Incomes of the Upper Middle Class". In: *Urban Institute* 21.June (2016), pp. 1–28.

[9] V Masson-Delmotte, P Zhai, A Pirani, S Connors, C Péan, S Berger, N Caud, Y Chen, L Goldfarb, M Gomis, M Huang, K Leitzell, E Lonnoy, J Matthews, T

Maycock, T Waterfield, O Yelekçi, R Yu, and B Zhou. *Climate Change 2021: The Physical Science Basis. Contribution of Working Group I to the Sixth Assessment Report of the Intergovernmental Panel on Climate Change*. Tech. rep. IPCC, 2021. URL: https://www.ipcc.ch/report/ar6/wg1/#SPM.

[10] J Mohtasham. "Review Article-Renewable Energies". In: *Energy Procedia* 74 (2015), pp. 1289–1297. ISSN: 18766102. DOI: 10.1016/j.egypro.2015.07.774. URL: http://dx.doi.org/10.1016/j.egypro.2015.07.774.

[11] JJ Bozell and GR Petersen. "Technology development for the production of biobased products from biorefinery carbohydrates - The US Department of Energy's "top 10" revisited". In: *Green Chemistry* 12.4 (2010), pp. 539–554. ISSN: 14639262. DOI: 10.1039/b922014c.

[12] T Werpy and G Petersen. *Top Value Added Chemicals from Biomass: Volume I – Results of Screening for Potential Candidates from Sugars and Synthesis Gas*. Tech. rep. Golden, CO (United States): National Renewable Energy Laboratory (NREL), Aug. 2004, p. 76. DOI: 10.2172/15008859. URL: http://www.osti.gov/scitech//servlets/purl/15008859-s6ri0N/native/%20http://www.osti.gov/servlets/purl/15008859/.

[13] JW Langeveld, J Dixon, and JF Jaworski. "Development perspectives of the biobased economy: A review". In: *Crop Science* 50.April (2010), S–142–S–151. ISSN: 14350653. DOI: 10.2135/cropsci2009.09.0529.

[14] J Villadsen, J Nielsen, and G Lidén. *Bioreaction Engineering Principles*. Vol. 53. Boston, MA: Springer US, 2011, pp. 1689–1699. ISBN: 978-1-4419-9687-9. DOI: 10.1007/978-1-4419-9688-6. arXiv: arXiv:1011.1669v3. URL: http://link.springer.com/10.1007/978-1-4419-9688-6.

[15] Q Qi and Q Liang. "Single-Cell Biorefinery". In: *Industrial Biorefineries & White Biotechnology*. Elsevier, 2015, pp. 369–388. ISBN: 9780444634535. DOI: 10.1016/B978-0-444-63453-5.00011-2. URL: https://linkinghub.elsevier.com/retrieve/pii/B9780444634535000112.

[16] ML Jansen and WM van Gulik. "Towards large scale fermentative production of succinic acid". In: *Current Opinion in Biotechnology* 30 (2014), pp. 190–197. ISSN: 18790429. DOI: 10.1016/j.copbio.2014.07.003. URL: http://dx.doi.org/10.1016/j.copbio.2014.07.003.

[17] Grand View Research. *Maleic Anhydride Market Size, Share & Trends Analysis Report By Application (1,4-BDO, UPR, Additives, Copolymers), By Region (Asia Pacific, North America, Europe, Central & South America, MEA), And Segment Forecasts, 2019-2025*. Tech. rep. Grand View Research, 2019. URL: https://www.grandviewresearch.com/industry-analysis/maleic-anhydride-market.

[18] Imarc. *Fumaric Acid Market: Global Industry Trends, Share, Size, Growth, Opportunity and Forecast 2021-2026*. Tech. rep. Imarc, 2020. URL: https://www.imarcgroup.com/fumaric-acid-market.

[19] J Sebastian, K Hegde, P Kumar, T Rouissi, and SK Brar. "Bioproduction of fumaric acid: an insight into microbial strain improvement strategies". In: *Critical Reviews in Biotechnology* 39.6 (2019), pp. 817–834. ISSN: 15497801. DOI: 10.1080/07388551.2019.1620677. URL: https://doi.org/10.1080/07388551.2019.1620677.

[20] V Martin-Dominguez, J Estevez, F Ojembarrena, V Santos, and M Ladero. "Fumaric Acid Production: A Biorefinery Perspective". In: *Fermentation* 4.2 (2018), p. 33. DOI: 10.3390/fermentation4020033.

[21] TR Felthouse, JC Burnett, B Horrell, MJ Mummey, and YJ Kuo. "Maleic Anhydride, Maleic Acid, and Fumaric Acid". In: *Kirk-Othmer Encyclopedia of Chemical Technology* 15.10 (Oct. 2001). Ed. by TR Felthouse. DOI: 10.1002/0471238961.1301120506051220.a01.pub2. URL: http://doi.wiley.com/10.1002/0471740039.vec1569%20http://doi.wiley.com/10.1002/0471238961.1301120506051220.a01.pub2.

[22] CA Roa Engel, AJJ Straathof, TW Zijlmans, WM Van Gulik, and LAM Van Der Wielen. "Fumaric acid production by fermentation". In: *Applied Microbiology and Biotechnology* 78.3 (2008), pp. 379–389. ISSN: 01757598. DOI: 10.1007/s00253-007-1341-x.

[23] A Abe, Y Oda, K Asano, and T Sone. "*Rhizopus delemar* is the proper name for *Rhizopus oryzae* fumaric-malic acid producers". In: *Mycologia* 99.5 (2007), pp. 714–722. ISSN: 00275514. DOI: 10.3852/mycologia.99.5.714.

[24] Y Deng, S Li, Q Xu, M Gao, and H Huang. "Production of fumaric acid by simultaneous saccharification and fermentation of starchy materials with 2-deoxyglucose-resistant mutant strains of *Rhizopus oryzae*". In: *Bioresource Technology* 107 (2012),

pp. 363–367. ISSN: 09608524. DOI: 10.1016/j.biortech.2011.11.117. URL: http://dx.doi.org/10.1016/j.biortech.2011.11.117.

[25] SW Kang, H Lee, D Kim, D Lee, S Kim, GT Chun, J Lee, SW Kim, and C Park. "Strain development and medium optimization for fumaric acid production". In: *Biotechnology and Bioprocess Engineering* 15.5 (2010), pp. 761–769. ISSN: 12268372. DOI: 10.1007/s12257-010-0081-4.

[26] Y Zhou, J Du, and GT Tsao. "Mycelial Pellet Formation by *Rhizopus oryzae* ATCC 20344". In: *Applied Biochemistry and Biotechnology* 84-86.1-9 (2000), pp. 779–790. ISSN: 0273-2289. DOI: 10.1385/ABAB:84-86:1-9:779. URL: http://link.springer.com/10.1385/ABAB:84-86:1-9:779.

[27] JC van Suijdam, NW Kossen, and PG Paul. "An inoculum technique for the production of fungal pellets". In: *European Journal of Applied Microbiology and Biotechnology* 10.3 (1980), pp. 211–221. ISSN: 01711741. DOI: 10.1007/BF00508608.

[28] W Liao, Y Liu, C Frear, and S Chen. "A new approach of pellet formation of a filamentous fungus - *Rhizopus oryzae*". In: *Bioresource Technology* 98.18 (2007), pp. 3415–3423. ISSN: 09608524. DOI: 10.1016/j.biortech.2006.10.028.

[29] DI Odoni, JA Tamayo-Ramos, J Sloothaak, RG van Heck, VA Martins dos Santos, LH de Graaff, M Suarez-Diez, and PJ Schaap. "Comparative proteomics of *Rhizopus delemar* ATCC 20344 unravels the role of amino acid catabolism in fumarate accumulation". In: *PeerJ* 5 (Mar. 2017), e3133. ISSN: 2167-8359. DOI: 10.7717/peerj.3133. URL: https://peerj.com/articles/3133.

[30] Z Zhou, G Du, Z Hua, J Zhou, and J Chen. "Optimization of fumaric acid production by *Rhizopus delemar* based on the morphology formation". In: *Bioresource Technology* 102.20 (2011), pp. 9345–9349. ISSN: 09608524. DOI: 10.1016/j.biortech.2011.07.120. URL: http://dx.doi.org/10.1016/j.biortech.2011.07.120.

[31] A Papadaki, N Androutsopoulos, M Patsalou, M Koutinas, N Kopsahelis, A Castro, S Papanikolaou, and A Koutinas. "Biotechnological Production of Fumaric Acid: The Effect of Morphology of *Rhizopus arrhizus* NRRL 2582". In: *Fermentation* 3.3 (2017), p. 33. DOI: 10.3390/fermentation3030033.

[32] A Naude and W Nicol. "Fumaric acid fermentation with immobilised *Rhizopus oryzae*: Quantifying time-dependent variations in catabolic flux". In: *Process Biochemistry* 56 (2017), pp. 8–20. ISSN: 13595113. DOI: 10.1016/j.procbio.2017.02.027. URL: http://dx.doi.org/10.1016/j.procbio.2017.02.027.

[33] A Naude and W Nicol. "Improved continuous fumaric acid production with immobilised *Rhizopus oryzae* by implementation of a revised nitrogen control strategy". In: *New Biotechnology* 44.July 2017 (2018), pp. 13–22. ISSN: 18764347. DOI: 10.1016/j.nbt.2018.02.012. URL: https://doi.org/10.1016/j.nbt.2018.02.012.

[34] A Naude and W Nicol. "Malic acid production through the whole-cell hydration of fumaric acid with immobilised *Rhizopus oryzae*". In: *Biochemical Engineering Journal* 137 (2018), pp. 152–161. ISSN: 1873295X. DOI: 10.1016/j.bej.2018.05.022. URL: https://doi.org/10.1016/j.bej.2018.05.022.

[35] R Das, S Brar, and M Verma. "Fumaric Acid". In: *Platform Chemical Biorefinery* June 2016 (2016), pp. 133–157. DOI: 10.1016/b978-0-12-802980-0.00008-0.

[36] H Taymaz-Nikerel, E Jamalzadeh, AE Borujeni, PJ Verheijen, WM Van Gulik, and SJ Heijnen. "A thermodynamic analysis of dicarboxylic acid production in microorganisms". In: *Biothermodynamics: The Role of Thermodynamics in Biochemical Engineering* (2013), pp. 547–579.

[37] A Zoghlami and G Paës. "Lignocellulosic Biomass: Understanding Recalcitrance and Predicting Hydrolysis". In: *Frontiers in Chemistry* 7.December (2019). ISSN: 22962646. DOI: 10.3389/fchem.2019.00874.

[38] Y Zhou, J Du, and GT Tsao. "Comparison of fumaric acid production by Rhizopus oryzae using different neutralizing agents". In: 25 (2002), pp. 179–181. DOI: 10.1007/s004490100224.

[39] Z Li, N Liu, Y Cao, C Jin, F Li, C Cai, and J Yao. "Effects of fumaric acid supplementation on methane production and rumen fermentation in goats fed diets varying in forage and concentrate particle size". In: *Journal of Animal Science and Biotechnology* 9.1 (2018), pp. 1–9. ISSN: 20491891. DOI: 10.1186/s40104-018-0235-3.

[40] KR Lassey. "Livestock methane emission and its perspective in the global methane cycle". In: Lassey 2007 (2008), pp. 114–118.

[41] D Smith. "Fumaric acid esters for psoriasis: a systematic review". In: *Irish Journal of Medical Science (1971 -)* 186.1 (Feb. 2017), pp. 161–177. ISSN: 0021-1265. DOI: 10.1007/s11845-016-1470-2. URL: http://link.springer.com/10.1007/s11845-016-1470-2.

[42] S Kourakis, CA Timpani, JB de Haan, N Gueven, D Fischer, and E Rybalka. "Dimethyl Fumarate and Its Esters: A Drug with Broad Clinical Utility?" In: *Pharmaceuticals* 13.10 (Oct. 2020), p. 306. ISSN: 1424-8247. DOI: 10.3390/ph13100306. URL: https://www.mdpi.com/1424-8247/13/10/306.

[43] RF Nystrom, YH Loo, and JC Leak. "Synthesis of Fumaric Acid-2-C 14 and Maleic Anhydride-2-C 14 1". In: *Journal of the American Chemical Society* 74.13 (July 1952), pp. 3434–3435. ISSN: 0002-7863. DOI: 10.1021/ja01133a521. URL: http://pubs.acs.org/doi/abs/10.1021/ja01133a521.

[44] M FitzPatrick, P Champagne, MF Cunningham, and RA Whitney. "A biorefinery processing perspective: Treatment of lignocellulosic materials for the production of value-added products". In: *Bioresource Technology* 101.23 (2010), pp. 8915–8922. ISSN: 09608524. DOI: 10.1016/j.biortech.2010.06.125. URL: http://dx.doi.org/10.1016/j.biortech.2010.06.125.

[45] K Amit, M Nakachew, B Yilkal, and Y Mukesh. "A review of factors affecting enzymatic hydrolysis of pretreated lignocellulosic biomass". In: *Research Journal of Chemistry and Environment* 22.7 (2018), pp. 62–67. ISSN: 22784527.

[46] Y Sun and J Cheng. "Hydrolysis of lignocellulosic materials for ethanol production: A review". In: *Bioresource Technology* 83.1 (2002), pp. 1–11. ISSN: 09608524. DOI: 10.1016/S0960-8524(01)00212-7.

[47] B Hahn-Hägerdal, K Karhumaa, C Fonseca, I Spencer-Martins, and MF Gorwa-Grauslund. "Towards industrial pentose-fermenting yeast strains". In: *Applied Microbiology and Biotechnology* 74.5 (2007), pp. 937–953. ISSN: 01757598. DOI: 10.1007/s00253-006-0827-2.

[48] JW Foster and SA Waksman. "The Production of Fumaric Acid by Molds Belonging to the Genus *Rhizopus*". In: *Journal of the American Chemical Society* 61.1 (1939), pp. 127–135. ISSN: 15205126. DOI: 10.1021/ja01870a043.

[49] A Abe, Y Oda, K Asano, and T Sone. "*Rhizopus delemar* is the proper name for *Rhizopus oryzae* fumaric-malic acid producers". In: *Mycologia* 99.5 (Sept. 2007), pp. 714–722. ISSN: 0027-5514. DOI: 10.3852/mycologia.99.5.714. URL: http://www.mycologia.org/cgi/doi/10.3852/mycologia.99.5.714.

[50] RA Rhodes, AA Lagoda, TJ Misenheimer, ML Smith, RF Anderson, and RW Jackson. "Production of Fumaric Acid in 20-Liter Fermentors." In: *Applied microbiology* 10.1 (1962), pp. 9–15. ISSN: 0003-6919. URL: http://www.ncbi.nlm.nih.gov/pubmed/16349614%0Ahttp://www.pubmedcentral.nih.gov/articlerender.fcgi?artid=PMC1057800.

[51] YQ Fu, S Li, Y Chen, Q Xu, H Huang, and XY Sheng. "Enhancement of fumaric acid production by *Rhizopus oryzae* using a two-stage dissolved oxygen control strategy". In: *Applied Biochemistry and Biotechnology* 162.4 (2010), pp. 1031–1038. ISSN: 02732289. DOI: 10.1007/s12010-009-8831-5.

[52] L Huang, P Wei, R Zang, and Z Xu. "High-throughput screening of high-yield colonies of *Rhizopus oryzae* for enhanced production of fumaric acid". In: (2010), pp. 287–292. DOI: 10.1007/s13213-010-0039-y.

[53] CA Roa Engel, WM van Gulik, L Marang, LA van der Wielen, and AJ Straathof. "Development of a low pH fermentation strategy for fumaric acid production by *Rhizopus oryzae*". In: *Enzyme and Microbial Technology* 48.1 (Jan. 2011), pp. 39–47. ISSN: 01410229. DOI: 10.1016/j.enzmictec.2010.09.001. URL: http://dx.doi.org/10.1016/j.enzmictec.2010.09.001%20https://linkinghub.elsevier.com/retrieve/pii/S0141022910001948.

[54] C Gu, Y Zhou, L Liu, T Tan, and L Deng. "Production of fumaric acid by immobilized *Rhizopus arrhizus* on net". In: *Bioresource Technology* 131 (Mar. 2013), pp. 303–307. ISSN: 09608524. DOI: 10.1016/j.biortech.2012.12.148. URL: https://linkinghub.elsevier.com/retrieve/pii/S0960852412020068.

[55] H Liu, S Zhao, Y Jin, X Yue, L Deng, F Wang, and T Tan. "Production of fumaric acid by immobilized Rhizopus arrhizus RH 7-13-9# on loofah fiber in a stirred-tank reactor". In: *Bioresource Technology* 244 (Nov. 2017), pp. 929–933. ISSN: 09608524.

DOI: 10.1016/j.biortech.2017.07.185. URL: https://linkinghub.elsevier.com/retrieve/pii/S0960852417313019.

[56] Y Zhou, K Nie, X Zhang, S Liu, M Wang, L Deng, F Wang, and T Tan. "Production of fumaric acid from biodiesel-derived crude glycerol by Rhizopus arrhizus". In: *Bioresource Technology* 163 (July 2014), pp. 48–53. ISSN: 09608524. DOI: 10.1016/j.biortech.2014.04.021. URL: https://linkinghub.elsevier.com/retrieve/pii/S0960852414005161.

[57] RK Das and SK Brar. "Enhanced Fumaric Acid Production from Brewery Wastewater and Insight into the Morphology of *Rhizopus oryzae* 1526". In: *Applied Biochemistry and Biotechnology* 172.6 (Mar. 2014), pp. 2974–2988. ISSN: 0273-2289. DOI: 10.1007/s12010-014-0739-z. URL: http://link.springer.com/10.1007/s12010-014-0739-z.

[58] RK Das, SK Brar, and M Verma. "A fermentative approach towards optimizing directed biosynthesis of fumaric acid by *Rhizopus oryzae* 1526 utilizing apple industry waste biomass". In: *Fungal Biology* 119.12 (Dec. 2015), pp. 1279–1290. ISSN: 18786146. DOI: 10.1016/j.funbio.2015.10.001. URL: https://linkinghub.elsevier.com/retrieve/pii/S1878614615001907.

[59] W Liao, Y Liu, C Frear, and S Chen. "Co-production of fumaric acid and chitin from a nitrogen-rich lignocellulosic material - dairy manure - using a pelletized filamentous fungus *Rhizopus oryzae* ATCC 20344". In: *Bioresource Technology* 99.13 (Sept. 2008), pp. 5859–5866. ISSN: 09608524. DOI: 10.1016/j.biortech.2007.10.006. URL: https://linkinghub.elsevier.com/retrieve/pii/S0960852407008437.

[60] RK Das, SK Brar, and M Verma. "Enhanced fumaric acid production from brewery wastewater by immobilization technique". In: *Journal of Chemical Technology & Biotechnology* 90.8 (Aug. 2015), pp. 1473–1479. ISSN: 02682575. DOI: 10.1002/jctb.4455. URL: http://doi.wiley.com/10.1002/jctb.4455.

[61] S Wen, L Liu, K Nie, L Deng, T Tan, and F Wang. "Enhanced Fumaric Acid Production by Fermentation of Xylose Using a Modified Strain of *Rhizopus arrhizus*". In: *Bioresources* 8 (2013). DOI: 10.15376/biores.8.2.2186-2194.

[62] H Liu, W Wang, L Deng, F Wang, and T Tan. "High production of fumaric acid from xylose by newly selected strain *Rhizopus arrhizus* RH 7-13-9#". In: *Bioresource Technology* 186 (June 2015), pp. 348–350. ISSN: 09608524. DOI: 10.1016/j.

biortech.2015.03.109. URL: https://linkinghub.elsevier.com/retrieve/pii/S0960852415004411.

[63] F Deng and GM Aita. "Fumaric Acid Production by *Rhizopus oryzae* ATCC® 20344™ from Lignocellulosic Syrup". In: *Bioenergy Research* 11.2 (2018), pp. 330–340. ISSN: 19391242. DOI: 10.1007/s12155-018-9899-y.

[64] H Liu, H Hu, Y Jin, X Yue, L Deng, F Wang, and T Tan. "Co-fermentation of a mixture of glucose and xylose to fumaric acid by Rhizopus arrhizus RH 7-13-9#". In: *Bioresource Technology* 233 (2017), pp. 30–33. ISSN: 18732976. DOI: 10.1016/j.biortech.2017.02.035. URL: http://dx.doi.org/10.1016/j.biortech.2017.02.035.

[65] Q Xu, S Li, Y Fu, C Tai, and H Huang. "Two-stage utilization of corn straw by *Rhizopus oryzae* for fumaric acid production". In: *Bioresource Technology* 101.15 (Aug. 2010), pp. 6262–6264. ISSN: 09608524. DOI: 10.1016/j.biortech.2010.02.086. URL: https://linkinghub.elsevier.com/retrieve/pii/S0960852410003974.

[66] SA Osmani and MC Scrutton. "The sub-cellular localisation and regulatory properties of pyruvate carboxylase from *Rhizopus arrhizus*". In: *European Journal of Biochemistry* 147.1 (Feb. 1985), pp. 119–128. ISSN: 0014-2956. DOI: 10.1111/j.1432-1033.1985.tb08727.x. URL: https://onlinelibrary.wiley.com/doi/10.1111/j.1432-1033.1985.tb08727.x.

[67] B Zhang, CD Skory, and ST Yang. "Metabolic engineering of *Rhizopus oryzae*: Effects of overexpressing pyc and pepc genes on fumaric acid biosynthesis from glucose". In: *Metabolic Engineering* 14.5 (Sept. 2012), pp. 512–520. ISSN: 10967176. DOI: 10.1016/j.ymben.2012.07.001. URL: https://linkinghub.elsevier.com/retrieve/pii/S1096717612000717.

[68] B Zhang and ST Yang. "Metabolic engineering of Rhizopus oryzae: Effects of overexpressing fumR gene on cell growth and fumaric acid biosynthesis from glucose". In: *Process Biochemistry* 47.12 (2012), pp. 2159–2165. ISSN: 13595113. DOI: 10.1016/j.procbio.2012.08.009. URL: http://dx.doi.org/10.1016/j.procbio.2012.08.009.

[69] AY Skorokhodova, AY Gulevich, and VG Debabov. "Engineering Escherichia coli for efficient aerobic conversion of glucose to fumaric acid". In: *Biotechnology Reports*

33 (2022), e00703. ISSN: 2215017X. DOI: 10.1016/j.btre.2022.e00703. URL: https://doi.org/10.1016/j.btre.2022.e00703.

[70] CW Song, DI Kim, S Choi, JW Jang, and SY Lee. "Metabolic engineering of Escherichia coli for the production of fumaric acid". In: *Biotechnology and Bioengineering* 110.7 (2013), pp. 2025–2034. ISSN: 00063592. DOI: 10.1002/bit.24868. URL: https://onlinelibrary.wiley.com/doi/abs/10.1002/bit.24868.

[71] G Xu, X Chen, L Liu, and L Jiang. "Fumaric acid production in Saccharomyces cerevisiae by simultaneous use of oxidative and reductive routes". In: *Bioresource Technology* 148 (2013), pp. 91–96. ISSN: 18732976. DOI: 10.1016/j.biortech.2013.08.115. URL: http://dx.doi.org/10.1016/j.biortech.2013.08.115.

[72] G Xu, L Liu, and J Chen. "Reconstruction of cytosolic fumaric acid biosynthetic pathways in Saccharomyces cerevisiae". In: *Microbial Cell Factories* 11.1 (Dec. 2012), p. 24. ISSN: 1475-2859. DOI: 10.1186/1475-2859-11-24. URL: https://microbialcellfactories.biomedcentral.com/articles/10.1186/1475-2859-11-24.

[73] Y Ding, S Li, C Dou, Y Yu, and H He. "Production of fumaric acid by Rhizopus oryzae: Role of carbon-nitrogen ratio". In: *Applied Biochemistry and Biotechnology* 164.8 (2011), pp. 1461–1467. ISSN: 02732289. DOI: 10.1007/s12010-011-9226-y.

[74] Q Xu, S Li, H Huang, and J Wen. "Key technologies for the industrial production of fumaric acid by fermentation". In: *Biotechnology Advances* 30.6 (2012), pp. 1685–1696. ISSN: 07349750. DOI: 10.1016/j.biotechadv.2012.08.007. URL: http://dx.doi.org/10.1016/j.biotechadv.2012.08.007.

[75] RH Maas, J Springer, G Eggink, and RA Weusthuis. "Xylose metabolism in the fungus Rhizopus oryzae: Effect of growth and respiration on l(+)-lactic acid production". In: *Journal of Industrial Microbiology and Biotechnology* 35.6 (2008), pp. 569–578. ISSN: 13675435. DOI: 10.1007/s10295-008-0318-9.

[76] Y Peleg, E Battat, MC Scrutton, and I Goldberg. "Isoenzyme pattern and subcellular localisation of enzymes involved in fumaric acid accumulation by *Rhizopus oryzae*". In: *Applied Microbiology and Biotechnology* 32.3 (1989), pp. 334–339. ISSN: 01757598. DOI: 10.1007/BF00184985.

[77] MT Madigan, JM Martinko, KS Bender, DH Buckley, DA Stahl, and T Brock. *Brock biology of microorganisms*. 14th ed. Pearson, 2015, pp. 86–94. ISBN: 978-0-321-89739-8.

[78] BJ Meussen, LH De Graaff, JP Sanders, and RA Weusthuis. "Metabolic engineering of Rhizopus oryzae for the production of platform chemicals". In: *Applied Microbiology and Biotechnology* 94.4 (2012), pp. 875–886. ISSN: 01757598. DOI: 10.1007/s00253-012-4033-0.

[79] W Kenealy, E Zaady, and JC Du Preez. "Biochemical aspects of fumaric acid accumulation by *Rhizopus arrhizus*". In: *Applied and Environmental Microbiology* 52.1 (1986), pp. 128–133. ISSN: 00992240. DOI: 10.1128/aem.52.1.128-133.1986.

[80] S FazeliNejad, JA Ferreira, T Brandberg, PR Lennartsson, and MJ Taherzadeh. "Fungal protein and ethanol from lignocelluloses using *Rhizopus* pellets under simultaneous saccharification, filtration and fermentation (SSFF)". In: *Biofuel Research Journal* 3.1 (2016), pp. 372–378. DOI: 10.18331/brj2016.3.1.7.

[81] RH De Deken. "The Crabtree Effect: A Regulatory System in Yeast". In: *Journal of General Microbiology* 44.2 (1966), pp. 149–156. ISSN: 0022-1287. DOI: 10.1099/00221287-44-2-149. URL: http://mic.microbiologyresearch.org/content/journal/micro/10.1099/00221287-44-2-149.

[82] JP Barford and RJ Hall. "An Examination of the Crabtree Effect in Saccharomyces cerevisiae: the Role of Respiratory Adaptation". In: *Journal of General Microbiology* 114.2 (Oct. 1979), pp. 267–275. ISSN: 0022-1287. DOI: 10.1099/00221287-114-2-267. URL: http://mic.microbiologyresearch.org/content/journal/micro/10.1099/00221287-114-2-267%20https://www.microbiologyresearch.org/content/journal/micro/10.1099/00221287-114-2-267.

[83] E Postma, C Verduyn, WA Scheffers, and JP Van Dijken. "Enzymic analysis of the crabtree effect in glucose-limited chemostat cultures of Saccharomyces cerevisiae." In: *Applied and Environmental Microbiology* 55.2 (1989), pp. 468–477. ISSN: 00992240. DOI: 0099-2240/89/020468-10{\$}02.00/0.

[84] L Habegger, KR Crespo, and M Dabros. "Preventing overflow metabolism in crabtree-positive microorganisms through on-line monitoring and control of fed-batch fermentations". In: *Fermentation* 4.3 (2018). ISSN: 23115637. DOI: 10.3390/fermentation4030079.

[85] W Mager and M Siderius. "Novel insights into the osmotic stress response of yeast". In: *FEMS Yeast Research* 2.3 (Aug. 2002), pp. 251–257. ISSN: 15671356. DOI: 10.1016/S1567-1356(02)00116-2. URL: https://academic.oup.com/femsyr/article-lookup/doi/10.1016/S1567-1356(02)00116-2.

[86] DA Abbott, E Suir, AJ Van Maris, and JT Pronk. "Physiological and transcriptional responses to high concentrations of lactic acid in anaerobic chemostat cultures of Saccharomyces cerevisiae". In: *Applied and Environmental Microbiology* 74.18 (2008), pp. 5759–5768. ISSN: 00992240. DOI: 10.1128/AEM.01030-08.

[87] AJ Maris, WN Konings, JP Dijken, and JT Pronk. "Microbial export of lactic and 3-hydroxypropanoic acid: Implications for industrial fermentation processes". In: *Metabolic Engineering* 6.4 (2004), pp. 245–255. ISSN: 10967176. DOI: 10.1016/j.ymben.2004.05.001.

[88] Q Xu, S Li, Y Fu, C Tai, and H Huang. "Two-stage utilization of corn straw by Rhizopus oryzae for fumaric acid production". In: *Bioresource Technology* 101.15 (2010), pp. 6262–6264. ISSN: 09608524. DOI: 10.1016/j.biortech.2010.02.086. URL: http://dx.doi.org/10.1016/j.biortech.2010.02.086.

[89] Z Zhao, M Xian, M Liu, and G Zhao. "Biochemical routes for uptake and conversion of xylose by microorganisms". In: *Biotechnology for Biofuels* 13.1 (2020), pp. 1–12. ISSN: 17546834. DOI: 10.1186/s13068-020-1662-x. URL: https://doi.org/10.1186/s13068-020-1662-x.

[90] P Vinuselvi, MK Kim, SK Lee, and CM Ghim. "Rewiring carbon catabolite repression for microbial cell factory". In: *BMB Reports* 45.2 (2012), pp. 59–70. ISSN: 19766696. DOI: 10.5483/BMBRep.2012.45.2.59.

[91] DE Seborg, DA Mellichamp, TF Edgar, and FJ Doyle III. *Process Dynamics and Control*. 4th ed. Danvers, MA: John Wiley & Sons Inc., 2017. ISBN: 9781119285915.

[92] C Verduyn, TPL Zomerdijk, JP van Dijken, and WA Scheffers. "Continuous measurement of ethanol production by aerobic yeast suspensions with an enzyme electrode". In: *Applied Microbiology and Biotechnology* 19.3 (1984), pp. 181–185. ISSN: 01757598. DOI: 10.1007/BF00256451.

[93] S Aiba, S Nagai, and Y Nishi. "A Perspective of Computer Control to Enhance the Productivity in Baker 's Yeast Cultivation". In: *Biotechnology* XVIII (1976), pp. 1001–1016.

[94] Y Liu, C Lv, Q Xu, S Li, H Huang, and P Ouyang. "Enhanced acid tolerance of *Rhizopus oryzae* during fumaric acid production". In: *Bioprocess and Biosystems Engineering* 38.2 (Feb. 2015), pp. 323–328. ISSN: 1615-7591. DOI: 10.1007/s00449-014-1272-8. URL: http://link.springer.com/10.1007/s00449-014-1272-8.

[95] F Di Caprio. "A fattening factor to quantify the accumulation ability of microorganisms under N-starvation". In: *New Biotechnology* 66.April (2021). ISSN: 18764347. DOI: 10.1016/j.nbt.2021.04.001. URL: https://doi.org/10.1016/j.nbt.2021.04.001.

[96] F Feillet and JV Leonard. "Alternative pathway therapy for urea cycle disorders". In: *Journal of Inherited Metabolic Disease* 21.SUPPL. 1 (1998), pp. 101–111. ISSN: 01418955. DOI: 10.1023/a:1005365825875.

[97] X Kan, Z Yao, J Zhang, YW Tong, W Yang, Y Dai, and CH Wang. "Energy performance of an integrated bio and thermal hybrid system for lignocellulosic biomass waste treatment". In: *Bioresource Technology* 228 (2017), pp. 77–88. ISSN: 18732976. DOI: 10.1016/j.biortech.2016.12.064. URL: http://dx.doi.org/10.1016/j.biortech.2016.12.064.

[98] SR Kim, YC Park, YS Jin, and JH Seo. "Strain engineering of Saccharomyces cerevisiae for enhanced xylose metabolism". In: *Biotechnology Advances* 31.6 (2013), pp. 851–861. ISSN: 07349750. DOI: 10.1016/j.biotechadv.2013.03.004. URL: http://dx.doi.org/10.1016/j.biotechadv.2013.03.004.

[99] A Matsushika, A Nagashima, T Goshima, and T Hoshino. "Fermentation of Xylose Causes Inefficient Metabolic State Due to Carbon/Energy Starvation and Reduced Glycolytic Flux in Recombinant Industrial Saccharomyces cerevisiae". In: *PLoS ONE* 8.7 (2013). ISSN: 19326203. DOI: 10.1371/journal.pone.0069005.

A Appendix

$$
\begin{bmatrix}
 & v_0 & v_1 & v_2 & v_3 & v_4 & v_5 & v_6 & v_7 & v_8 & v_9 & v_{10} & v_{11} & v_{12} & v_{13} & v_{14} & v_{15} & v_{16} & v_{17} & v_{18} & v_{19} & v_{20} & v_{21} & v_{22} & v_{23} & v_{24} & v_{25} & v_{26} \\
A & 0 & -1 & 1.116 & 1 & 0 & 0 & 1 & 0 & 0 & 0 & 0 & 0 & 0 & 0 & 0 & 0 & 0 & 0 & 0 & 0 & 0 & 0 & 0 & 0 & 0 & 0 & 0 \\
B & 0 & 0 & 0 & 0 & 0 & 0 & -1 & 1 & -5/6 & 0 & 0 & 0 & 0 & 0 & 0 & 0 & 0 & 0 & 0 & 0 & 0 & 0 & 0 & 0 & 0 & 0 & 0 \\
C & -1 & 0 & 0 & 0 & 1.116 & 1 & 0 & 0 & 0 & 1 & 0 & 0 & 0 & 0 & 0 & 0 & 0 & 0 & 0 & 0 & 0 & 0 & 0 & 0 & 0 & 0 & 0 \\
D & 0 & 0 & 0 & 0 & 0 & 0 & 0 & -1 & 1 & -1 & 1 & 0 & 0 & 0 & 0 & 0 & 0 & 0 & 0 & 0 & 0 & 0 & 0 & 0 & 0 & 0 & 0 \\
E & 0 & 0 & 0 & 0 & 0 & 0 & 0 & 0 & 0 & 0 & -1 & 1 & 1 & 0 & 0 & 0 & 0 & 0 & 0 & 0 & 0 & 0 & 0 & 0 & 0 & 0 & 0 \\
F & 0 & 0 & 0 & 0 & 0 & 0 & 0 & 0 & 0 & 0 & 0 & 0 & -1 & 3/4 & 0 & 0 & 1.5 & 0 & 0 & 0 & 0 & 0 & 0 & 1 & 1.5 & 0 & 0 \\
G & 0 & 0 & 0 & 0 & 0 & 0 & 0 & 0 & 0 & 0 & 0 & 0 & 0 & -1 & 1 & 1 & 0 & 0 & 0 & 0 & 0 & 0 & 0 & 0 & 0 & 0 & 0 \\
H & 0 & 0 & 0 & 0 & 0 & 0 & 0 & 0 & 0 & 0 & 0 & 0 & 0 & 0 & 0 & 0 & -1 & 1 & 0 & 0 & 0 & 0 & 0 & 0 & 0 & -1 & 0 \\
I & 0 & 0 & 0 & 0 & 0 & 0 & 0 & 0 & 0 & 0 & 0 & 0 & 0 & 0 & 0 & 0 & 0 & -1 & 1.5 & 0 & 0 & 0 & -1 & 0 & 0 & 0 & 0 \\
J & 0 & 0 & 0 & 0 & 0 & 0 & 0 & 0 & 0 & 0 & 0 & 0 & 0 & 0 & 0 & 0 & 0 & 0 & -1 & 1 & 1 & 0 & 0 & 0 & 0 & 0 & 0 \\
K & 0 & 0 & 0 & 0 & 0 & 0 & 0 & 0 & 0 & 0 & 0 & 0 & 0 & 0 & 0 & 0 & 0 & 0 & 0 & 0 & -1 & 1 & 1 & 0 & 0 & 0 & 0 \\
M & 0 & 0 & 0 & 0 & 0 & 0 & 0 & 0 & 0 & 0 & 0 & 0 & 0 & 0 & 0 & 0 & 0 & 1 & 0 & 0 & 0 & 0 & -0.5 & 0 & 0 & 0 & 0 \\
NADPH & 0 & -0.6 & 0 & 0 & 0 & 0 & 0 & 0 & 1 & 0 & 0 & 0 & 0 & 0 & 0 & 0 & 0 & 0 & 0 & 0 & 0 & 0 & 0 & 0 & 0 & 0 & 0 \\
NADH & 0 & 0 & 0.116 & 0 & 0.116 & 0 & 0.2 & 0 & 0 & 0 & 0 & -1/3 & 1/3 & -1/4 & 0 & 0 & 0.5 & 0 & 0.5 & 0 & 1/4 & 0 & 1/4 & 0 & -0.5 & 1 & -2 \\
ATP & 0 & 0 & -2.5 & 0 & -2.5 & 0 & 0 & 0 & 0 & -1/6 & -1/6 & 0 & 2/3 & -1/4 & 0 & 0 & 0 & 0 & 1/4 & 0 & 0 & 0 & 0 & 0 & 0 & -0.5 & 3 \\
S_1 & 1 & 0 & 0 & 0 & 0 & 0 & 0 & 0 & 0 & 0 & 0 & 0 & 0 & 0 & 0 & 0 & 0 & 0 & 0 & 0 & 0 & 0 & 0 & 0 & 0 & 0 & 0 \\
S_2 & 0 & 1 & 0 & 0 & 0 & 0 & 0 & 0 & 0 & 0 & 0 & 0 & 0 & 0 & 0 & 0 & 0 & 0 & 0 & 0 & 0 & 0 & 0 & 0 & 0 & 0 & 0 \\
S_3 & 0 & 0 & 1 & 0 & 0 & 0 & 0 & 0 & 0 & 0 & 0 & 0 & 0 & 0 & 0 & 0 & 0 & 0 & 0 & 0 & 0 & 0 & 0 & 0 & 0 & 0 & 0 \\
S_4 & 0 & 0 & 0 & 1 & 0 & 0 & 0 & 0 & 0 & 0 & 0 & 0 & 0 & 0 & 0 & 0 & 0 & 0 & 0 & 0 & 0 & 0 & 0 & 0 & 0 & 0 & 0 \\
S_5 & 0 & 0 & 0 & 0 & 1 & 0 & 0 & 0 & 0 & 0 & 0 & 0 & 0 & 0 & 0 & 0 & 0 & 0 & 0 & 0 & 0 & 0 & 0 & 0 & 0 & 0 & 0 \\
S_6 & 0 & 0 & 0 & 0 & 0 & 1 & 0 & 0 & 0 & 0 & 0 & 0 & 0 & 0 & 0 & 0 & 0 & 0 & 0 & 0 & 0 & 0 & 0 & 0 & 0 & 0 & 0 \\
S_7 & 0 & 0 & 0 & 0 & 0 & 0 & 0 & 0 & 0 & 0 & 0 & 0 & 0 & 0 & 0 & 0 & 0 & 0 & 0 & 0 & 0 & 0 & 0 & 1 & 0 & 0 & 0 \\
S_8 & 0 & 0 & 0 & 0 & 0 & 0 & 0 & 0 & 0 & 0 & 0 & 1 & 0 & 0 & 0 & 0 & 0 & 0 & 0 & 0 & 0 & 0 & 0 & 0 & 0 & 0 & 0 \\
S_9 & 0 & 0 & 0 & 0 & 0 & 0 & 0 & 0 & 0 & 0 & 0 & 0 & 0 & 0 & 0 & 1 & 0 & 0 & 0 & 0 & 0 & 1 & 0 & 0 & 0 & 0 & 0 \\
S_{10} & 0 & 0 & 0 & 0 & 0 & 0 & 0 & 0 & 0 & 0 & 0 & 0 & 0 & 0 & 1 & 0 & 0 & 0 & 0 & 0 & 0 & 0 & 0 & 0 & 0 & 0 & 0 \\
S_{11} & 0 & 0 & 0 & 0 & 0 & 0 & 0 & 0 & 0 & 0 & 0 & 0 & 0 & 0 & 0 & 0 & 0 & 0 & 0 & 1 & 0 & 0 & 0 & 0 & 0 & 0 & 0 \\
S_{12} & 0 & 0 & 0 & 0 & 0 & 0 & 0 & 0 & 0 & 0 & 0 & 0 & 0 & 0 & 0 & 0 & 0 & 0 & 0 & 0 & 0 & 0 & 0 & 0 & 1 & 0 & 0 \\
S_{13} & 0 & 0 & 0 & 0 & 0 & 0 & 0 & 0 & 0 & 0 & 0 & 0 & 0 & 0 & 0 & 0 & 0 & 0 & 0 & 0 & 0 & 0 & 0 & 0 & 0 & 1 & 0 \\
S_{14} & 0 & 0 & 0 & 0 & 0 & 0 & 0 & 0 & 0 & 0 & 0 & 0 & 0 & 0 & 0 & 0 & 0 & 0 & 0 & 0 & 0 & 0 & 0 & 0 & 0 & 0 & 1 \\
S_{15} & 0 & 0 & 0.116 & 0 & 0.116 & 0 & 0 & 0 & 1/6 & 0 & 0 & 0 & 0 & -1/4 & 0 & 0 & 0.5 & 0 & 0.5 & 0 & 0 & 0 & 0 & 0 & 0 & 0.5 & 0 & 0
\end{bmatrix}
\mathbf{v} =
\begin{bmatrix}
0 \\ 0 \\ 0 \\ 0 \\ 0 \\ 0 \\ 0 \\ 0 \\ 0 \\ 0 \\ 0 \\ 0 \\ 0 \\ 0 \\ 0 \\ 0 \\ -r_g \\ -r_x \\ r_{bx} \\ r_{gyx} \\ r_{bg} \\ r_{gyg} \\ r_{py} \\ r_{gl} \\ r_{ma} \\ r_{fa} \\ r_{sa} \\ r_{et} \\ -r_{et} \\ r_{O_2} \\ r_{CO_2}
\end{bmatrix}
$$